ENGINEERED MICROTOPOGRAPHIES AND SURFACE CHEMISTRIES DIRECT CELL ATTACHMENT AND FUNCTION

By

CHELSEA MARIE MAGIN

A DISSERTATION PRESENTED TO THE GRADUATE SCHOOL
OF THE UNIVERSITY OF FLORIDA IN PARTIAL FULFILLMENT
OF THE REQUIREMENTS FOR THE DEGREE OF
DOCTOR OF PHILOSOPHY

UNIVERSITY OF FLORIDA

2010

To my fiancé, Steven J. Kirschner

ACKNOWLEDGMENTS

I would like to express my sincere gratitude to my advisor Dr. Anthony Brennan for his guidance and support. I also appreciate the advice and guidance provided by my doctoral committee: Dr. Christopher Batich, Dr. Benjamin Keselowsky, and Dr. Daniel Purich. I must also acknowledge and thank my research collaborators: Dr. Mark Segal, Ms. Larysa (Laura) Sautina, Dr. Maureen Callow, Dr. James Callow, Dr. John Finlay, Dr. Gabriel Lopez, Ms. Linnea Ista, and Dr. Michael Schultz. I extend special thanks to Jennifer Wrighton her administrative assistance and friendship throughout my graduate studies.

Graduate and undergraduate students, past and present, have been essential to my progress. I must first thank Dr. Michelle Carman, Drs. James and Iris Schumacher, Dr. Leslie Wilson, Dr. Christopher Long, and Mr. Kenneth Chung for their guidance and support as mentors. I would also like to thank Dr. Sheema Freeman for teaching me how to properly dispose of biohazardous waste. I must acknowledge the friendship and collaboration provided by my peers and current members of the Brennan Research Group: Scott Cooper, Angel Eijiasi, Dave Jackson, Jack (Jiun-Jeng) Chen, and Julian Sheats. Undergraduate students that worked with me to make my research possible include Matthew Blackburn, Cristina Fernandez, Sara Mendelson, Kern Hast and Michael Showalter.

I also express my great appreciation for the loving support from my mother, Tina Capizzi, and my father, Greg Magin who inspired me to grow up to be an engineer. I am truly grateful for the constant encouragement from my dearest friend, Johannah Mahfood, and my loving fiancé, Steve Kirschner.

TABLE OF CONTENTS

LIST OF TABLES

LIST OF FIGURES

LIST OF ABBREVIATIONS

α	describes the risk of making a Type I error in statistical analysis
ANOVA	Analysis of Variance
ATR-FTIR	Attenuated Total Reflectance Fourier Transform Infrared Spectrometry
C. marina	*Cobetia marina*
CSI	Cell Shape Index
EC	Endothelial Cell
ERI	Engineered Roughness Index
Fn	Fibronectin
GMA	Glycidyl methacrylate
HCAEC	Human Coronary Artery Endothelial Cell
HCASMC	Human Coronary Artery Smooth Muscle Cell
HEMA	2-Hydroxyethylmethacrylate
Navicula	*Navicula incerta*
p	p-value or observed significance level
PDMSe	Polydimethylsiloxane elastomer Silastic T2® Dow Corning Corporation
PEG	Poly(ethylene glycol)
PEGDMA	Poly(ethylene glycol) dimethacrylate
PVEC	Porcine Vascular Endothelial Cell
SMC	Smooth Muscle Cell
Re	Reynolds Number
Seminavis	*Seminavis robusta*
TCPS	Tissue culture polystyrene
Ulva	*Ulva linza*

Abstract of Dissertation Presented to the Graduate School
of the University of Florida in Partial Fulfillment of the
Requirements for the Degree of Doctor of Philosophy

ENGINEERED MICROTOPOGRAPHIES AND SURFACE CHEMISTRIES DIRECT CELL ATTACHMENT AND FUNCTION

By

Chelsea Marie Magin

December 2010

Chair: Anthony B. Brennan
Major: Biomedical Engineering

Harrison, in 1914, first recognized that cells respond to physicochemical cues such as substratum topography when he observed that fibroblasts elongated while cultured on spider silk. Recently, techniques developed in the micro-electronics industry have been used to create molds for producing microscaled topographies with various shapes and spatial arrangements. Although these patterning techniques are well-established, very little is known about the mechanisms underlying cell sensing and response to microtopographies. In this work cellular micro-environments with varying surface topographies and chemistries were evaluated with marine organisms and mammalian cells to investigate cellular sensing and response.

Biofouling – the accumulation of micro-organisms, plants, and animals on submerged surfaces – is an environmental and economic concern. Engineered topographies, replicated in polydimethylsiloxane elastomer (PDMSe) and functionalized poly(ethylene glycol)-dimethacrylate (PEGDMA) hydrogels, were evaluated for inhibition of marine fouling organism attachment. Microtopographies replicated in PDMSe inhibited attachment of the marine bacterium, *Cobetia marina* up to 99% versus smooth.

The average normalized attachment densities of cells of *C. marina* and zoospores of the green algae *Ulva* on PDMSe topographies scaled inversely with the Engineered Roughness Index (ERI_{II}), a representation of surface energy. Attachment densities of *Ulva* from four assays and *C. marina* from two growth phases to PDMSe surfaces scaled inversely with one equation: ERI_{II} multiplied by the Reynolds number of the organism (Re) ($R^2 = 0.77$).

The same microtopographies created in PDMSe reduced the initial attachment density and attachment strength of cells of the diatoms *Navicula incerta* and *Seminavis robusta* compared to smooth PDMSe. The average normalized attachment density of *Navicula* after exposure to shear stress (48 Pa) was correlated with the contact area between the diatom and a topographically modified surface (R^2=0.82).

Functionalized PEGDMA hydrogels significantly reduced attachment and attachment strength of *Navicula* and *C. marina*. These hydrogels also reduced attachment of zoospores of *Ulva* compared to PDMSe. Attachment of *Ulva* to microtopographies in PDMSe and PEGDMA-co-HEMA negatively correlated with ERI_{II}*Re ($R^2 = 0.94$ and $R^2 = 0.99$, respectively). Incorporating a surface energy term into this equation created a correlation between the attachment densities of cells from two evolutionarily diverse groups on substrates of two surface chemistries with an equation that describes the various microtopographies and surface chemistries in terms of surface energy ($R^2 = 0.80$). The current Attachment Model can now be used to design engineered antifouling surface microtopographies and chemistries that inhibit the attachment of organisms from three evoluntionarily diverse groups.

Hydrogels based on PEGDMA were also chosen as a substratum material for mammalian cell culture. Capturing endothelial progenitor cells (EPCs) and inducing differentiation into the endothelial cell (EC) phenotype is the ideal way to re-endothelialize a small-diameter vascular graft. Substratum elasticity has been reported to direct stem cell differentiation into specific lineages. Functionalized PEGDMA hydrogels provided good compliance, high fidelity of topographic features and sites for surface modification with biomolecules. Fibronectin grafting and topography both increased EC attachment. This combination of adjustable elasticity, surface chemistry and topography has the potential to promote the capture and differentiation of EPCs into a confluent EC monolayer. Engineered microtopographies replicated in PDMSe directed elongation and alignment of human coronary artery endothelial cells (HCAECs) and human coronary artery smooth muscle cells (HCASMCs) compared to smooth surfaces. Engineered cellular micro-environments were created with specific surface energies defined by chemistry and topography to successfully direct cell attachment and function.

CHAPTER 1
INTRODUCTION

Scope of Research

It is widely recognized that cells and organisms respond to physicochemical cues presented by their micro-environment (Harrison 1914, Callow et al. 2002, Dalby 2005, Engler et al. 2006, Schumacher et al. 2007b, Schilp et al. 2009). In this work the influence of engineered microtopographies and surface chemistries on cell attachment and function is investigated for two different applications: marine antifouling and substrates for mammalian cell culture. Combinations of surface topography and chemistry were evaluated for the deterrence of fouling cells and organisms in the marine environment and as substrates for mammalian cell culture.

Specific Aims

Specific Aim 1: Determine the Contribution of Organism Size and Shape to the Slope of the Attachment Model using *Cobetia marina*

A model that relates the normalized, transformed attachment density of the green algae *Ulva linza* to engineered microtopographies was previously developed. The attachment densities from four separate *Ulva* attachment assays performed over three years correlated with the ERI_{II} ($R^2 = 0.88$) (Long et al. 2010). It was hypothesized that the normalized, transformed attachment density of cells of *C. marina* would also have a negative correlation with ERI_{II} (Regression: HA: $\beta 1 \neq 0$, $\alpha = 0.05$).

Specific Aim 2: Predict Attachment Densities and Attachment Strength of Cells of the Diatoms *Navicula incerta* and *Seminavis robusta* to Engineered Microtopographies

The attachment model was hypothesized to predict the initial attachment densities of cells of the diatoms *Navicula* and *Seminavis* to engineered microtopographies (Long,

et al. 2010). The normalized, transformed attachment densities were hypothesized to have a negative correlation with ERI_{II} (Regression: HA: $\beta 1 \neq 0$, $\alpha = 0.05$).

Substrates for antifouling applications were also exposed to shear stress to test fouling-release after initial attachment. Attachment Point Theory states that the retention of cells by surface microtopographies provides protection from shear stresses in the surrounding environment. Organisms that are provided with larger numbers of points of contact to the surface will therefore have increased attachment strength (Verran and Boyd 2001, Scardino et al. 2006). The attachment strength of cells of both diatoms to engineered microtopographies was hypothesized to correlate with the number of attachment points available to the cell on each surface. The attachment densities of cells after exposure to shear stress were hypothesized to have a negative correlation with the number of attachment points (Regression: HA: $\beta 1 \neq 0$, $\alpha = 0.05$).

Specific Aim 3: Determine the Contribution of Surface Chemistry to the Slope of the Attachment Model using Functionalized Poly(ethylene glycol) Dimethacrylate Hydrogels

Surfaces coated with poly(ethylene glycol) (PEG) and its oligomers exhibit resistance to protein adsorption and biofouling (Ostuni et al. 2001, Balamurugan et al. 2005, Ekblad et al. 2008, Schilp, et al. 2009). It was hypothesized that initial attachment of *Ulva, Navicula* and *C. marina* would be lower on functionalized PEG-dimethacrylate (PEGDMA) hydrogels than on PDMSe and that cell and spore densities remaining on hydrogels after exposure to shear stress would be lower than those on PDMSe. It was also hypothesized that the negative correlation of the normalized, transformed attachment density of spores of *Ulva* on functionalized hydrogels with the attachment model (Long, et al. 2010) (Regression: HA: $\beta 1 \neq 0$, $\alpha = 0.05$) would have a slope and intercept lower than those for the correlation with attachment densities on PDMSe.

Specific Aim 4: Identify a Combination of Surface Chemistry and Topography that Enhances the Attachment of Human Coronary Artery Endothelial Cells or Human Coronary Artery Smooth Muscle Cells

The clinical application of synthetic small-diameter (d<6mm) vascular grafts has been limited due to high rates of occlusion from thrombosis and intimal hyperplasia. Intimal hyperplasia can be caused by compliance mismatch between the graft and the vessel wall and poor re-endothelialization of the luminal surface. Capturing endothelial progenitor cells (EPCs) and inducing their differentiation into the endothelial cell (EC) phenotype could be the ideal way to re-endothelialize a small-diameter vascular graft (Asahara et al. 1997). Substratum elasticity can direct stem cell differentiation into specific lineages (Engler, et al. 2006). Therefore, PEGDMA hydrogels which have a highly adjustable shear modulus (Pfister et al. 2007) (G=10k Pa to 1 Mpa) were chosen as a substratum material. This combination of adjustable elasticity, surface chemistry and topography has the potential to promote the capture and differentiation of EPCs into a confluent EC monolayer that is non-thrombogenic and stable to shear stress. Such capture and differentiation would make small diameter artificial vascular grafts feasible. It was hypothesized that PEGDMA-co-glycidyl methacrylate (GMA)-graft-fibronectin (Fn) hydrogels would increase EC attachment 2-fold versus PEGDMA hydrogels (Markway et al. 2008). The effects of topography, i.e., cell elongation or cell phenotype were hypothesized to increase with increasing ERI_{II} value (Schumacher, et al. 2007b, Long, et al. 2010) (Regression: HA: $\beta 1 \neq 0$, $\alpha = 0.05$).

CHAPTER 2
BACKGROUND

The chemistry and physical properties of a substratum are critical in directing cell attachment and function. Control of bioadhesion is vital in both the marine environment and in the creation of biomaterials for cell culture substrates. Several reviews have been written describing the effects of surface chemistry (Marmur 2006), topography (Verran and Boyd 2001) and combinations of the two (Abarzua and Jakubowski 1995, Yebra et al. 2004, Genzer and Efimenko 2006, Ralston and Swain 2009, Magin et al. 2010a) on the attachment of marine fouling cells and organisms. Likewise, biomaterials are designed with a focus on the influence of chemistry (Hoffman 2002, Stegemann et al. 2007, de Mel et al. 2008) and topography (Dalby et al. 2002, Lim and Donahue 2007, Moon et al. 2009, Liliensiek et al. 2010) on cell attachment and function.

The energy required to wet (or dewet) a surface controls bioadhesion. Topographical modification of a surface is a parameter that controls the wetting (or dewetting) of a surface (Bico et al. 1999, Bico et al. 2002, Quere 2008). The contact angle of a liquid drop on a flat, homogeneous solid is given by Young's equation:

$$cos\theta = \frac{\gamma_{SV} - \gamma_{SL}}{\gamma} \quad (2\text{-}1)$$

The different surface tensions, solid/vapor, solid/liquid and liquid/vapor are given by γ_{SV}, γ_{SL} and γ, respectively. Wettability of a topographically modified surface can be described by two different models. Wenzel proposed the first model in 1936 (Wenzel 1936)

$$cos\theta^* = rcos\theta \quad (2\text{-}2)$$

where θ is Young's angle given in Equation 2-1 and r is the solid roughness. The solid roughness (r) is defined as the ratio between the actual surface area and the projected surface area (Bico, et al. 1999). A drop will spread on a rough surface until it reaches an equilibrium characterized by a contact angle θ^*, which is not the same as the Young's angle. Wenzel's model assumes that the topography becomes fully wetted and that the change in contact angle is due to the increased wetted surface area. Wenzel's Equation (2-2) shows that the effect of surface topography is to amplify wetting, since r > 1 in all cases, i.e., a hydrophilic surface is more easily wetted and hydrophobic surface is less easily wetted.

Cassie and Baxter proposed a second model for the wetting of rough surfaces while investigating waxy surfaces which were not only rough, but also porous (Cassie and Baxter 1944). Under these conditions water drops did not simply follow the contours of the topography as described by Wenzel. Instead, two wetting regimes were described: air entrapment and wicking. When air was entrapped within the features of the topography, drops rested on a composite of the surface and entrapped air. In the case of wicking, the liquid was drawn into the topography at the advancing edge so that the drop rested on a combination of the surface and liquid. The Cassie-Baxter wetting model is described by the following equations:

Air entrapment:

$$cos\theta^* = -1 + \varphi_s(cos\theta + 1) \quad (2\text{-}3)$$

Wicking:

$$cos\theta^* = 1 - \varphi_s + \varphi_s(cos\theta) \quad (2\text{-}4)$$

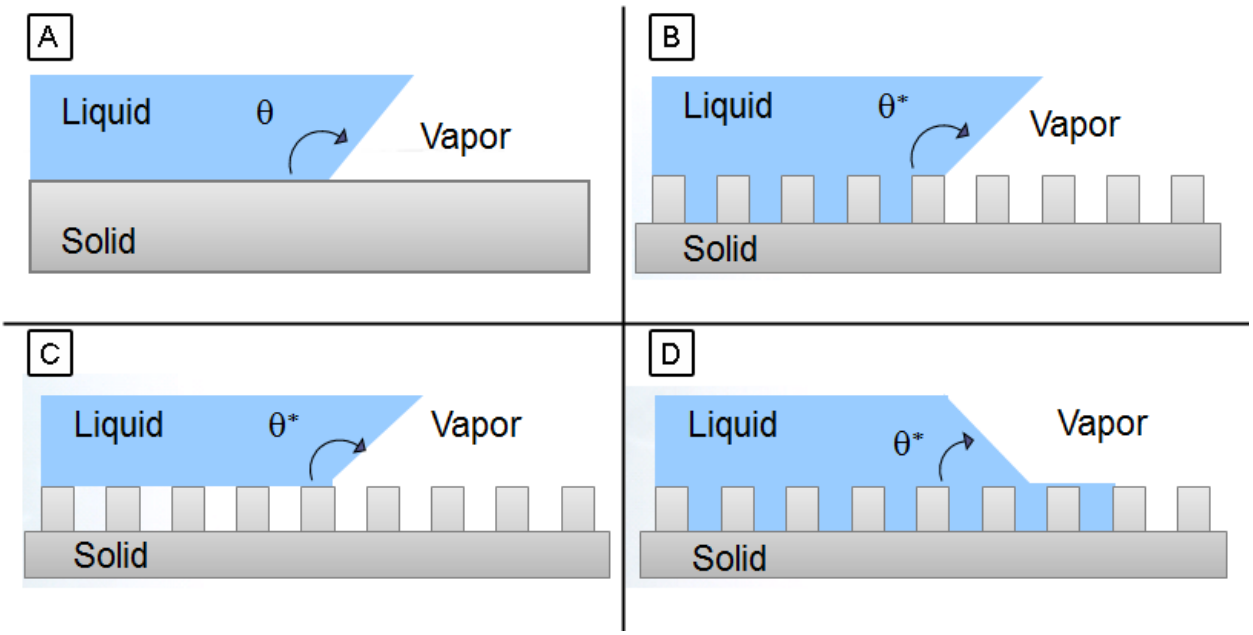

Figure 2-1. Schematic of various wetting models: A) Young's Model, B) Wenzel's Model, C) Cassie-Baxter Model – Air Entrapment and D) Cassie-Baxter Model – Wicking.

Topographically modified surfaces have also been tested in the biomedical field. The adhesion and spreading of mammalian cells (Hatcher et al. 2002, Carman et al. 2006) was changed by topographical modification. The attachment and biofilm formation of the of the bacteria *Staphyloccocus aureus* (Chung et al. 2007b) has been also been inhibited using topography.

Hatcher and Seegert (Hatcher, et al. 2002) demonstrated that scaffolds of various porosities made from polyvinylpyrrolidone modified bioactive glass fibers could increase proliferation of rat mesenchymal stem cells preceding differentiation. More recently, a pattern of 3 μm-diameter circles of the ECM protein fibronectin on PDMSe was used to direct formation of focal adhesions and grow an EC monolayer with density and morphology similar to that of the native artery (Feinberg et al. 2009). Additionally, topographical cues were used to induce EC morphologies *in vitro* that were stable to the shear stresses that would be experienced *in vivo* (Carman 2007). Several of the

topographies investigated in this work are shown in the schematic below (Figure 2-2). Surfaces are designated by a nomenclature that includes feature orientation, feature height, surface design, feature width, feature spacing and the number of distinct features. All feature dimensions are reported in µm. The Sharklet AF™ surface in Figure 2-2 Part A would be designated as +3SK2x2_n4. The channels surface in Figure 2-2 Part D would be designated +3CH2x2.

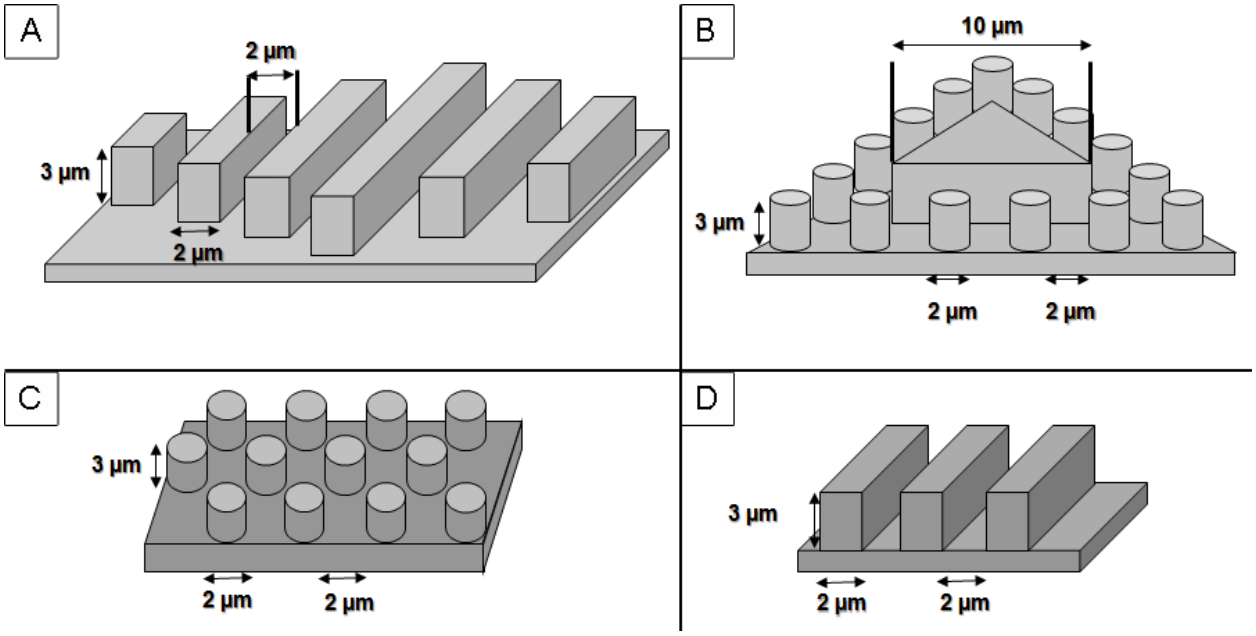

Figure 2-2. Schematic of various surface topographies and the associated dimensions. A) Sharklet AF™ (+3SK2x2), B) Triangle/Pillars (+3T10P2x2), C) Pillars (+3P2x2) and D) Channels (+3SK2x2). Adapted from an image created by Christopher J. Long.

In the current work, a model that relates surface energy and topography to cell response is used to control bioadhesion and cell function in both marine antifouling and biomedical applications.

Non-toxic Antifouling Strategies[1]

Introduction

Biofouling of marine vessels continues to plague sailors as it has for thousands of years (Wahl 1989, Callow and Callow 2002a, Yebra et al. 2004b, Chambers et al. 2006, Genzer and Efimenko 2006b, Grozea and Walker 2009a, Ralston and Swain 2009). The ancient Phoenicians, inventors of the earliest recorded anti-fouling coatings, covered ships with lead sheets (Yebra, et al. 2004b). Later in the 17th century metals containing copper were also shown to be effective biofouling deterrents. Metals, such as lead, are effective antifouling agents, but have a negative impact on the environment. Ships are still slowed today by the growth of algae, barnacles, and slime on their hulls due to the absence of a universal, green, antifouling system (Figure 2-1). The United States (US) Naval Sea Systems Command estimates that biofouling on ship hulls results in a speed loss of approximately 2 percent and increases fuel costs 6 to 45 percent depending on the size of the ship (Ingle 2008). One source cites total costs associated with biofouling of nearly $1 billion annually (Callow and Callow 2002b).

Antifouling, in this review, refers to all systems that prevent an organism from attaching to a surface. Historically, the term antifouling was associated only with biocidal compounds. Current antifouling strategies focus on green, non-toxic technologies. Fouling-release describes the force required to remove an organism that is already attached to a surface. These two terms have been used interchangeably in the literature; however they are truly different phenomena.

[1] Reprinted with permission from Elsevier from Magin CM, Cooper SP and Brennan AB. 2010a. Non-Toxic Antifouling Strategies. Materials Today. 13(4):36-44.

Figure 2-3. Macrofouling on the hull of a ship increases drag and fuel consumption. Image courtesy of North Florida Shipyards, Jacksonville FL. [Reprinted with permission from Magin CM, Cooper SP and Brennan AB. 2010a. Non-Toxic Antifouling Strategies. Materials Today. 13(4):36-44 (Page 37, Figure 1)].

Antifouling paints have been and remain the primary strategy for combating biofouling in the marine industry. Biocides such as tributyltin (TBT) were developed in the middle of the 20th century and were the active components of antifouling paints until recently (Yebra, et al. 2004b). Biocidal paints based on TBT have been effective at reducing biofouling (Yebra et al. 2004a, Chambers, et al. 2006, Howell and Behrends 2006). However, the use of TBT-based paints has been prohibited because they are detrimental to non-target organisms and the surrounding environment (Sonak et al. 2008). The response to this ban has been the use of copper, zinc, and a variety of organic compounds as the active, antifouling components. The ideal replacement for TBT is an environmentally neutral coating with both antifouling and fouling-release

properties (Goupil et al. 1973, Yebra, et al. 2004a, Genzer and Efimenko 2006a, Marmur 2006).

Biofouling is a major challenge for the biomedical industry as well. Healthcare associated-infections are attributed to biofilms on surfaces such as countertops, doors, beds, surgical tools, or medical devices such as catheters. The Centers for Disease Control and Prevention have reported that these healthcare-associated infections account for an estimated 1.7 million infections and 99,000 deaths annually in the US (Klevens et al. 2002). Furthermore, these infections accounted for nearly $45 billion of patient costs in 2007 (Scott 2009). The formation of an atherosclerotic plaque within the arterial wall can be broadly described as a biofouling process (Libby and Theroux 2005). The American Heart Association reported that 16.8 million people in the US were diagnosed with coronary heart disease in 2006. Coronary heart disease is the leading cause of death in the US. The estimated direct and indirect costs of treating this disease total approximately $165.4 billion per year (Heart Disease & Stroke Statistics 2010).

Biofouling is a very dynamic process, which spans numerous length and time scales (Figures 2-2 and 2-3). Fouling of a new surface is typically described as a four phase process: formation of a conditioning layer of organic molecules, primary colonization by micro-organisms such as bacteria and diatoms, unicellular colonization by algal spores, and attachment of multicellular macrofoulers (Wahl 1989, Abarzua and Jakubowski 1995, Chambers, et al. 2006).

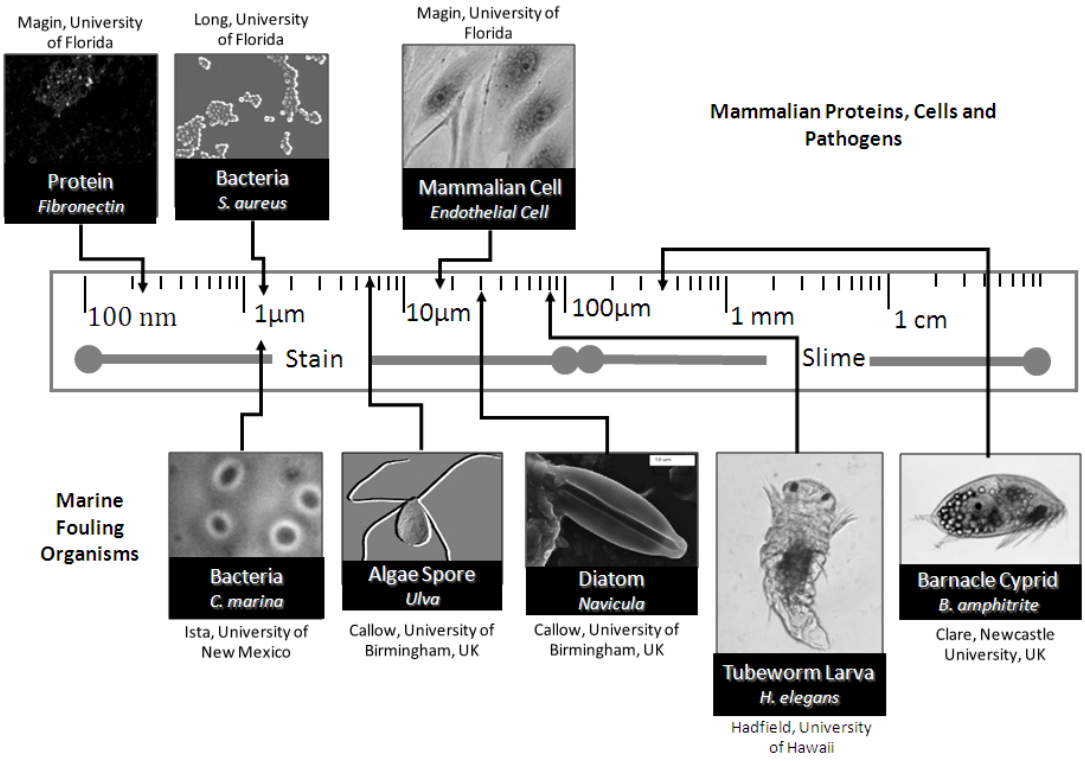

Figure 2-4. Schematic demonstrating the hierarchy of fouling organisms. Cells and compounds relevant to biomedical applications are shown above the scale axis. Marine organisms are shown below the scale. [Reprinted with permission from Magin CM, Cooper SP and Brennan AB. 2010a. Non-Toxic Antifouling Strategies. Materials Today. 13(4):36-44 (Page 37, Figure 2)]

Since fouling occurs in an aqueous solution, the properties of the fluid mediate the interaction of the fouling organism and material. Ions and water molecules adsorb to a biomaterial surface to form an electric double layer immediately upon immersion. This electric double layer effectively establishes the charge associated with surface. This electrostatic charge affects the nature of the interaction of proteins and cells with the surface. Antifouling performance scales with both density and sign of the charge (Ostuni et al. 2001a).

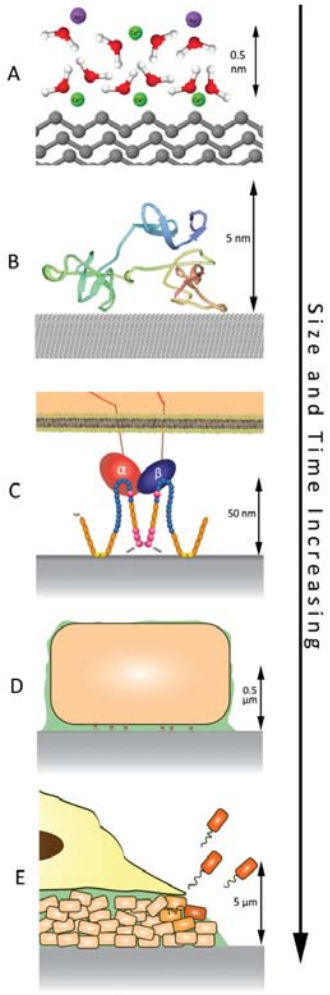

Figure 2-5. Schematic of the dynamic biofouling process which takes place over numerous length scales. (a) An electric double layer is established at the surface of a solid such as a linear polymer in less than a second. This electric double layer mediates the adsorption and conformation of proteins. (b) The type-II subunits of fibronectin are shown adsorbed to the surface. These subunits are responsible for binding to gelatin (Pickford et al. 2001). (c) Fibronectin mediates the binding of a cell to the surface via integrins (shown as α and β subunits) in the cell membrane. The type II domains of fibronectin are shown in yellow. (d) If a bacterial cell is bound to the surface, it undergoes a phenotypic change and excretes an EPS coating. (e) Over time, the cells replicate and continue to build the EPS. The biofilm creates "swarmer" cells, which leave the biofilm to inoculate another surface. Larger cells such as *Ulva* (in the marine environment) or phagocytes (in the human body) may subsequently interact with the initial biofilm. Figure created by co-author Scott P. Cooper. [Reprinted with permission from Magin CM, Cooper SP and Brennan AB. 2010a. Non-Toxic Antifouling Strategies. Materials Today. 13(4):36-44 (Page 38, Figure 3)]

A layer of proteins adsorbs to a pristine surface within seconds to minutes following immersion (Vroman et al. 1982). The protein conformation is strongly influenced by both the physical and chemical structure, including electrostatic charge, of the surface. Protein conformation defines functionality with respect to cell adhesion (Williams et al. 1982, Bergkvist et al. 2003). This protein layer acts as a conditioning film for the settlement of micro-organisms such as diatoms and bacteria.

A biofilm can be defined as a community of attached micro-organisms connected by an extracellular polysaccharide (EPS) coating. Bacteria undergo multiple developmental stages from planktonic to attached cells. This transformation from the planktonic to attached state induces a phenotypic change that facilitates increased secretion of an EPS coating (Stewart and Franklin 2008). The EPS coating is both an adhesive and protective layer that modulates the diffusion of molecules in the biofilm. Consequently, cells in biofilms are more resistant to antibiotics and antibacterial agents (Costerton et al. 1987). Natural biofilms are composed of several microbial species and their EPS coatings. These cells along with protein and enzyme structures form complex, functional micro-colonies. It was first observed by Zobell and Allen in 1935 that biofilms could stimulate the settlement of secondary macro-organisms (Zobell and Allen 1935) such as algal spores (Joint et al. 2002, Patel et al. 2003, Marshall et al. 2006) and larvae of barnacles and tubeworms (Hadfield and Paul 2001, Zardus et al. 2008). Reviews on the subject indicate that marine biofilms can also inhibit or have no effect at all on settlement of macro-organisms (Qian et al. 2007, Dobretsov 2008). The interaction between a marine biofilm and secondary colonizers is a complex interplay of surface chemistry, micro-topography, and microbial products i.e., low molecular weight

metabolites involved in quorum sensing (Qian, et al. 2007).The diversity of species resulting from various geographic locations creates a broad spectrum of physical, chemical and biological attributes. We have investigated natural structures that are able to resist the adhesion of these complex fouling communities. This review discusses natural surfaces as well as physicochemical and physical antifouling strategies.

Natural Antifouling Surfaces

There are natural surfaces that resist biofouling in the marine and the biomedical environments. These natural antifouling surfaces appear to use a combination of chemical and physical structures to inhibit biofouling. Marine organisms such as sharks, mussels, and crabs have natural antifouling defenses. The endothelium of a healthy artery is another example of a natural antifouling system (Figure 2-4). However, it is also recognized that these surfaces will lose their antifouling characteristics due to age, injury or disease.

The skin of the approximately 900 species of Elasmobranchii, which include sharks, skates, and rays is embedded with placoid scales (Bone and Moore 1995). These scales have a vascular core of dentine surrounded by an acellular “enamel” layer similar to human teeth. For this reason, placoid scales are commonly referred to as dermal denticles. Denticles serve several functions including reduction of mechanical abrasion, reduced hydrodynamic drag (Lang et al. 2008) and most interestingly protection from ectoparasites (Raschi and Tabit 1992). The skin of two members of the porpoise family, i.e., the bottlenose dolphin *Tursiops truncatus* and the killer whale *Orcinus orca*, forms a system of ridges and grooves oriented transversely to the direction of flow. The natural wavelength of the ridges and grooves is 0.3 to 0.4 mm with a trough to crest wave height of about 10 µm (Gucinski et al. 1984). These

topographic features and a mucosal coating secreted by epidermal cells contribute to the antifouling properties of these marine animals.

The microtopographically structured periostraca on shells of the blue mussels *Mytilus galloprovincialis* (Scardino et al. 2002) and *Mytilus edulis* (Bers and Wahl 2004) are also effective antifouling surfaces. The grooves and ridges of the periostraca are 1 to 2µm wide with an average depth of 1.5 µm. The shells of *M. galloprovincialis* significantly reduced settlement of barnacle larvae during a 14 week field exposure trial (Scardino, et al. 2002). Microtopography replicates cast in epoxy resin from the blue mussel *M. edulis*, edible crabs *Cancer pagurus*, the egg-case of the lesser-spotted dogfish *Scyliorhinus canicula*, and the brittle star *Ophiura texturata* reduced fouling for three to four weeks (Bers and Wahl 2004). The short-term performance implies that natural antifouling is a combination of chemistry and microtopography.

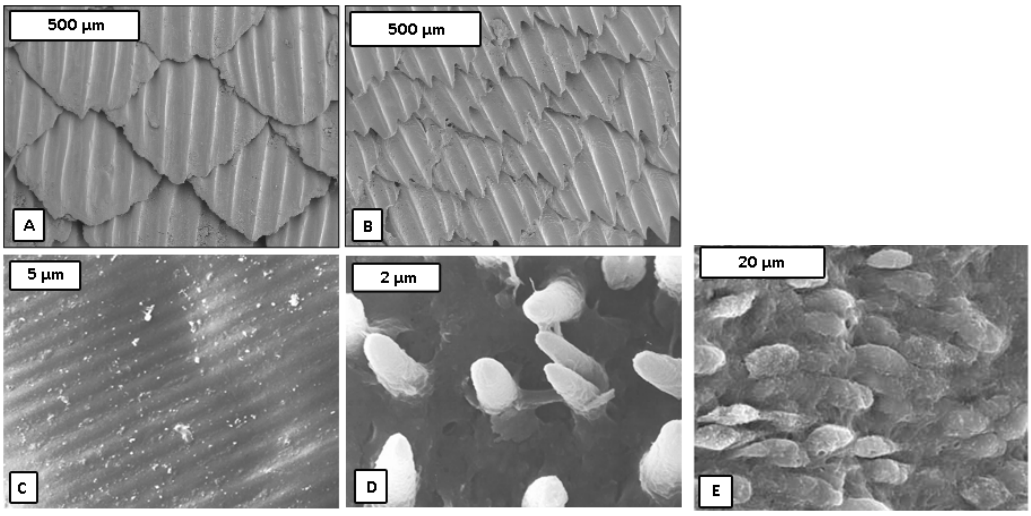

Figure 2-6. Scanning electron micrographs of natural textured surfaces: a) Spinner shark skin, b) Galapagos shark skin, c) Mussel shell (*M. edulis*) and d) Crab shell (*C. pagurus*) reprinted from (Bers and Wahl 2004) with permission from the publisher Taylor & Francis Group (http://www.informaworld.com), e) Porcine pulmonary artery reprinted from (Feinberg, et al. 2009) with permission from Elsevier. [Reprinted with permission from Magin CM, Cooper SP and Brennan AB. 2010a. Non-Toxic Antifouling Strategies. Materials Today. 13(4):36-44 (Page 39, Figure 4)]

The inner surface of a blood vessel is another natural surface that resists the constant presence of fouling proteins and cells. The endothelium consists of a continuous monolayer of endothelial cells with a cobblestone-like morphology and a distinct topography (Figure 2-4). Endothelial cells express a negatively charged glycoprotein coat that repels platelets and leukocytes. These cells also secrete bioactive substances that inhibit thrombosis and smooth muscle cell proliferation (Biology of the Arterial Wall 1999, Xue and Greisler 2000). This combination of chemistry and microtopography creates an ideal anti-thrombogenic, i.e., antifouling, surface.

Physicochemical Antifouling Strategies

Surface chemistry is a significant factor in the formation, stability and release of adhesion by fouling organisms to surfaces. The work by Baier in the late 1960s demonstrated a correlation between relative adhesion of fouling organisms and the energy of the surface (Baier 2006). The Baier curve (Figure 2-5), as this relationship is known, has been confirmed in several marine and biomedical environments (Goupil, et al. 1973, Baier 2006). A key characteristic of the Baier curve is that minimal fouling is typically achieved at a critical surface tension of 22-24 mN/m. This surface tension, often referred to as surface energy, is approximately equal to the dispersive component for water. In an aqueous system, water must rewet the system when proteins and cells are removed. For solids with a surface energy of ~22 mN/m, the thermodynamic “cost” for water to re-wet the surface is minimized.

One way of systematically varying surface energy without altering the bulk material is through self-assembled monolayer (SAMs). In an extensive study, Whitesides and co-workers tested the ability of a wide range of SAM chemistries to resist protein adsorption.

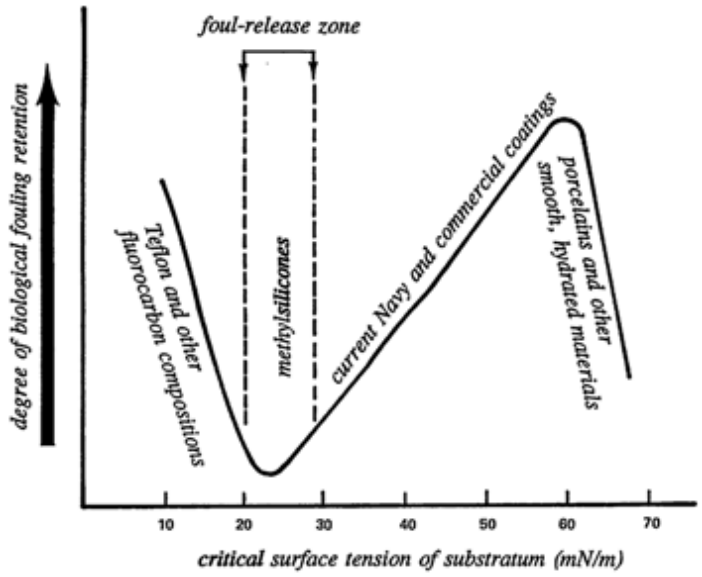

Figure 2-7. The Baier curve demonstrates the relative amount of biofouling versus critical surface tension of the substrate. Reprinted from (Baier 2006) with kind permission from Springer Science + Business Media. [Reprinted with permission from Magin CM, Cooper SP and Brennan AB. 2010a. Non-Toxic Antifouling Strategies. Materials Today. 13(4):36-44 (Page 40, Figure 5)]

The authors conclude that SAMs, which are hydrophilic, electrically neutral, and contain hydrogen bond acceptors, are most effective at resisting protein adhesion. Zwitterionic structures have both positive and negative domains, but remain electrically neutral overall. It has been demonstrated that zwitterionic compounds similar to phosphorylcholine such as sulfobetaine resisted protein adsorption when the surface density and chain length of the SAMS were carefully controlled (Ostuni et al. 2001b, Chang et al. 2008).

Even though surface energies for poly(ethylene glycol)(PEG) and its oligomers typically fall above the zone of low cell adhesion defined by Baier, it is widely recognized that these materials exhibit resistance to protein adsorption and biofouling (Ostuni, et al. 2001b, Balamurugan et al. 2005, Schilp et al. 2007, Ekblad et al. 2008). The mechanism for protein resistance for high molecular weight PEG is well explained

by steric repulsion (Jeon et al. 1991). Andrade and de Gennes postulated that during protein adsorption water must be removed from the PEG structure. This dehydration is thermodynamically unfavorable because it leads to confinement of polymer chains which previously had high conformational entropy. Even though the model system of oligo(ethylene glycol) SAMs tested by Whitesides restricted conformational freedom of end groups into densely packed films, these surfaces also showed protein repellent properties. Grunze and others have proposed that the chain conformation and packing of SAMs affect the penetration of water into the SAM surface and are also important determinants of resistance to protein adsorption (Herrwerth et al. 2003, Balamurugan, et al. 2005).

The surface chemistry of SAMs is strongly influenced by their physical structure. Ethylene-glycol terminated SAMs have been shown to be especially fouling-resistant in numerous studies. *Ulva* zoospore attachment to SAMs systematically increased with decreasing wettability and correlated with adsorption of the protein fibrinogen (Schilp, et al. 2007). Experiments have shown that higher numbers of *Ulva* spores attach to hydrophobic SAMs versus hydrophilic ones in static assays (Callow et al. 2000). However, the attachment strength of *Ulva* spores is greater on hydrophilic SAMs (Finlay et al. 2002). The mechanism for delay of *Ulva* attachment by PEG-based surfaces is not fully understood. However, like resistance to protein adsorption, infiltration of water into the SAM surfaces may create a hydration energy that prevents effective interaction of the adhesive used by *Ulva* with the surface (Schilp, et al. 2007).

Bowen, et al. tested the effect of SAM chain length on the settlement and release of zoospores of *Ulva* and cells of the diatom *Navicula incerta*. This study showed that

chain length affected release more than settlement. Alkane chains greater than 12 carbons long corresponded to higher release of these organisms under flow. This fouling-release behavior is associated with greater rigidity of the alkane chain and subsequently higher lubricity (Bowen et al. 2007).

Attachment of a medically relevant bacterium (*Staphylococcus epidermidis*) and a marine bacterium (*Cobetia marina*) was reduced up to 99.7% by surfaces coated with hexa(ethylene glycol)-terminated SAMs(Ista et al. 1996). The response of *C. marina* to surface energy was opposite of that predicted by the Baier curve, i.e., attachment density increased with decreasing surface energy. Attachment of *Ulva* showed the same relationship only when the cosine of the advancing water contact angle was greater than zero ($\cos\theta_{AW} \geq 0$) (Ista et al. 2004).

Hydrogels – crosslinked polymer networks that swell in the presence of water – have also been investigated for antifouling applications. Rasmussen et al. demonstrated that hydrogel surfaces of alginate, chitosan, and polyvinyl alcohol substituted with stilbazolium groups (PVA-SbQ) inhibited settlement of *Balanus amphitrite* (Rasmussen et al. 2002). This group also showed that the PVA-SbQ surface inhibited adhesion of the marine bacterium *Pseudomonas* sp. NCIMB2021 (Rasmussen and Ostgaard 2003). Hydrogels based on 2-hydroxyethyl methacrylate (HEMA) reduced fouling in two algal colonization bioassays and with the addition of benzalkonium chloride remained visually clean in field testing for up to 12 weeks (Cowling et al. 2000). Crosslinked poly(ethylene glycol) diacrylate surfaces were evaluated as fouling-resistant membrane coatings. Surfaces that were more hydrophilic based on contact angle measurements exhibited less protein adsorption (Ju et al.

2009). The antifouling character of these surfaces is representative of high surface energy regime of the Baier curve.

Amphiphilic surfaces and heterogenous surfaces formed by patterning or mixing chemistries are other examples of nontoxic polymer coating designs that have shown antifouling properties (Grozea and Walker 2009b). Self-assembled and nano-structured polymer thin films were also reviewed in the context of antifouling (Krishnan et al. 2008). Another class of chemical deterrents to biofouling includes naturally occurring biomolecules. For instance, it has been proposed that enzymes could break down the EPS of attached cells (Dobretsov et al. 2007, Olsen et al. 2007) or catalyze the production of repellent compounds (Kristensen et al. 2008, McMaster et al. 2009). However, it remains difficult to identify a single enzyme which is effective universally. Numerous chemicals have been isolated from natural sources and several reviews discuss specific strategies in detail (Pawlik 1992, Clare 1996, Rittschof 2000, Fusetani 2004). Dalsin, et al. (Dalsin and Messersmith 2005) have provided an extensive review of bioinspired polymers. These chemistries attempt to mimic the complex biopolymers which naturally resist fouling, such as the adhesive pad of the mussel.

It is clear that protein adsorption and subsequent biofouling are strongly influenced by surface chemistry. Correlations have been observed between protein adsorption and biofouling in both the marine and biomedical environments. Resistance to protein adsorption could be used as an inexpensive way to screen new materials for antifouling properties. A single chemistry has not yet emerged as a universal antifouling strategy. However, a variety of surface chemistries have shown promise as fouling-release

coatings. A combination of chemical and physical antifouling strategies is therefore necessary to produce an optimal coating.

Physical Antifouling Strategies

It has been recognized that cells respond to substratum topography since 1914 when Harrison observed that fibroblasts found in the embryonic nervous tissue of frogs elongated when cultured on spider silk (Harrison 1914). This phenomenon was later termed “contact guidance” by Paul Weiss after obtaining similar results when growing nerve cells on glass fibers (Weiss 1945). Recently, techniques developed in the microelectronics industry, such as photolithography and electron beam lithography, have been used by several research groups including our own to create molds for producing micro- and nano-scaled topographies with various shapes and spatial arrangements (Curtis and Wilkinson 1998, van Kooten and von Recum 1999, Carman et al. 2006). Microtopography, in the marine environment, has been shown to deter biofouling on mollusk shells (Scardino, et al. 2002, Bers and Wahl 2004) and affect attachment of barnacles (Berntsson et al. 2000, Schumacher et al. 2007a) and bacteria (Scheuerman et al. 1998).

Nearly eight years ago our group designed engineered microtopographies composed of pillars or ridges with various heights (5 or 1.5µm) and spacings (5 or 20 µm) using photolithographic techniques. These particular patterns were found to systematically enhance settlement of the spores of *Ulva* when created in poly(dimethyl siloxane) elastomer (PDMSe) (Callow et al. 2002). The addition of silicone oils to the PDMSe reduced overall *Ulva* settlement, but did not decrease settlement on microtopographies compared to smooth control surfaces (Feinberg et al. 2003, Hoipemeier-Wilson et al. 2004). Carman et al. demonstrated in 2006 that a bio-inspired

surface, Sharklet AF™ (Figure 2-5), reduced *Ulva* settlement by 86% compared to smooth when feature width and spacing were 2µm (Carman, et al. 2006). These dimensions are smaller than the average diameter of the spore body of Ulva (~5µm). These experiments implied that the width and spacing of topographical features necessary to deter biofouling must be tailored to the size of the organism.

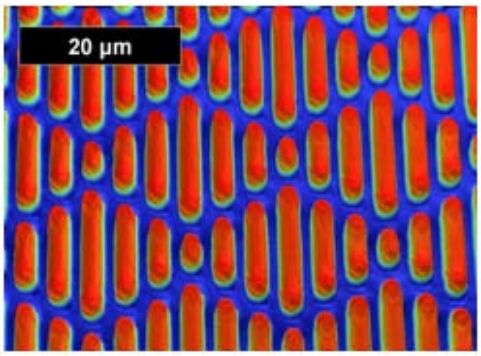

Figure 2-8. White light optical profilometry image of Sharklet AF™. [Reprinted with permission from Magin CM, Cooper SP and Brennan AB. 2010a. Non-Toxic Antifouling Strategies. Materials Today. 13(4):36-44 (Page 41, Figure 6)]

Contact guidance was observed for endothelial cells cultured on ridges, pillars, and Sharklet AF™ topographies (Feinberg, et al. 2003, Carman, et al. 2006). Additionally, Feinberg (Feinberg 2004) demonstrated that a pattern of 3µm diameter circles of the ECM protein fibronectin on PDMSe could be used to direct formation of focal adhesions and grow an endothelial cell monolayer with density and morphology similar to that of the native artery (Feinberg et al. 2009). Hatcher and Seegert (Hatcher et al. 2002) showed that scaffolds of various porosities made from polyvinylpyrrolidone modified bioactive glass fibers could increase proliferation of rat mesenchymal stem cells preceding differentiation. Chung and others demonstrated that the Sharklet AF™ topography inhibited biofilm formation of *Staphylococcus aureus* over a period of 21 days (Chung et al. 2007).

The change in wettability of a surface due to microtopographical roughness is also likely to be a contributing factor to antifouling properties. The topic of wetting and dewetting on rough surfaces has been thoroughly reviewed by Quéré and colleagues (Bico et al. 1999, Bico et al. 2002, Quere 2008). The application of surface roughness to alter wettability for antifouling coatings especially superhydrophobic coatings has also been reviewed extensively (Genzer and Efimenko 2006a, Howell and Behrends 2006, Marmur 2006). Long and others reported recently that seven different engineered microtopographies exhibited contact angle anisotropy between contact angles measured parallel and perpendicular to the features (Long et al. 2009). This work demonstrates the importance of anisotropy in the design and study of antifouling surfaces.

An engineered roughness index was developed that demonstrated a negative correlation between the settlement behavior of the zoospore of *Ulva* with wettability of engineered microtopographies (Figure 2-6). The original ERI empirically ratios the product of Wenzel's roughness factor (Wenzel 1936) (r) and the degrees of freedom of the pattern (*df*) to the depressed surface area fraction (1- Φ_s) (Schumacher et al. 2007b). Bico, Quéré, and others (Bico, et al. 1999, Bico, et al. 2002, Quere 2008) described the surface solid fraction (1- Φ_s) as the ratio of the depressed surface area between features and the projected planar surface area. The surface solid fraction is equivalent to 1-f_1, the solid-liquid interface term of the Cassie-Baxter equation for wetting (Cassie and Baxter 1944).

A biological attachment model based on a modified ERI was recently proposed by Long et al (Long, et al. 2010). In this model the ERI was changed by replacing the

degrees of freedom (*df*) of the pattern with the number of distinct features in the pattern (n).

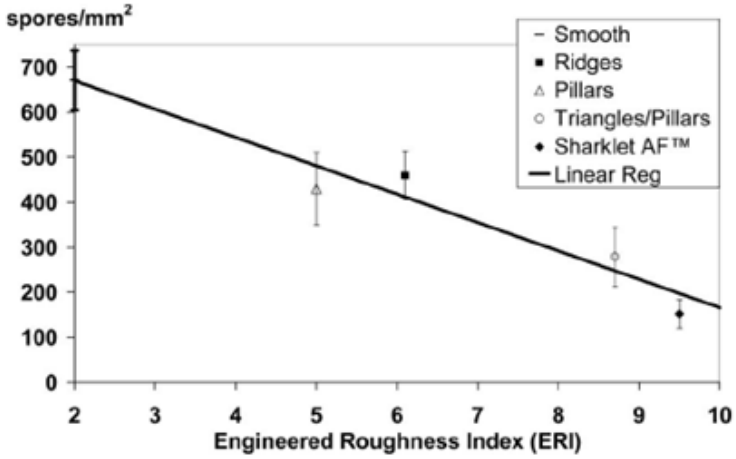

Figure 2-9. Correlation of Ulva spore settlement density and Engineered Roughness Index (ERI). The calculated ERI for the tested PDMSe surfaces is plotted against the experimental mean spore density (spores/mm2)+SE (n=3). Reprinted from (Schumacher, et al. 2007b) with permission from the publisher Taylor & Francis Group (http://www.informaworld.com). [Reprinted with permission from Magin CM, Cooper SP and Brennan AB. 2010a. Non-Toxic Antifouling Strategies. Materials Today. 13(4):36-44 (Page 42, Figure 7)]

The number of attached organisms per area was normalized to the number of organisms attached to a smooth control. The data were transformed by taking the natural logarithm (Equation 2-1).

$$\ln\left(\frac{A}{A_{SM}}\right) = m^* \frac{r^* n}{1-\varphi_s} - b \qquad (2\text{-}1)$$

This transformation unified the data from numerous experiments onto a single plot. The attachment density of spores of *Ulva* for all of the experiments showed a high statistical correlation (R^2=0.88) to the attachment model. The attachment model also correctly predicted a further reduction of *Ulva* attachment on a newly designed topography with a higher ERI value (Long, et al. 2010). This relationship can be used to create new engineered microtopographies that further reduce *Ulva* attachment.

The elastic modulus of a substratum is another physical factor that has been shown to influence bioadhesion. The adhesion strength of a disc to an elastomeric substrate was proposed by Kendall (Kendall 1971) as:

$$P = \frac{F_c}{\pi a^2} = \left(\frac{8\pi\gamma E\, a^3}{(1-\nu^2)}\right)^{1/2} \quad (2\text{-}2)$$

in which P = critical stress for removing the disc, F_c = critical force, a = radius of the disc, γ = interfacial energy between the disc and substrate, E = elastic modulus of the substrate, and v is Poisson's ratio. A similar analysis by Brady demonstrated a correlation between elastic modulus and surface energy of a material (Kendall 1971, Brady 1999). Vascular graft research has shown that intimal hyperplasia can be caused by compliance mismatch between the graft and the vessel wall and poor re-endothelialization of the luminal surface (Tai et al. 2000). It has also been reported that substratum elasticity directs stem cell differentiation into specific lineages (Engler et al. 2006). Likewise, in the area of marine biofouling it has been proposed that the release behavior of pseudobarnacles and spores from various coatings is inversely proportional to the pull-off stress and scales with elastic modulus ($E^{1/2}$) (Brady 2001, Chaudhury et al. 2005).

The importance of hydrodynamics to the fouling process cannot be overlooked. Work by Crisp in 1955 showed that there is a critical velocity gradient at the surface for barnacle cyprids to attach (Crisp 1955). A critical observation by Purcell (Purcell 1977) states that our physical intuition of swimming does not apply to microorganisms. Bacteria and cells swim in an environment of very low Reynolds number (*E. coli*, Re~10^{-5}). As a result, these organisms live in a world where viscous forces dominate over inertial forces. It has been demonstrated both empirically and experimentally that *E. coli*

is attracted to the walls of a container purely by hydrodynamic interactions (Berke et al. 2008, Lauga and Powers 2009). This hydrodynamic attraction is similar to other phenomena described by Vogel (Vogel 1994). For instance, if two spheres fall next to each other in a fluid, they are attracted to each other by viscous forces. These hydrodynamic interactions may initiate the settlement process by allowing the organism to "find" the surface.

One approach to create new antifouling surfaces may be to utilize the concept of fluid slip. Fluid slip is the boundary condition in which the fluid has a finite velocity at an interface (Granick et al. 2003). This is in contrast to the "no slip" boundary condition which is commonly assumed in fluid mechanics. The no slip boundary condition is relevant to a fluids moving over air, which occurs in the case of superhydrophobic materials in the "non-wetted" or Cassie-Baxter state (Ybert et al. 2007, Voronov et al. 2008, Lee and Kim 2009). It may be possible to prevent hydrodynamic attraction of swimming organisms through the use of fluid slip.

Fluid hydrodynamics also contributes to the antifouling character of biological tissues. In the case of vascular implants, thrombus formation is a common problem. Thrombogenesis follows a typical biofouling cascade in which proteins that are present in blood adsorb to the surface, followed by platelets and red blood cells. Therefore, a healthy endothelium requires a constant supply of both thrombogenic and anti-coagulant factors. These factors are maintained by fluid flow through the blood vessel (Edmunds 1996). Fluid shear affects platelet and red blood cell physiology and subsequent thrombus formation (Spijker et al. 2003). The disruption of native fluid flow in a vessel – either by injury or placement of an implant – influences the balance of

these thrombogenic factors. Therefore, fluid flow plays an integral role in the fouling process.

Conclusion

Biofouling is a dynamic process which spans numerous length scales and involves a complex variety of molecules and organisms. Antifouling strategies, therefore, must include both chemical and physical concepts. Nature provides examples of antifouling and fouling-release surfaces that emphasize the importance of these factors. Physical cues, such as surface roughness and fluid hydrodynamics, can act singularly or in concert with surface chemistry to enhance or inhibit the attachment of organisms to a surface. Chemical cues, especially surface energy, influence not only the ability of an organism to initially attach to a surface, but also the degree of fouling-release from the surface once adhesion has been established. At this point, no single technology has been demonstrated universally effective at either antifouling or fouling-release. The environmental impacts of biofouling demonstrate the need to continue the development of strategies that are truly non-toxic and broadly effective. Confronting the complexity of biofouling requires the cooperative effort of industry and academia in all disciplines of science and engineering.

Influence of Surface Chemistry and Topography on Cell Culture

Contact Guidance

The first evidence of contact guidance was reported nearly a century ago when it was observed that fibroblasts found in the embryonic nervous tissue of frogs elongated when cultured on spider silk (Harrison 1914, Weiss 1945). Recently, techniques such as photolithography and electron beam lithography have been used by several research groups to create molds for producing micro- and nano-scaled topographies with various

shapes and spatial arrangements (Curtis and Wilkinson 1998, van Kooten and von Recum 1999, Carman, et al. 2006). Even though these patterning techniques are now well-established, very little is known about the mechanisms underlying cell sensing and response to topographies. It is clear that by altering substratum topography, it is possible to change cell morphology. In recent studies cellular micro-environments have been shown to direct cell function, (Dalby 2005, Bettinger et al. 2009, Moon, et al. 2009, Schulte et al. 2009, Liliensiek, et al. 2010) and topography has been used to direct differentiation of stem or progenitor cells into a specific lineage (Engler, et al. 2006, Chai and Leong 2007, Saha et al. 2007, Reilly and Engler 2010). In 2007 it was demonstrated that topography could enhance differentiation of human mesenchymal stem cells into the neuronal lineage (Yim et al. 2007). The aim of the current research was to create a cell culture substrate for small-diameter vascular graft applications that uses a combination of surface chemistry and microtopography to re-endothelialize *in situ* through the capture and differentiation of circulating EPCs into the EC phenotype.

Medical and Economic Impact of Controlling Cell Adhesion

Coronary heart disease is the leading cause of death in the United States (U.S). According to the latest mortality data, nearly 2,300 Americans die from cardiovascular disease every day, an average of one death every 38 seconds (Heart Disease & Stroke Statistics 2010). Coronary heart disease is a result of atherosclerosis, the narrowing and hardening of artery walls due to a buildup of fatty substances including cholesterol in the arteries that supply blood to the heart muscle. This buildup can disrupt or even block the blood flow and oxygen supply to the heart ultimately resulting in acute myocardial infarction (heart attack).

Angioplasty and stenting have been used to increase lumen size and restore blood flow in small-diameter vessels such as the coronary arteries when heart attack is imminent or has already occurred, but not without complications. In-stent restenosis – renarrowing of the blood vessels – occurs within 6 months in 50% of patients that undergo stenting (Padera and Schoen 2004). For this reason, the most common way to treat coronary blockages is to create new passages for blood flow by grafting. Since there are currently no FDA approved small-diameter vascular grafts, autogenous veins or arteries are typically used to reroute blood flow around the blocked arteries (Heart Disease & Stroke Statistics 2010). The patient's internal mammary artery or saphenous vein are the most common grafts; however, damage to the native vasculature or a previous grafting procedure may make bypass surgery impossible, especially for procedures that require multiple grafts. Even when healthy autogenous vessels are available, it is less desirable to remove them from their positions than it would be to insert a prosthetic graft (Nerem and Seliktar 2001).

In 2006, approximately 448,000 inpatient bypass procedures were performed. The American Heart Association estimates that the total cost direct and indirect of coronary heart disease in 2010 was $177.1 billion (Heart Disease & Stroke Statistics 2010). As the average age and longevity of the U.S. population increases, these figures will certainly increase and the need for new small-diameter grafting techniques that have patency rates comparable to those of autogenous grafts will become more urgent.

Summary

Physicochemical cues presented by a surface influence bioadhesion and cellular function in both marine antifouling applications and mammalian cell culture substrates. The effects of engineered microtopographies and specifically designed surface

chemistries on cell attachment and function are investigated in this work. The findings are applied to two different applications: marine antifouling and direction of mammalian cell function. Various combinations of surface topography and chemistry were evaluated for the deterrence of fouling cells and organisms in the marine environment and as substrates for mammalian cell culture. A model is presented that relates the surface energy of a substratum and the size and motility of an organism to the attachment density of a variety of marine fouling organisms. Surface chemistries and topographies that direct the elongation and orientation of human vascular cells are also presented.

CHAPTER 3
ENGINEERED ANTIFOULING MICROTOPOGRAPHIES: THE ROLE OF REYNOLDS NUMBER IN A MODEL THAT PREDICTS ATTACHMENT OF ZOOSPORES OF *ULVA* AND CELLS OF *COBETIA MARINA*[2]

Introduction

Biofouling, the undesired accumulation of organic molecules, living organisms, and the metabolites of these organisms on a surface (Costerton et al. 1995, Shea et al. 1995, O'Toole et al. 2000), is a significant environmental concern with consequences beyond barnacles and bivalves. Biofouling increases drag on vessels by increasing hull roughness, which leads to higher fuel consumption and cost (Townsin 2003, Schultz 2007). The United States (US) Naval Sea Systems Command estimates that fuel costs increase 6 to 45 percent if the hull is fouled, depending on the size of the vessel. Slime layers composed of bacteria and diatoms that develop in the early stages of biofouling (Molino, Campbell et al. 2009, Molino, Childs et al. 2009) have been shown to significantly increase hydrodynamic drag and increase fuel consumption (Schultz 2007). Increased fossil fuel consumption is not the only environmental concern raised by biofouling. Hull fouling has been shown to be a primary cause for the introduction and spread of non-indigenous marine species (Otani et al. 2007, Pettengill et al. 2007, Piola and Johnston 2008, Yamaguchi et al. 2009). The ideal solution to the detrimental effects of biofouling will be a green technology possessing both antifouling and fouling-release properties (Genzer and Efimenko 2006, Marmur 2006) to reduce drag and fuel consumption while remaining non-toxic.

[2] Reprinted with permission from the publisher Taylor & Francis Group (http://www.informaworld.com) from Magin CM, Long CJ, Cooper SP, Ista LK, Lopez GP and Brennan AB. 2010b. Engineered Antifouling Microtopographies: The role of Reynolds number in a model that predicts attachment of zoospores of Ulva and cells of Cobetia marina. Biofouling. 26(6):719-727.

Polydimethylsiloxane elastomers (PDMSe), more commonly known as silicones, are currently marketed as non-toxic marine coatings. These coatings are known to have fouling-release properties (Chaudhury et al. 2005, Holm et al. 2006, Wendt et al. 2006) due to their low surface energy and low modulus (Brady and Singer 2000, Chaudhury, et al. 2005); however, they are not inherently antifouling (Molino, Campbell, et al. 2009, Molino, Childs, et al. 2009). Non-toxic antifouling technologies that focus on the manipulation of surface topography in PDMSe have been designed to deter attachment of fouling organisms (Carman et al. 2006, Schumacher, Aldred et al. 2007, Schumacher, Carman et al. 2007, Schumacher et al. 2008, Long et al. 2010). Carman et al. presented a biomimetically inspired surface topography, Sharklet AF™ that reduced attachment of *Ulva* zoospores by 86% (Carman, et al. 2006). *Ulva* is a common green alga commonly found in marine biofilms found on ships, submarines, and other underwater structures. The *Ulva* plant produces motile spores that disperse and colonize surrounding surfaces (Callow and Callow 2000). Evidence suggests that the swimming spores are able to select a surface suitable for attachment based on topographical, biological (Joint et al. 2002), chemical, and physicochemical cues (Ederth et al. 2009, Schilp et al. 2009). A recent report proposes that the flagellar motion of a swimming unicellular alga, *Chlamydomonas*, is coupled to its hydrodynamic environment (Polin et al. 2009). An empirical relationship called the Engineered Roughness Index (ERI) has been proposed to quantify topographical “roughness” based on parameters that describe surface energy. Results have demonstrated a correlation between the attachment behavior of *Ulva* zoospores and ERI (Schumacher, et al. 2007). A predictive attachment model was developed based on the second-

generation ERI (ERI_{II}) and correctly predicted spore density on three newly designed surface topographies. Four separate *Ulva* attachment data sets showed excellent correlation (R^2=0.88) with the attachment model (Long, et al. 2010).

The ERI is a dimensionless ratio based on Wenzel's roughness factor (r), the depressed surface area fraction (1- Φ_s), and originally the degrees of freedom of the pattern (*df*) (Schumacher, et al. 2007). Recently, the ERI was extended to include additional topographical designs (Long, et al. 2010). The *df* term was replaced with n, which is the number of unique features in each topography. The ridges topography is comprised of one distinct feature thus an n-value of one. The triangle/pillars topography is composed of two unique features: an equilateral triangle and a round pillar (n=2). ERI_{II} is represented as

$$ERI_{II} = (r * n)/(1 - \Phi s) \quad (3\text{-}1)$$

Wenzel's roughness factor (r) is the ratio of the actual surface area to the projected planar surface area (Wenzel 1936). The actual surface area includes the surface area of the feature tops, sides, and depressed surface area between features. The depressed surface fraction (1- Φ_s) described by Bico, Quéré, and others (Bico et al. 1999, Bico et al. 2002, Quere 2008) is the ratio of the depressed surface area between features and the projected planar surface area. The depressed surface fraction is equivalent to 1-f_1, where f_1 is the solid-liquid interface term of the Cassie-Baxter equation for wetting (Cassie and Baxter 1944). The topographies studied were selected to cover a range of ERI_{II} values (Figure 3-1).

In this study it was hypothesized that marine bacteria attachment and biofilm formation would be inhibited by engineered microtopographies in PDMSe and this

inhibition would scale with the ERI_{II} value. *Cobetia marina*, originally isolated from a marine biofilm (Baumann et al. 1983), was used as a model marine fouling organism.

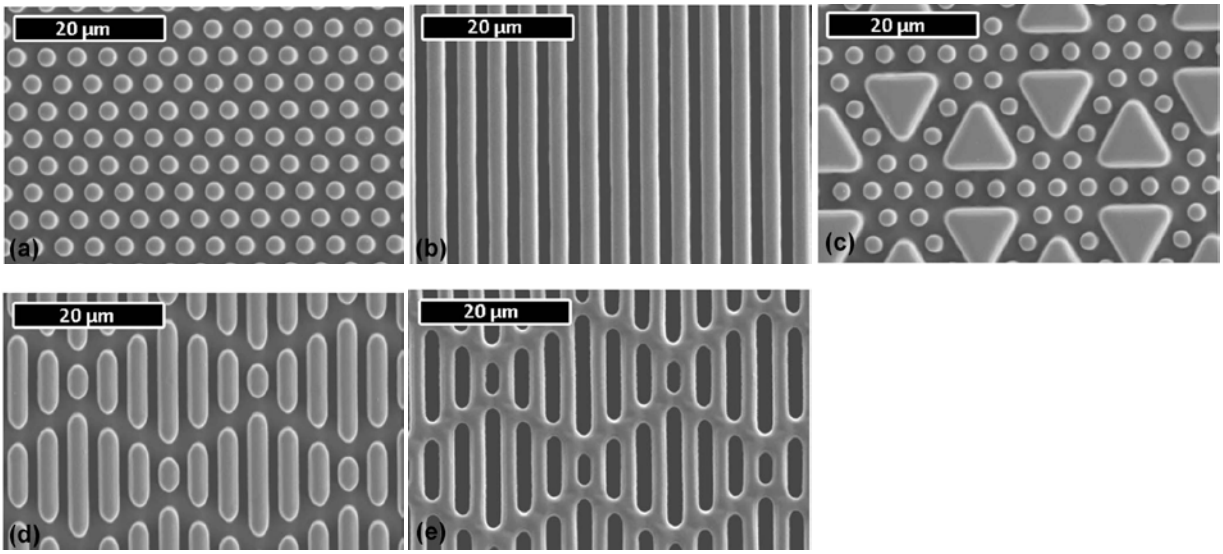

Figure 3-1. Scanning electron micrographs of (a) pillars, (b) ridges, (c) triangle/pillars, (d) Sharklet AF™, (e) Recessed Sharklet AF™ surfaces in PDMSe. The topographies of the Sharklet AF™ and the ridges were positioned so that the features were parallel to the direction of flow when mounted in the flow cell. [Reprinted with permission from Magin CM, Long CJ, Cooper SP, Ista LK, Lopez GP and Brennan AB. 2010b. Engineered Antifouling Microtopographies: The role of Reynolds number in a model that predicts attachment of zoospores of *Ulva* and cells of *Cobetia marina*. Biofouling. 26(6):719-727 (Page 720, Figure 1)].

C. marina attachment to defined solid surfaces has been studied extensively through the use of self-assembled monolayers (SAMs) (Ista et al. 1996, Ista et al. 1999, Ista et al. 2004, Ista et al. 2010) and has been reported to influence secondary colonization (Shea, et al. 1995). The present report shows the correlation between ERI_{II} value and attachment of the marine bacterium *C. marina*. Additionally, a single equation is presented that relates attachment densities of *Ulva* and *C. marina* to the ERI multiplied by the estimated Reynolds number for the individual organisms.

Materials and Methods

Materials

The base material used for engineered topographical modification was a platinum-catalysed polydimethysiloxane elastomer (PDMSe), Silastic® T-2 (Dow Corning Corporation). The elastomer was prepared by hand mixing ten parts resin and one part curing agent by weight for 5 min. The mixture was degassed under vacuum (28-30 in. Hg) for 30 min, removed from the vacuum chamber, and poured into negative topographical molds to cure for 24 h at ~22°C.

Pattern Designs

The patterns studied included Sharklet AF™, recessed Sharklet AF™, ridges, pillars, and triangle/pillars (Schumacher, et al. 2007). Sharklet AF™ previously described (Carman, et al. 2006, Schumacher, et al. 2007) consists of 2 µm wide ribs of various lengths (4, 8, 12, and 16 µm) that are combined by feature length in the following order: 4, 8, 12, 16, 12, 8, and 4 µm at a feature spacing of 2 µm to form a diamond. This diamond of protruding features was the repeat unit for the arrayed pattern. The spacing between each diamond unit was 2 µm. This pattern was inspired by and is similar to the skin of a shark (Bechert et al. 2000) in terms of feature arrangement. Recessed Sharklet AF™ is the negative of Sharklet AF™. It has the same arrangement of features indented into the surface instead of protruding out from the surface. Ridges and pillars were designed with an analogous feature spacing of 2 µm. Ridges were continuous in length and separated by 2 µm. The pillars were hexagonally packed so the distance between any two adjacent pillars was 2 µm. The triangle/pillars pattern is a multi-feature pattern formed by replacing a set of six hexagonally packed 2 µm pillars with a 10 µm equilateral triangle. This triangle

placement maintained a 2 µm feature spacing between the edges of the triangle and the pillars.

Pattern Fabrication

Pattern designs were transferred to photoresist-coated silicon wafers using standard photolithographic techniques described previously (Schumacher, et al. 2008). The patterned wafers were deep reactive ion etched using the Bosch process to a depth of approximately 3 µm to create negative molds of the engineered topographies. Wafers were subsequently stripped of photoresist with an O_2 plasma etch. Hexamethyldisilazane was vapor deposited onto the processed wafers to methylate the surfaces and prevent adhesion of PDMSe during the replication process.

Topographical Replication

Engineered topographies were transferred to PDMSe by replication of the patterned and etched silicon wafer. The resulting engineered topographies contained features that protrude from the surface at a height of approximately 3 µm. Pattern fidelity and feature height were evaluated with light and scanning electron microscopy.

Sample Preparation

Samples were provided as smooth PDMSe surrounding two 13 mm x 13 mm squares of engineered topographies of interest adhered to glass coverslips (60 mm x 24 mm, No. 2 thickness). Engineered topographies were attached to glass coverslips using a two-step process previously described (Carman, et al. 2006). Topographies (smooth, Sharklet AF™, recessed Sharklet AF™, ridges, pillars, and triangles/pillars) were randomly assigned to one of two positions on each coverslip. Sharklet AF™ and ridges topographies were positioned on coverslips so that features were parallel to the direction of flow when mounted in the flow cell. The resulting coverslip was

approximately 0.8 mm thick and contained an adhered PDMSe film with two 13 mm x 13 mm square areas containing topography bordered on all sides by smooth (no topography) areas.

Bacteria

Chemostat culture

A logarithmic chemostat culture of *C. marina* ATCC 25374 (American Type Culture Collection, Manassas, VA) strain (Baumann, et al. 1983, Arahal et al. 2002) was established in modified basal medium (200 mM NaCl, 50 mM MgSO4•7H2O, 10 mM KCl, 10 mM CaCl2•2H2O, 19 mM NH4Cl, 0.33 mM K2HPO4, 0.1 mM FeSO4 •7H2O, 5 mM Tris-HCl (pH 7.5), and 2 mM glycerol) as described previously (Ista, et al. 1996). The chemostat was maintained at a flow rate of 1 ml min^{-1} with constant stirring resulting in a cellular concentration of 5 x 10^7 cells ml^{-1}.

Stationary phase culture

A stationary phase culture of *C. marina* was grown in 1 L of modified basal medium described above. The inoculated culture grew for 21 h at 25°C while shaking at 400 RPM.

***C. marina* Attachment Assay**

Two bacterial attachment assays were performed with *C. marina*, one using the chemostat culture and one the stationary phase culture described above. Samples were sterilized by immersion in ethanol for 20 min, soaked in artificial seawater for 1 h and then placed into a laminar flow cell apparatus (Ista, et al. 1996) that was mounted onto the stage of an optical microscope (Zeiss Axioscope 40). The sample coverslip forms the top plate of the flow chamber to minimize gravitational effects on attachment. The flow cell was then connected to the culture vessel through tubing and a peristaltic

pump (Ista, et al. 1996, Ista, et al. 2004). The cells were introduced into the flow cell at a rate of $2x10^{-5}$ L s^{-1} for 2 h. Under these conditions for a flat surface, the Reynolds number was ~2×10^{-3}, indicating laminar flow and the surface shear rate was $6.6x10^{2}$ s^{-1} (Ista, et al. 2004). Bacterial attachment was monitored through a camera attached to a phase contrast microscope. Ten random images were taken for each topography at 15 min intervals. Images were acquired with Axiovision software and processed with ImageJ software (Rasband 1997-2009). Each image was first converted to 8 bit format and then processed using the Fast Fourier Transform (FFT) bandpass filter associated with ImageJ to eliminate background unevenness. The cell densities were determined through direct counting using the ImageJ Cell Counter plug-in. The attached cells in 10 randomly selected fields of view were counted at each time point. The average number of cells per square millimeter (cells mm^{-2}) was calculated for each replicate. Three replicates were analyzed for each topography. The position of each topography was varied in the flow stream.

Statistical Methods

Cell counts were reported as the mean number of cells mm^{-2} from 10 counts on each of three replicate topographies (n=30) with 95% confidence intervals. The cell count data were transformed using a natural logarithm. Statistical differences between surfaces were evaluated with the transformed data using one-way analysis of variance (ANOVA) and Tukey's test for multiple comparisons.

The transformed mean number of cells mm^{-2} for each engineered topography was plotted versus time for kinetics analysis. The transformed data was also plotted against the calculated ERI_{II} to determine if any correlations existed between *C. marina*

attachment and the ERI_{II}. Regression analysis was performed to evaluate the strength of the correlation.

Results and Discussion

Only slight variations in attachment densities were measured over the entire assay period. This includes samples exposed to both logarithmic growth phase and stationary growth phase *C. marina* (Figure 3-2).

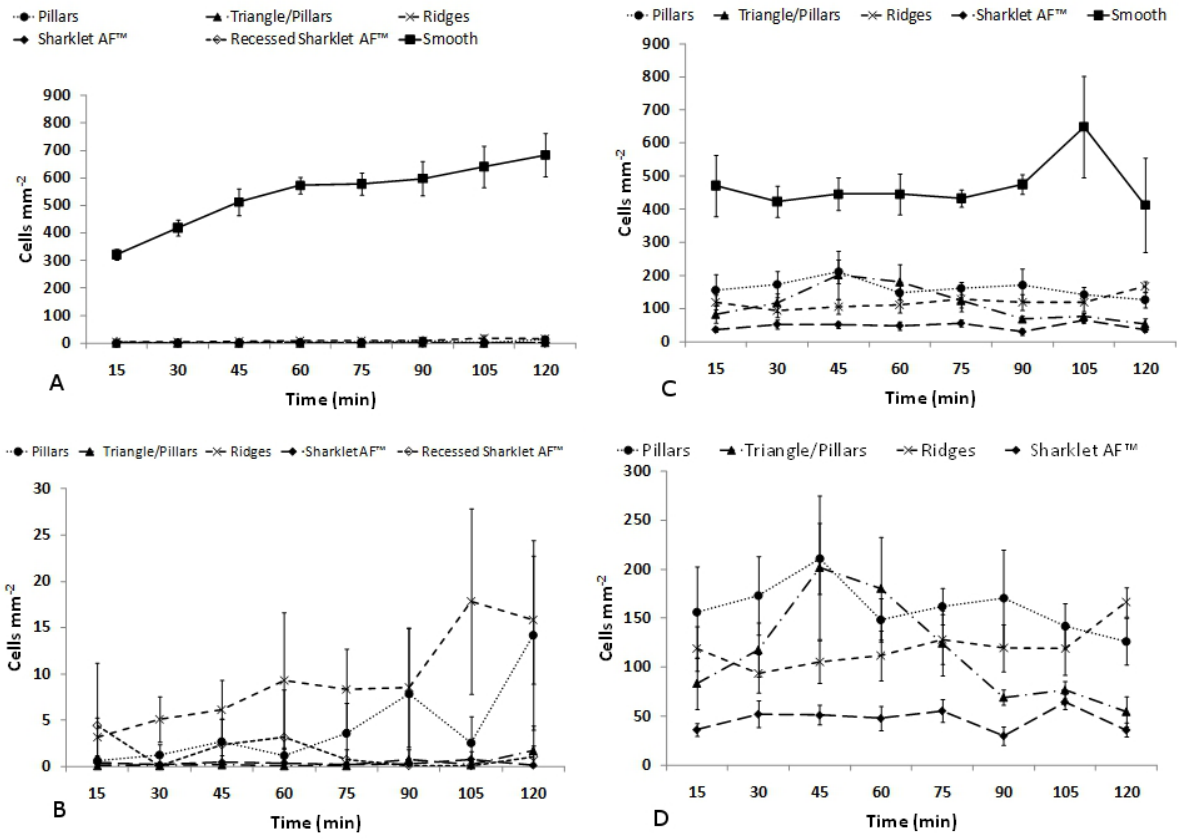

Figure 3-2. *C. marina* attachment vs time for (A) chemostat culture (logarithmic growth phase), all surfaces; (B) chemostat culture (logarithmic growth phase), topographically modified surfaces only; (C) overnight culture (stationary growth phase), all surfaces; and (D) overnight culture (stationary growth phase), topographically modified surfaces only. Error bars represent 95% confidence intervals. [Reprinted with permission from Magin CM, Long CJ, Cooper SP, Ista LK, Lopez GP and Brennan AB. 2010b. Engineered Antifouling Microtopographies: The role of Reynolds number in a model that predicts attachment of zoospores of *Ulva* and cells of *Cobetia marina*. Biofouling. 26(6):719-727 (Page 723, Figure 2)]

C. marina was calculated to attach at a mean density of 683 ± 79 cells mm^{-2} and 413 ± 51 cells mm^{-2} on the smooth PDMSe at the 120 min time point for the logarithmic growth phase and stationary growth phase, respectively. The cell density for both growth phases was reduced significantly (Figure 3-3) on all topographies relative to the smooth surface at 120 min. The logarithmic growth phase cell density was lower on the triangle/pillars (1.7 ± 2.6), Sharklet AF™ (0.1 ± 0.2), and recessed Sharklet AF™ (1.0 ± 1.2) topographies compared to cell density on pillars (14.2 ± 10.2) and ridges (15.8 ± 7). Attachment density of C. marina cells in the stationary growth phase followed the same order; i.e., lower attachment density was measured on triangle/pillars (55 ± 0.3) and Sharklet AF™ (36 ± 0.2) patterns than on pillars (126 ± 0.3) and ridges (166 ± 0.1).

Nearly all of the attached cells were singular or in small clusters. Cells appeared to attach in clusters around pillars on the pillar pattern. The majority of cells were attached within the ~2 µm wide channels of the ridge patterns. Nearly all cells settled next to the edges of the triangle or clustered around the pillars of the triangle/pillar patterns. Cells did not attach to the tops of the 10 µm triangles. Cells were attached either between the features of the Sharklet AF™ pattern or around the edges of the diamond repeat units. On the recessed Sharklet AF™ pattern cells attached within the ~2 µm wide depressions.

The feature dimensions of the topographies used in each study were measured and the average heights, widths and spacings were used to calculate the ERI_{II} value. Due to slight variations in feature height the value of the ERI_{II} for each pattern varied between the two bacterial attachment assays (Tables 3-1 and 3-2). Recessed Sharklet AF™ is a newly designed topography with a higher ERI_{II} value (24) than Sharklet AF™

that was included in the logarithmic growth phase attachment assay to further the ERI_{II} series.

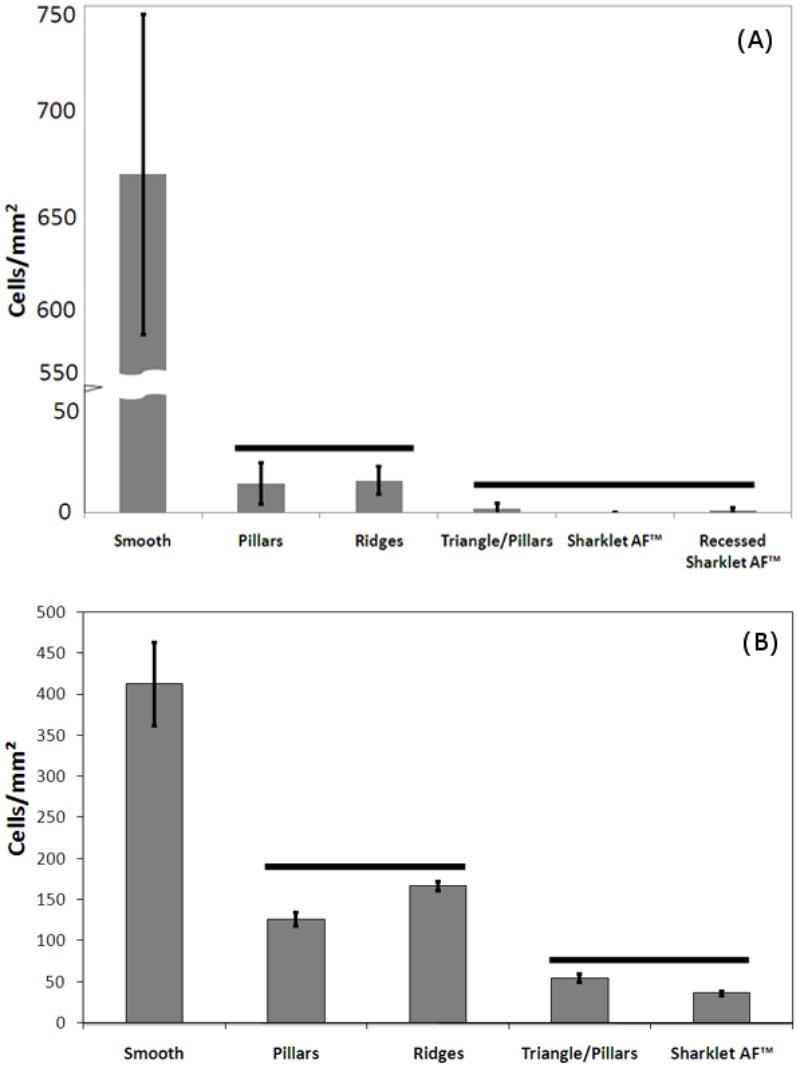

Figure 3-3. *C. marina* attachment data on PDMSe surfaces represented as mean cell density (cells-mm^{-2}) +95% confidence interval (n = 30). (A) surfaces exposed to *C. marina* cells in the logarithmic growth phase established in a chemostat culture for 120 min; (B) surfaces exposed to *C. marina* cells in the stationary growth phase established through an overnight culture for 120 min. Solid horizontal bars = statistically different groups (ANOVA p = 0.05, Tukey test p = 0.05). [Reprinted with permission from Magin CM, Long CJ, Cooper SP, Ista LK, Lopez GP and Brennan AB. 2010b. Engineered Antifouling Microtopographies: The role of Reynolds number in a model that predicts attachment of zoospores of *Ulva* and cells of *Cobetia marina*. Biofouling. 26(6):719-727 (Page 723, Figure 3)]

Table 3-1. Feature geometry and engineered roughness index calculations for topographies exposed to the chemostat culture. The Table includes the calculated values for Wenzel's roughness factor (r), the depressed surface area fraction (1-Φs) and the number of unique features in each pattern.

	Feature geometry			Engineered Roughness Index			
	Height (μm)	Width (μm)	Spacing (μm)	r	n	$1-\Phi_s$	ERI_{II} $(r \times n)/(1-\Phi_s)$
Pillars	3.2 ± 0.1	2 ± 0.1	2 ± 0.1	2.5	1	0.77	3.2
Ridges	2.6 ± 0.1	2.4 ± 0.1	1.7 ± 0.1	2.3	1	0.41	5.5
Triangles/Pillars	3.2 ± 0.1	1.9 ± 0.1, 8.0 ± 0.1	2.1 ± 0.1	2.1	2	0.74	5.8
Sharklet AF™	2.9 ± 0.1	2.3 ± 0.1	1.7 ± 0.1	2.5	4	0.52	19
Recessed Sharklet AF™	3.1 ± 0.2	2.1 ± 0.1	2.0 ± 0.1	2.5	4	0.42	24
Smooth	n/a	n/a	n/a	1	0	1	0

Table 3-2. Feature geometry and engineered roughness index calculations for topographies exposed to the overnight culture. The Table includes the calculated values for Wenzel's roughness factor (r), the depressed surface area fraction (1-Φs) and the number of unique features in each pattern.

	Feature geometry			Engineered Roughness Index			
	Height (μm)	Width (μm)	Spacing (μm)	r	n	$1-\Phi_s$	ERI_{II} $(r \times n)/(1-\Phi_s)$
Pillars	3.2 ± 0.1	2.0 ± 0.1	2.0 ± 0.1	2.5	1	0.77	3.2
Ridges	3.0 ± 0.1	2.3 ± 0.1	1.7 ± 0.1	2.5	1	0.42	5.9
Triangle/Pillars	3.2 ± 0.1	2.0 ± 0.1, 8.1 ± 0.1	2.1 ± 0.1	2.2	2	0.72	6.1
Sharklet AF™	1.8 ± 0.1	1.8 ± 0.1	2.0 ± 0.1	1.9	4	0.57	13
Smooth	n/a	n/a	n/a	1	0	1	0

The natural logarithm of the normalized mean cell density measured on each surface at 120 min was plotted against ERI_{II} of each pattern (Figure 3-4). A linear

regression model was fit to each set of data. An inverse linear relationship existed between mean cell density and ERI_{II} for bacterial attachment in both the stationary (R^2=0.78, p=0.047) and logarithmic (R^2=0.40, p=0.038) growth phases.

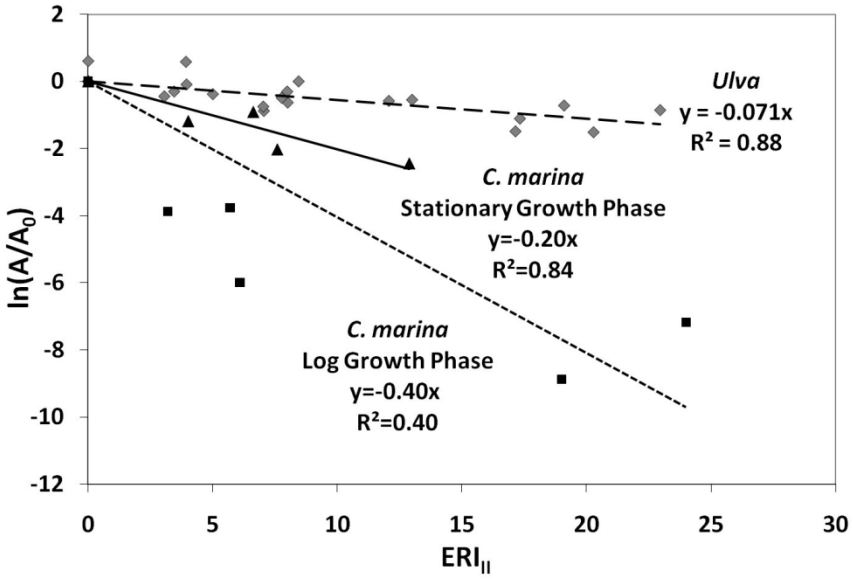

Figure 3-4. The attachment model shows the correlation between *C. marina* attachment normalized to attachment on a smooth surface and the engineered roughness index (ERI_{II}) at 120 min for the stationary and logarithmic growth phases. Plotted is the calculated ERI_{II} for each pattern tested vs the natural logarithm of the experimental mean bacterial cell density at the 120 min time point minus the mean bacterial cell density on a smooth surface at the same time point ($\ln(A/A_0)$) (n = 30). Data for attachment of zoospores of *Ulva*, taken from Long et al. (2010) are also plotted. [Reprinted with permission from Magin CM, Long CJ, Cooper SP, Ista LK, Lopez GP and Brennan AB. 2010b. Engineered Antifouling Microtopographies: The role of Reynolds number in a model that predicts attachment of zoospores of *Ulva* and cells of *Cobetia marina*. Biofouling. 26(6):719-727 (Page 724, Figure 4)]

The lowest mean cell densities for the logarithmic growth phase *C. marina* correlated with the highest ERI_{II} values, e.g. triangle/pillars (5.8), Sharklet AF™ (19), and Recessed Sharklet AF™ (24), but were not different statistically. The second lowest cell densities were measured on ridges and pillars (ERI_{II} values of 5.5 and 3.2, respectively). Cell densities measured in the stationary phase attachment assay followed a similar trend. Triangle/pillars and Sharklet AF™ with the highest ERI_{II} values

(6.1 and 13 respectively) had the lowest cell densities. Ridges and pillars had the next highest ERI_{II} values (5.9 and 3.2) and the second lowest attachment densities.

The regression analysis for the cell attachment to the surfaces established a statistically significant trend for both the logarithmic growth phase and stationary growth phase. These trends were analyzed in terms of the attachment model as Equations (3-2) and (3-3). The variable A is the attachment on a surface with a given ERI_{II} value and A_0 is the attachment on a smooth surface (ERI_{II}=0).

$$\ln\left(\frac{A}{A_0}\right) = -0.40 * ERI_{II} \quad (3\text{-}2)$$

$$\ln\left(\frac{A}{A_0}\right) = -0.20 * ERI_{II} \quad (3\text{-}3)$$

Adhesion of marine bacteria to surfaces has been attributed to many factors: substratum composition (Ista, et al. 2004, Ekblad et al. 2008), surface chemistry (Ista, et al. 1996, Ista, et al. 1999, Poolman et al. 2004, Cordiero et al. 2009), substratum mechanical properties (Ekblad, et al. 2008, Cordiero, et al. 2009), and surface roughness (Kerr and Cowling 2003). Substratum composition, substratum mechanical properties and surface chemistry were kept constant in this study by using PDMSe for all surfaces. Surface roughness was systematically studied by using the ERI_{II} algorithm to describe engineered microtopographies.

Plots of *C. marina* attachment over time indicated that bacteria in both the logarithmic and stationary growth phase reacted to surface topography nearly instantaneously (Figure 3-2). Bacterial attachment did not change significantly from the first time point (15 min) to the last (120 min). This response was due to physical, not chemical, changes in the substratum. These results are consistent with the work of Kerr

and Cowling in which the effect of surface roughness on bacterial adhesion was observed to be almost instantaneous (Kerr and Cowling 2003).

Cell densities measured at the last time point indicated that all topographies showed a statistically significant reduction in the density of attached cells in both growth phases relative to the smooth surface (Figure 3). A fairly strong inverse linear relationship existed between the natural logarithm of the mean cell density and ERI_{II} value for both bacterial attachment assays (Figure 3-4). These relationships, however, did not follow the same regression line. Attachment of *C. marina* established in a chemostat culture (logarithmic growth phase) correlated with a line with a steeper slope (m = -0.40) than the cells in the stationary growth phase (m = -0.20). The slopes of these lines were both different from the slope of the regression line for *Ulva* spore attachment versus ERI_{II} value (m = -0.071) from four separate studies reported in previous work (Long, et al. 2010).

It is possible that the slope of the line in the attachment model (m) encompasses the organism's sensitivity to a surface (Equation 3-4).

$$\ln\left(\frac{A}{A_0}\right) = m * ERI_{II} \qquad (3\text{-}4)$$

This sensitivity could be related to a number of factors including, the size and shape (Kerr and Cowling 2003, Carman, et al. 2006), motility (Shea, et al. 1995), and surface chemistry (Shea et al. 1991, Ista, et al. 2004, Poolman, et al. 2004, Cordiero, et al. 2009, Ista, et al. 2010) of the attaching organism and/or conditioning of the surface by culture medium and secreted products (Jain and Bhosle 2009). It has been observed that in the late stationary phase *C. marina* cells tend to shrink to approximately 1 µm in diameter and take on a more rounded shape. The same bacteria cells in the logarithmic

growth phase are rod-shaped, approximately 2 μm in length and often joined in pairs. This size and shape difference may influence bacterial attachment. The results from this study also showed stationary-phase cells adhered to hydrophobic topographic surfaces in higher numbers than logarithmic-phase cells. The higher densities of bacteria attached to surfaces exposed to the stationary phase culture could be due to the fact that there were simply more bacteria cells in the overnight culture than the chemostat culture. A standard overnight culture has approximately 10^9 cells mL^{-1} whereas the chemostat is maintained at approximately 10^7 cells mL^{-1}.

The Reynolds number is the ratio of inertial forces to viscous forces in fluid flow. Viscous forces dominate inertial forces in conditions such as those experienced by *C. marina* and spores of *Ulva* while moving through water (Purcell 1977, Berg 1983, Dusenbery 2009). Therefore *C. marina* and *Ulva* operate at low Reynolds number. Alternatively, the Reynolds number can be considered to represent the scale separation in the flow. That is to say the bacteria and alga spores are not large compared to the smallest scales in the flow at which viscosity dissipates kinetic energy. *Ulva* is a flagellated cell capable of propelling itself through the water. The *C. marina* in this study is not flagellated. The Reynolds numbers for the swimming *Ulva* spore and the *C. marina* in both growth phases were calculated using the following equation:

$$Re = \frac{\rho V L}{\mu} \tag{3-5}$$

where ρ and μ are the density and viscosity of the fluid used in the assay, V is the velocity of the organism relative to that of the fluid, and L is the characteristic length of the organism (see Appendix A for full calculation). The characteristic length is a dimension relevant to the geometry of the flow; in this case it is the diameter of the body

moving through the fluid. The characteristic length, i.e., the diameter of the spore body at its widest point, and velocity of the *Ulva* spore were taken to be 5 µm and 150 µm s^{-1}, respectively (Callow et al. 2002, Heydt et al. 2009). The characteristic length of *C. marina* varies with growth phase. It is 2 µm for the logarithmic growth phase and 1 µm for the stationary growth phase. The velocity of the bacteria relative to the fluid near the wall was estimated to be 20% of the average fluid velocity in the flow cell. When the bacteria enter the boundary layer near the wall, the velocity will be considerably less than the average bulk velocity due to the no-slip boundary condition. Flow velocity of the fluid, i.e., a key component of the Reynolds number, has been demonstrated to affect attachment density of *Ulva* (Granhag et al. 2007). The size and motion of the organisms were incorporated into the slope of the attachment model by multiplying the ERI_{II} value by the Reynolds number of the organism.

$$\mathrm{m} = m'Re \tag{3-6}$$

$$\ln\left(\frac{A}{A_0}\right) = -(m'Re) * ERI_{II} \tag{3-7}$$

The incorporation of the Reynolds number into the attachment model allowed four separate *Ulva* attachment assays (Schumacher, et al. 2007, Schumacher, et al. 2008, Long, et al. 2010) to be combined with both *C. marina* attachment assays into a single data set that yields a regression with high correlation to ERI_{II}•Re ($R^2 = 0.77$) (Figure 3-5).

Further work is planned to investigate the role of the slope of the attachment model line as an indicator of the organism's sensitivity to a surface. This work could include attachment of different species or organisms such as new or mutant strains of bacteria to elucidate which factors contribute to the sensing of topographically modified

surfaces. It could also include altering flow conditions to change the organism's Reynolds number and investigate the role of the hydrodynamic environment on biological attachment.

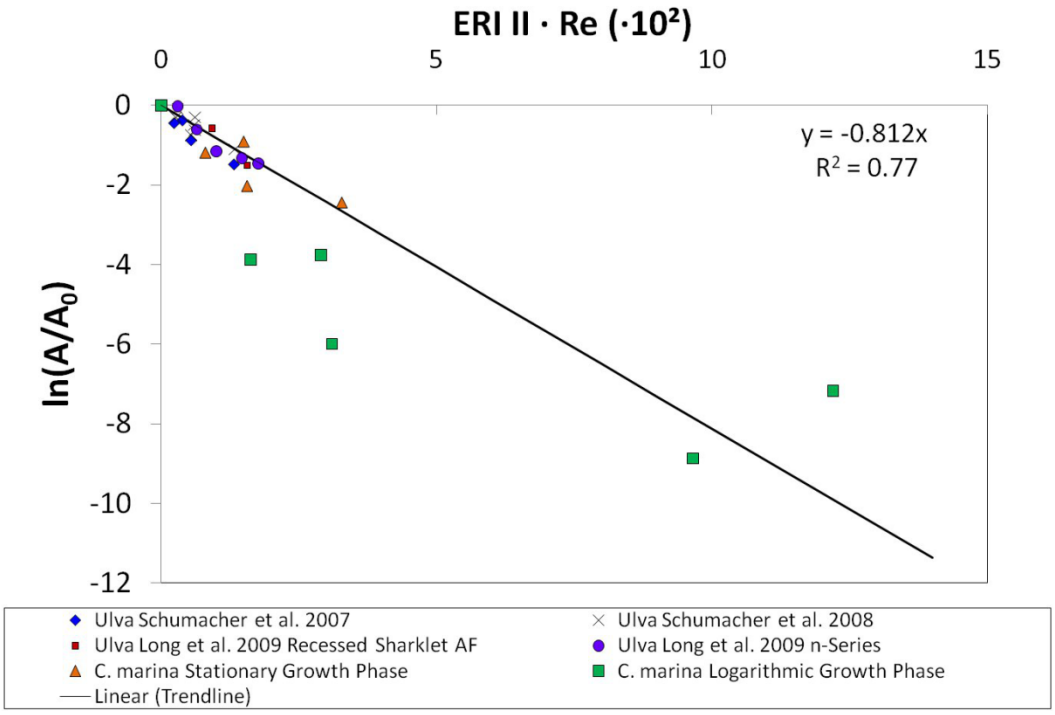

Figure 3-5. The attachment model shows the correlation between attachment of zoospores of *Ulva* and cells of *C. marina* normalized to attachment on a smooth surface and the engineered roughness index (ERI_{II}) multiplied by the Reynolds number of the organism. [Reprinted with permission from Magin CM, Long CJ, Cooper SP, Ista LK, Lopez GP and Brennan AB. 2010b. Engineered Antifouling Microtopographies: The role of Reynolds number in a model that predicts attachment of zoospores of *Ulva* and cells of *Cobetia marina*. Biofouling. 26(6):719-727 (Page 725, Figure 5)]

Microtopographies created in non-toxic materials such as PDMSe are a green alternative to biocidal methods for reducing biofouling. The attachment model has been demonstrated to correlate the ERI_{II} value multiplied by the Reynolds number for the organism to the attachment density of cells from the kingdoms bacteria and plantae. An inverse linear relationship exists between mean cell densities for the two different organisms and ERI_{II}•Re. Plots of *C. marina* attachment over time indicate that both

logarithmic-phase and stationary-phase cells reacted to surface topography within 15 min of exposure to the surface. At the 120 min time point all topographically modified surfaces showed statistically significant reduction in attachment compared to smooth for both bacterial attachment assays. The incorporation of the Reynolds number to the attachment model created a regression model with high correlation of attachment of *Ulva* and *C. marina* in both growth phases to ERI_{II}•Re.

CHAPTER 4
ENGINEERED ANTIFOULING TOPOGRAPHIES: INHIBITION OF ATTACHMENT, MOVEMENT AND BIOFILM ADHESION OF *NAVICULA INCERTA* AND *SEMINAVIS ROBUSTA*

Background

Biofouling is an environmental and economic concern. The biofouling process begins immediately upon immersion of a clean surface in seawater. Within seconds to minutes the surface becomes coated with a conditioning film. This film typically consists of glycoproteins, humic acids, proteins, carbohydrates and other macromolecules (Jain and Bhosle 2009). The nature of a conditioning film plays an important role in subsequent microbial adhesion to the surface (Bakker et al. 2004, Jain and Bhosle 2009). Diatoms are a diverse group of unicellular algae that along with bacteria form a major component of microbial slime layers (Molino and Wetherbee 2008). Raphid diatoms, in particular, are the most common early algal colonizers (Wetherbee et al. 1998). Raphid diatoms approach a surface passively through water currents or gravity and adhere to the surface through secretion of extracellular polymeric substances (EPS) (Hoagland et al. 1993, Wetherbee, et al. 1998, Chiovitti et al. 2006). The EPS facilitates a gliding motility whereby raphid diatoms can select a position more suitable for colonization (Edgar and Pickett-Heaps 1984, Wetherbee, et al. 1998, Chiovitti, et al. 2006). Diatom slimes foul surfaces in both freshwater and marine environments. Diatom biofilms of 5-10 mm in thickness developed in 6 months in the high flow conditions through canals feeding a power station increasing drag and impeding efficiency (Andrewartha et al. 2010, Perkins et al. 2010). Layers of diatoms and their byproducts have been shown to develop on both marine antifouling and fouling-release

paints (Holland et al. 2004, Molino et al. 2009a, Molino et al. 2009b) and increase hydrodynamic drag leading to an increase in fuel consumption and cost (Schultz 2007).

The attachment strength of diatoms has been shown to correlate with surface energy. Cells of the diatoms *Navicula perminuta* (Holland, et al. 2004) and *Seminavis robusta* (Thompson et al. 2008) adhered more firmly to hydrophobic silicone elastomers than to hydrophilic surfaces. On self-assembled monolayers (SAMs) the raphid diatom *Amphora* also adhered more strongly to hydrophobic than hydrophilic surfaces (Finlay et al. 2002b). Recently, the adhesion strength of *Navicula* was strongly correlated with the wettability (35-105°) and surface tension of a series of nine xerogel surfaces (Finlay et al. 2010). In studies by Scardino et al. (2006), the attachment strength of four different species of diatoms was influenced by sinusoidal ripple and peak patterns created in polyimides (Scardino, et al. 2006). Cells remained attached in higher numbers on surfaces where the numbers of attachment points were the highest. These results support the Attachment Point Theory (reviewed by (Verran and Boyd 2001), which states that cells are retained on surface microtopographies due to protection from shear stresses in the surrounding environment. Therefore, organisms provided with larger numbers of contact points by the surface, will have increased attachment strength. The Attachment Point Theory was further examined by testing attachment of the diatom *Amphora*, the green alga *Ulva rigida*, the red alga *Centroceras clavulatum*, the serpulid tubeworm *Hydroides elegans*, and the bryozoans *Bugula neritina* to microtextured polycarbonate surfaces (Scardino et al. 2008). The effect of attachment points was weak for motile microfoulers, strong for large macrofouling larvae, and non-existent for non-motile algal spores (Scardino, et al. 2008). To further investigate the

influence of surface topography, the surface parameters of 36 species of shelled marine mollusks were characterized and correlated with fouling-resistance and fouling-release. Fouling-release was shown to correlate positively with the mean waviness of the surface. Shell surfaces with the highest waviness profiles showed greater fouling-release (Scardino et al. 2009a).

Silicones, a major component in antifouling-paints, are currently marketed as a non-toxic alternative to biocidal marine coatings. Silicones exhibit fouling-release properties (Chaudhury et al. 2005, Holm et al. 2006, Wendt et al. 2006) due to their low surface energy and low modulus (Brady and Singer 2000, Chaudhury, et al. 2005). Since these materials are not inherently antifouling, i.e., do not prevent cells and larvae from attaching (Molino, et al. 2009a, Molino, et al. 2009b), engineered antifouling topographies have been created in polydimethylsiloxane elastomer (PDMSe) to deter the initial attachment of fouling organisms (Carman, et al. 2006, Schumacher et al. 2007a, Schumacher, et al. 2007b, Schumacher et al. 2008, Long, et al. 2010). A biomimetically inspired surface topography, Sharklet AF™, reduced attachment of zoospores of *Ulva* by 86% (Carman, et al. 2006) and cells of *Cobetia marina* by up to 91% compared to smooth standards (Magin et al. 2010b).

A model that predicts attachment of zoospores of the green algae *Ulva* to various surface microtopographies created in PDMSe was developed (Schumacher, et al. 2007b, Long, et al. 2010). The attachment model was extended to describe the attachment of cells of the bacteria *C. marina* to these surfaces (Magin, et al. 2010b). The current attachment model equation relates the attachment density of a spore or cell to the Engineered Roughness Index (ERI_{II}), a representation of surface energy, (Long,

et al. 2010) multiplied by the Reynolds number of the organism (Magin, et al. 2010b). It is important to consider the size and physical characteristics of diatoms when evaluating their responses to topographically modified surfaces. All diatom cells are encased by a rigid silica wall, which determines the size of topographical features that could deter settlement. The initial attachment of cells of the diatom *Navicula incerta* was reduced by approximately 35% on surfaces with 2 μm feature width and 2 μm spacing versus a smooth standard (Long 2009). These results are consistent with the findings of Scardino, et al (2008) that the size of settling propagules/larvae relative to the size of microtopographies was important in the selection of attachment sites (Scardino, et al. 2008). Cells of the diatom *Navicula* are approximately 4 μm wide by 12 μm long. Surfaces with feature widths or spacings greater than or equal to the size of the diatom cells had attachment results similar to that of a smooth surface (Long 2009). Initial attachment did not correlate with the current attachment model (Magin, et al. 2010b).

Decreased attachment density of *Navicula* on topographically modified surfaces compared to smooth and other surfaces with multiple attachment points also supported attachment point theory (Long 2009). It was hypothesized in the current work that engineered antifouling topographies would inhibit the initial attachment of *Seminavis* compared to smooth standards. Cells of the diatom *Seminavis* are larger than those of *Navicula* (approximately 6 μm wide by 30 to 50 μm long) (Thompson, et al. 2008). It was also hypothesized that diatom attachment strength would follow Attachment Point Theory, i.e., engineered antifouling topographies would reduce attachment strength of cells and biofilms of diatoms. The influence of topography on diatom gliding motion across surfaces was also observed.

Materials and Methods

Materials

The base material used for all engineered antifouling topographies was a platinum-catalysed PDMSe, Silastic® T-2 (Dow Corning Corporation). The elastomer was prepared by hand mixing ten parts by weight resin and one part curing agent by weight for 5 min. The mixture was degassed under vacuum (28-30 in. Hg) for 30 min to remove bubbles, removed from the vacuum chamber, and poured into negative topographical molds to cure for 24 h at ambient temperature (~22°C).

Pattern Designs

The patterns tested in this report included Sharklet AF™ and recessed Sharklet AF™ (Schumacher, et al. 2007b). Sharklet AF™ consists of 2 µm wide ribs of various lengths (4, 8, 12, and 16 µm) that are combined by feature length in the following order: 4, 8, 12, 16, 12, 8, and 4 µm at a feature spacing of 2 µm to form a diamond (Carman, et al. 2006, Schumacher, et al. 2007b). The spacing between each diamond repeat unit was 2 µm. This pattern was inspired by the skin of a shark (Bechert et al. 2000) and is similar to it in terms of feature arrangement. Recessed Sharklet AF™ is the negative of Sharklet AF™. The features are depressed into the surface instead of protruding from the surface. Both patterns were designed with a height of approximately 3 µm. Sharklet AF™ and Recessed Sharklet AF™ are referred to as +2.8SK2x2 and -3.1SK2x2, respectively (Figure 4-1).

Sample Preparation

Engineered antifouling topographies were transferred to PDMSe by replication of a patterned and etched silicon wafer (Schumacher, et al. 2008). Pattern fidelity and feature height were evaluated with light and scanning electron microscopy. Engineered

topographies were attached to glass slides using a two-step process previously described (Carman, et al. 2006). Smooth, Sharklet AF™ and recessed Sharklet AF™ topographies were evaluated. Samples were provided as smooth PDMSe surrounding one 25 mm x 25 mm square of engineered antifouling topography adhered to glass microscope slides (75 mm x 25 mm).

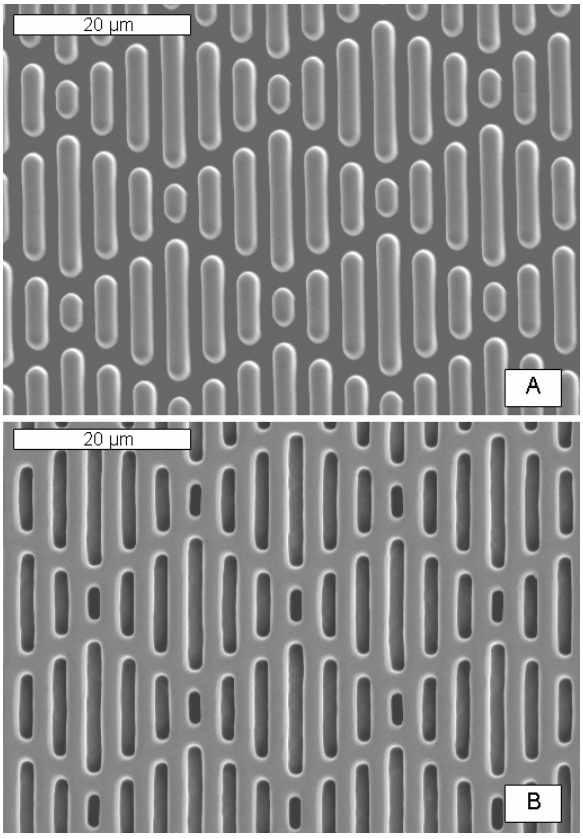

Figure 4-1. Topographies created in PDMSe A) Sharklet AF™ (+2.8SK2x2) and B) Recessed Sharklet AF™ (-3.1SK2x2).

Initial Attachment of Cells

Navicula incerta and *Seminavis robusta* cells were cultured in F/2 medium contained in 250 mL conical flasks for approximately 3 d until cells reached the logarithmic growth phase. Cells were washed 3 times in fresh medium before

harvesting and diluting to give a suspension with a chlorophyll *a* content of approximately 0.25 µg mL^{-1} (Holland, et al. 2004, Thompson, et al. 2008). Samples were placed in Quadriperm dishes to which 10 mL of a diatom suspension was added. Cells were allowed to attach on laboratory benches at ambient temperature (~20 °C) for 2 h. Samples for measuring initial attachment were exposed to a submerged wash in seawater to remove cells which had not attached. Samples were fixed in 2.5% glutaraldehyde, air dried and cell densities were counted manually on each slide using a fluorescence microscope. Counts were made for 30 fields of view (0.033 mm^2) on each sample.

Attachment Strength

Samples for attachment strength were exposed to a shear stress of 45 Pa for *Navicula* and 26 Pa for *Seminavis* in a water channel after initial attachment was established. The samples were subsequently fixed with 2.5% glutaraldehyde and air dried. The cell densities were determined, using the image analysis method described above, for cells remaining on each surface.

Assessment of Movement

Motility was assessed by examining the cells under a microscope (20 x magnification). The assessment took place after the allotted contact time with the surface, i.e. either 2 h or 6 d. Each slide was observed *in situ*, with a layer of water above it, covered by a 22 x 64 mm glass coverslip. Illumination from transmitted light stimulated movement of the diatoms. The total number of single cells (unclumped), the number orientated with the raphe-side down, and the number moving per field of view were counted after 1.5 min of illumination. Clumped diatoms were not counted in any field of view as these are less likely to be able to orientate or move than free cells.

Counts were made for 7 fields of view on each topography and the smooth standard. The counts were made in two rounds so that the observations for any single slide were not consecutive to avoid any time-dependence factors on movement. The counts on all surfaces were completed within 1.5 h after the initial settlement period.

Biofilm Growth and Attachment Strength

Samples for biofilm growth were not washed after initial attachment so that initial cell density was the same on all surfaces. The samples were placed in an illuminated incubator at 18 °C with a 16:8 light to dark cycle for 6 d. Biomass of the biofilms was quantified as autofluorescence of chlorophyll using an adapted multi-well plate reader (Tecan Genios Plus) ($430_{ex}/670_{em}$ nm). Biomass was measured before exposure to shear stress in the water channel (46 Pa) and after.

Statistical Methods

The cell or biofilm density per mm-squared was calculated for each sample and condition (n = 90 counts). Confidence intervals were calculated at 95% using either cell counts for the attachment density data or the arcsine transformed counts for proportions. The mean densities were compared using one-way analysis of variance (ANOVA) and Tukey's test for multiple comparisons.

Results

Seminavis Initial Attachment and Attachment Strength

Diatom cells, unlike *Ulva* spores, are not motile in the water column. Cells move in the water by gravity and water currents so at the end of a 2 h incubation period, the cell density will be nearly constant for all test surfaces. Therefore, differences in initial cell density were quantified following a gentle underwater washing. There was no

significant difference in initial attachment density of *Seminavis* between the smooth surface and -3.1SK2x2 or between +2.8SK2x2 and -3.1SK2x2 (Figure 4-2).

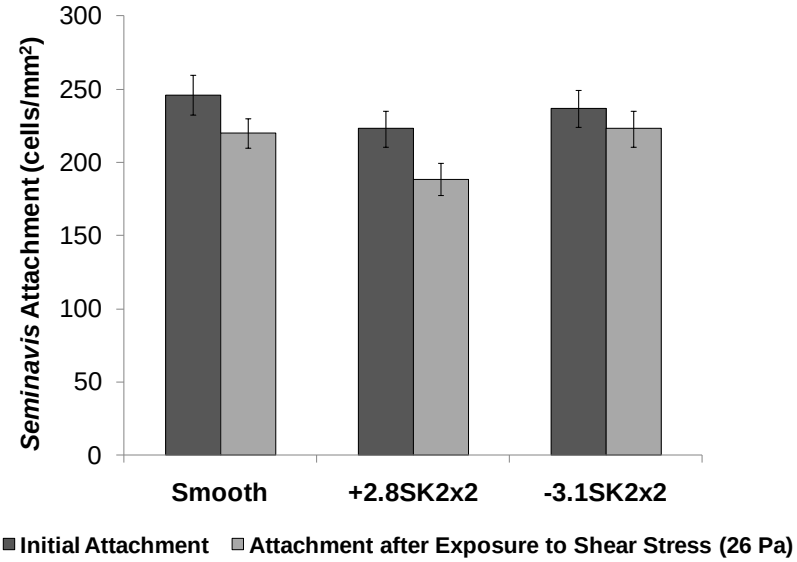

Figure 4-2. Initial attachment and attachment after exposure to shear stress (26 Pa) of *Seminavis* on smooth, +2.8SK2x2 and -3.1SK2x2 patterns in PDMSe. Each bar is a mean of 90 counts from 3 replicate samples. Error bars represent 95% confidence intervals.

Exposure to shear stress of 26 Pa removed more cells from +2.8SK2x2 than from the smooth surface and -3.1SK2x2 however the only significant difference was between the two Sharklet AF™ topographies ($F = 3.95$, $p = 0.02$, df = 2). Removal of 5, 10 and 15% of the total cells occurred from -3.1SK2x2, smooth and +2.8SK2x2, respectively (Figure 4-2). Previous experiments with *Navicula* also showed lower cell density on the +2.8SK2x2 topography compared to smooth after gentle rinsing (Long 2009). In contrast to initial attachment of *Navicula*, there was only a small but statistically significant decrease of 8.5% in initial attachment of *Seminavis* on +2.8SK2x2 compared to the smooth surface ($F = 3.17$, $p = 0.044$, df = 2) (Figure 4-2).

Assessment of Movement of *Seminavis* and *Navicula*

Orientation of diatoms was assessed after 1 h of settlement. The majority of *Seminavis* cells, 88 to 96%, were in the raphe-down orientation on all three topographies. There were no differences in the number of *Navicula* cells that were raphe-side down among topographies. However, the average proportions of *Navicula* cells that were raphe-side down were lower, 53 to 60%. The raphe-down orientation is the optimal position of adhesion and motility for diatoms.

Movement of diatom cells was evaluated after 1 h of settlement. The motility of *Seminavis* was much lower on the engineered antifouling topographies +2.8SK2x2 and -3.1SK2x2 than on the smooth PDMSe standard. Only one cell was seen to move on -3.1SK2x2 over the 15 min observation period and no cells were observed moving on +2.8SK2x2. Approximately 7% of raphe-side down cells of *Seminavis* moved across the smooth PDMSe standard. The percent of raphe-side down *Navicula* cells moving on all three surfaces was not statistically different. Only 8% of raphe-side down cells were observed to be moving on the on +2.8SK2x2 and -3.1SK2x2 compared to approximately 15% on the smooth standard. Diatoms of *Navicula* were observed to glide across microtopographies with spacings approximately half as wide as the diatom is long.

Navicula was able to glide across spacings between topographies because only a small section of the raphe needs to contact the substratum at any one time to enable movement (Edgar and Pickett-Heaps 1984). Diatoms gliding on a surface, like *Ulva* swimming through water, operate under low Reynolds number conditions in the region of 10^{-4} (Edgar 1982). Diatoms were moving at the solid-liquid interface with a thin film of water or secreted material between the cell and the substratum when movement was

assessed. Decreased movement of *Seminavis* across the Sharklet AF™ patterns indicates that topographical modification could influence the hydrodynamic properties of this fluid layer. The large size of the *Seminavis* diatom compared to *Navicula* (Figure 4-3) could be a reason for reduced motion. Drag is proportional to the surface area in close contact with the substratum (Edgar 1982) and *Seminavis* cells had a higher contact area than *Navicula*. In addition, as can be seen from Figure 4-3, if a *Navicula* cell orientates itself it can fit so that the entire cell is in contact with a surface on all but one of the features in the Sharklet AF™ pattern allowing the cells to move in 'tracks' across the surface. *Seminavis* cells must straddle several features which will make them unstable and perhaps less able to move as the raphe will not be in continuous contact with any surface.

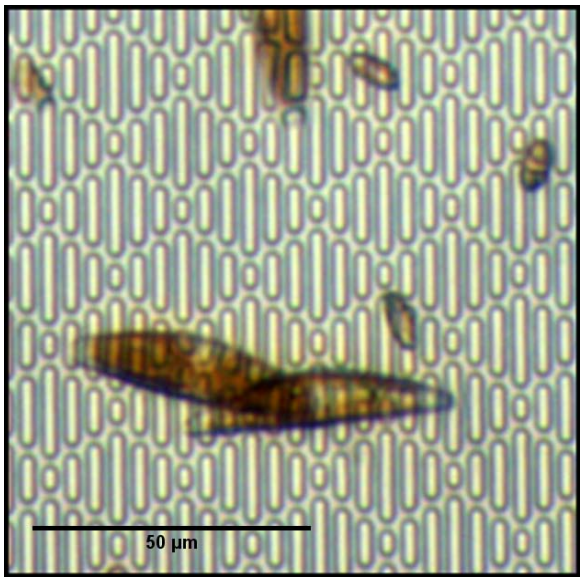

Figure 4-3. *Seminavis* (larger diatom) and *Navicula* (smaller diatom) on +2.8SK2x2 replicated in PDMSe.

Seminavis Biofilm Growth and Attachment Strength

Biofilm growth was assessed after 6 d. Initial biofilm density for *Seminavis* was lowest on +2.8SK2x2, higher on the smooth standard and highest on -3.1SK2x2 (Tukey

Test α = 0.5). After exposure to shear stress (26 Pa) biofilm density remained highest on -3.1SK2x2 and lower on +2.8SK2x2 and the smooth standard (Figure 4-4).

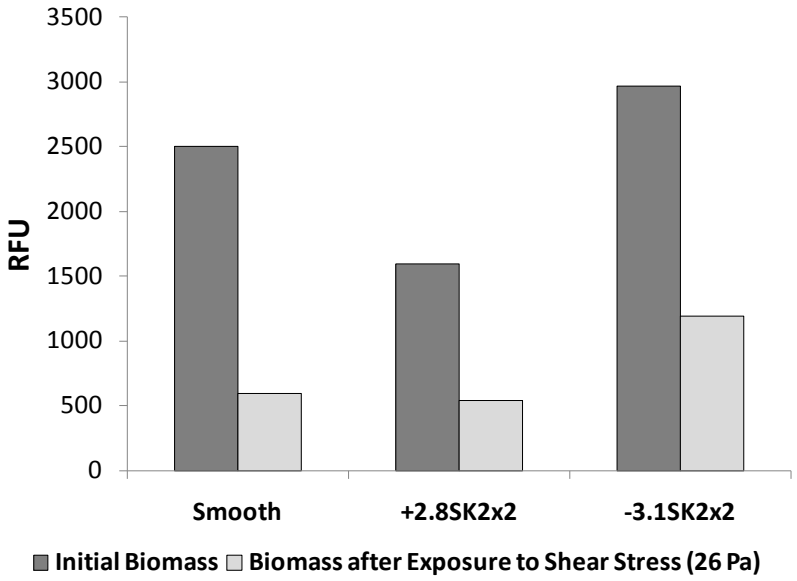

Figure 4-4. Density of attached diatoms of *Seminavis* after 6 d, before and after exposure to a shear stress of 26 Pa. Bars represent findings from single samples of each treatment.

Navicula Biofilm Growth and Attachment Strength

Densities of biofilms of *Navicula* were similar on all three surfaces after 6 d. Cells on +2.8SK2x2 and the smooth standard were clumped while those attached to the -3.1SK2x2 surface were evenly distributed. This distribution suggests the cells were more strongly bonded to the -3.1SK2x2 pattern than to +2.8SK2x2 or the smooth standard. After exposure to a shear stress of 45 Pa, biofilm density was lowest on +2.8SK2x2 and highest on -3.1SK2x2 (Figure 4-5). The strength of attachment of raphid diatoms to a surface is determined by the interaction energies between the substratum and EPS. The greater attachment strength of diatoms on -3.1SK2x2 could indicate that the EPS wetted the depressed areas of the surface topography causing stronger adhesion. Biofilms dominated by diatoms attach to (Molino, et al. 2009a) and

are not readily released from PDMS-based fouling release coatings (Holland, et al. 2004, Holm et al. 2004).

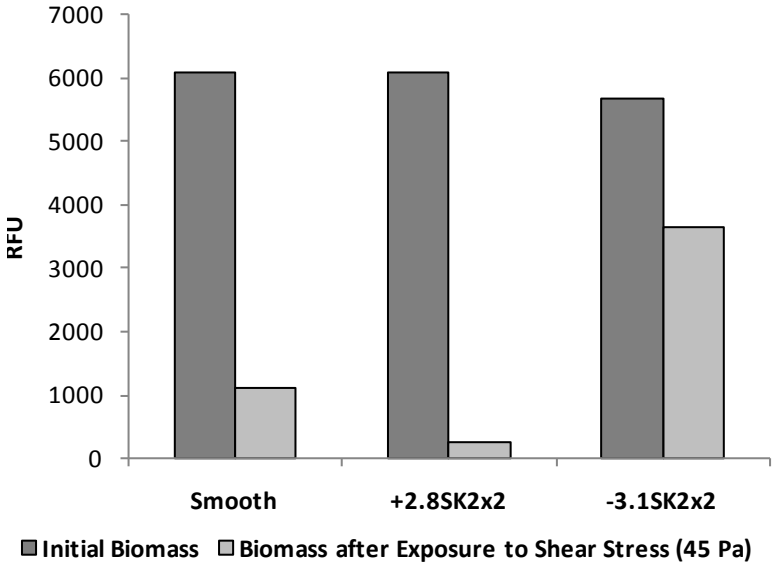

Figure 4-5. Density of attached diatoms of *Navicula* after 6 d, before and after exposure to a shear stress of 45 Pa. Bars represent findings from single samples of each treatment.

Discussion

The +2.8SK2x2 engineered antifouling topography reduced initial attachment and attachment strength of *Seminavis* and attachment strength of *Navicula* compared to smooth PDMSe. Historical data from four *Navicula* attachment strength assays was analyzed to determine the relationship between the area of the diatom in contact with the substratum and attachment strength (Long 2009). Initial attachment of *Navicula* on various engineered antifouling topographies was reported (Long 2009). Pillars surfaces showed no difference in initial attachment compared to smooth. The +2.7SK2x2 surface reduced initial attachment by 35% versus a smooth standard while other surfaces based on the Sharklet AF™ pattern had initial attachment densities similar to smooth (Long 2009). The data from one assay was first analyzed in terms of the

Attachment Point Theory (Verran and Boyd 2001, Scardino, et al. 2006). The average attachment density of *Navicula* was plotted for each topography in order of decreasing number of attachment points (Figure 4-6). The topographies plotted are smooth, pillars, channels, triangle/pillars, Recessed Sharklet AF™ and Sharklet AF™. All topographies were created with an average feature height of 3 µm and average feature widths and spacings of 2 µm. It is clear that these data cannot be described by the current Attachment Point Theory, i.e. surfaces with the lowest number of attachment points should have the lowest diatom density after exposure to shear stress.

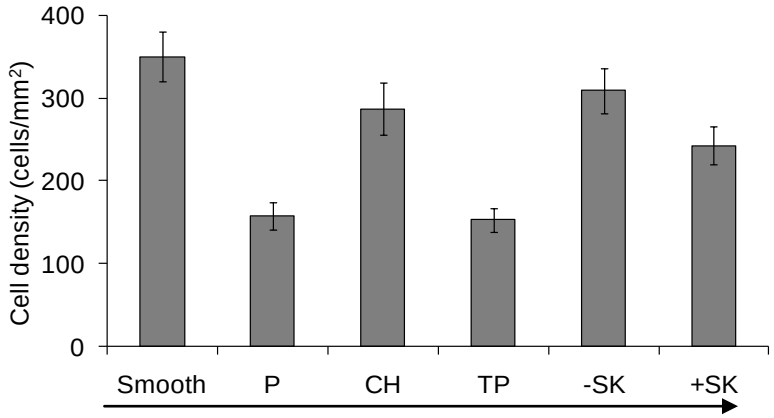

Figure 4-6. Attachment density of *Navicula* after exposure to shear stress (45 Pa) on each topography. Arrow indicates direction of decreasing number of attachment points.

The average attachment density of *Navicula* on a surface after exposure to shear stress (45 Pa) was then normalized by the average attachment density on a smooth standard and transformed with the natural logarithm. The normalized, transformed attachment data was plotted against the calculated contact area of a diatom on each surface. The contact area was determined by first calculating the projected area of a *Navicula* cell. The projected area was estimated as an ellipse with a = 12 µm and b = 4 µm. Since *Navicula* attachment before and after exposure to shear stress was evenly distributed across each surface, the solid surface fraction (φ_s) of each topography was

multiplied by the projected area of the diatom to calculate the contact area available on each surface (Figure 4-7). The solid surface fraction is the fraction of solid/liquid interface below a water drop or in this case diatom contacting a topographically modified surface (Bico, et al. 1999, Bico, et al. 2002). The width or spacing of topographic features on some of the surfaces tested allowed diatoms to fit either completely between or on top of features (Figure 4-7) (Long 2009). To calculate the contact area for these surfaces the proportion of diatoms completely between or on top of a feature was counted. The proportion of diatoms completely between or on top of a feature was multiplied by the projected area of the diatom and added to the proportion of diatoms spanning across features multiplied by the projected area of a diatom and by the solid surface fraction.

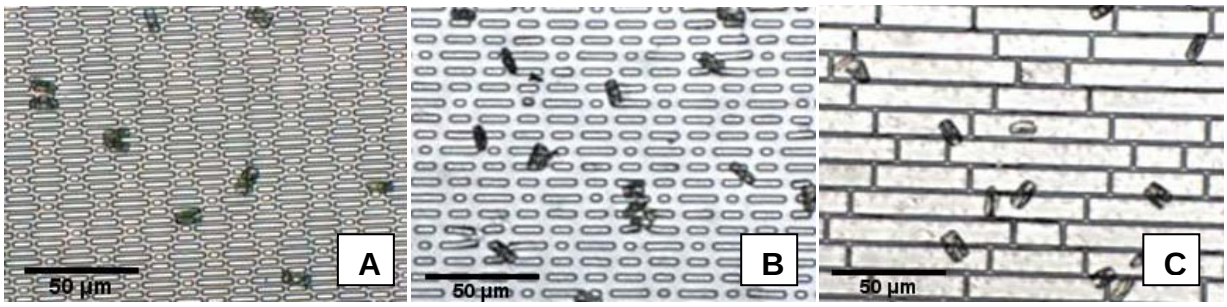

Figure 4-7. *Navicula* attachment after gentle washing on A) +2.8SK2x2, B)+2.8SK2x5 and C) +2.8SK10x2 topographies replicated in PDMSe.

The average normalized, transformed attachment density of *Navicula* after exposure to shear stress correlated with the contact area between the diatom and a topographically modified surface (R^2=0.82) (Figure 4-8). Attachment Point Theory states that organisms which are provided with larger numbers of contact points by the surface, will have increased attachment strength (Verran and Boyd 2001). The analysis in the current report shows that when diatoms are provided with a larger area of contact, attachment strength increases regardless of the number of attachment points.

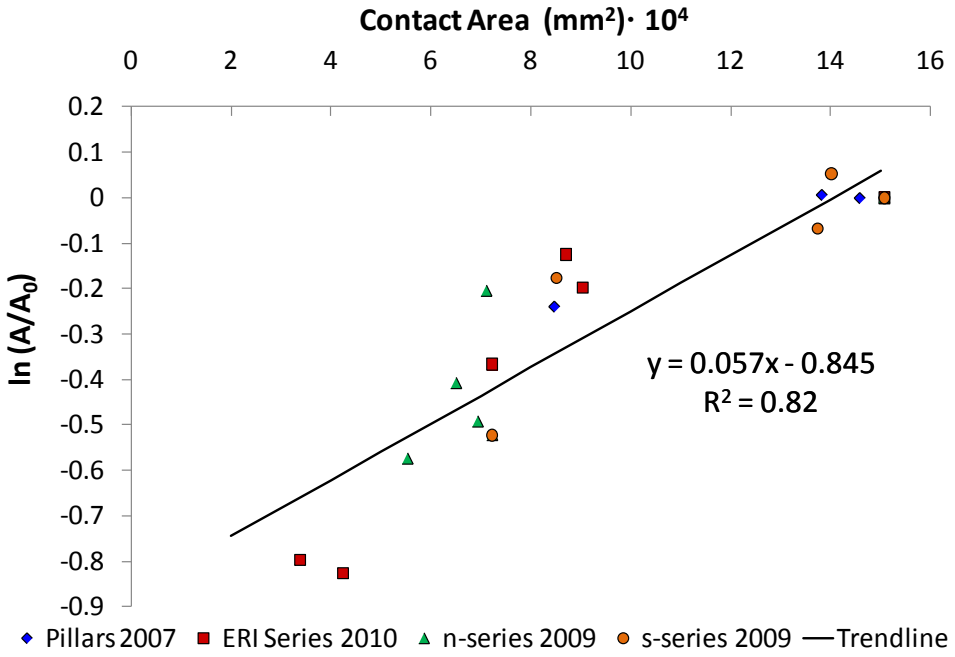

Figure 4-8. The normalized, transformed attachment density of *Navicula* after exposure to a shear stress of 45 Pa is plotted versus the maximum area of contact between the cell and the surface.

Diatoms have been shown to be a significant component of microbial biofilms on PDMS-based fouling-release surfaces (Molino, et al. 2009a). Engineered antifouling topographies were shown to decrease the attachment strength of *Seminavis* on PDMSe surfaces immediately after attachment and after 6 d of biofilm growth. Immediately after attachment and exposure to shear stress (26 Pa) removal of 5, 10 and 15% of the total cells occurred from -3.1SK2x2, smooth and +2.8SK2x2, respectively. Engineered antifouling topographies also reduced the movement of *Seminavis* across the surface. Only one cell was seen to move on -3.1SK2x2 over the observation period and no cells were observed moving on +2.8SK2x2 while 7% of raphe-side down cells moved across the smooth PDMSe standard. The percent of raphe-side down *Navicula* cells moving on +2.8SK2x2 and -3.1SK2x2 was 8% compared to approximately 15% on the smooth standard. Densities of *Seminavis* biofilms both before and after exposure to shear

stress were lowest on the +2.8SK2x2 topography. Densities of biofilms of *Navicula* were also lowest on +2.8SK2x2 after exposure to shear stress.

Attachment strength of *Navicula* on engineered antifouling topographies replicated in PDMSe was analyzed in terms of the Attachment Point Theory. It was shown that the data collected cannot be adequately described using the current Attachment Point Theory, i.e. surfaces with the lowest number of attachment points did not have the lowest diatom density after exposure to shear stress. The average normalized, transformed attachment density of *Navicula* after exposure to shear stress correlated with the contact area between the diatom and a topographically modified surface (R^2=0.82). The topographical modification of fouling-release coatings could decrease attachment strength of diatoms and biofilms on these surfaces.

CHAPTER 5
ENGINEERED ANTIFOULING MICROTOPOGRAPHIES: THE ROLE OF SURFACE ENERGY OF CROSSLINKED HYDROGELS IN A MODEL THAT PREDICTS ATTACHMENT OF ZOOSPORES OF *ULVA* AND CELLS OF *COBETIA MARINA* AND *NAVICULA INCERTA*[3]

Introduction

Biofouling – the accumulation of microorganisms, plants and animals on a wetted surface – is a widespread problem in the maritime industry. The biofouling process typically begins with conditioning of the surface (Jain and Bhosle 2009) and the development of microbial slime layers containing bacteria, diatoms (unicellular algae) and their extracellular products (Molino and Wetherbee 2008, Molino, et al. 2009a, Molino, et al. 2009b). As these slime layers foul a vessel, hydrodynamic drag and consequently fuel consumption significantly increase (Schultz 2007). Drag and fuel consumption increase further when macrofoulers, including macro-algae and invertebrates, colonize the surface (Schultz 2007). Fouling of ship hulls is also a primary cause for the introduction and spread of non-indigenous marine species worldwide (Otani et al. 2007, Pettengill et al. 2007, Piola and Johnston 2008, Yamaguchi et al. 2009). The green macro-alga (seaweed) *Ulva* is found all over the world and is well-known for fouling submerged structures such as ship hulls (Callow et al. 1997). *Ulva* colonizes substrata by releasing large numbers of motile spores (zoospores) that must select a suitable surface and transition to attached non-motile spores before germinating to produce new plants. Surface selection is influenced by chemical, physicochemical (Ederth et al. 2009, Schilp, et al. 2009), biological (Joint et

[3] Submitted to the American Chemical Society for publication. Magin CM, Finlay JA, Clay G, Callow ME, Callow JA, and Brennan AB. 2010. Engineered Antifouling Microtopographies: The role of surface energy of crosslinked hydrogels in a model that predicts attachment of zoospores of *Ulva* and cells of *Cobetia marina* and *Navicula incerta*. Biomacromolecules. (Submitted).

al. 2002), and topographic (Schumacher, et al. 2007a, Schumacher, et al. 2008) cues. Zoospores of *Ulva*, the cells of the diatom (unicellular alga) *Navicula perminuta* and the marine bacterium *Cobetia marina* are all used in this study as model soft fouling organisms representing three diverse phylogenetic groups, viz. the eukaryotic Plantae (*Ulva*), the eukaryotic Chromista (*Navicula*) and the prokaryotic Bacteria (*Cobetia*) (Cavalier-Smith 2004).

Surface chemistry is an important factor in the adhesion and release of a fouling organism (Magin, et al. 2010a, Rosenhahn et al. 2010). Self-assembled monolayers (SAMs) have been widely used to evaluate the influence of surface energy on attachment (Finlay et al. 2002a, Bowen et al. 2007, Schilp, et al. 2009, Zhao et al. 2009, Ista et al. 2010). Experiments have shown that higher numbers of spores of *Ulva* attach to hydrophobic SAMs versus hydrophilic ones in static assays (Callow et al. 2000). However, when attached spores were exposed to shear stress in a water channel, the attachment strength on hydrophilic SAMs was greater (Finlay, et al. 2002a). Materials composed of poly(ethylene glycol)(PEG) and its oligomers exhibit resistance to protein adsorption and have recently been evaluated as coatings for antifouling applications (Ostuni, et al. 2001, Balamurugan, et al. 2005, Schilp et al. 2007, Ekblad, et al. 2008). The number of zoospores of *Ulva* and cells of *Navicula* firmly attached to SAMs of hexa-(ethylene glycol)-containing alkanethiols with systematically changing end-group termination increased with decreasing wettability (Schilp, et al. 2007). This increase in attachment has also been correlated with an increase in adsorption of the protein fibrinogen (Schilp, et al. 2009). Monolayers of high molecular weight PEG (MW=2kg/mol, 5kg/mol) SAMs resisted spore attachment (Schilp, et al. 2009). The

mechanism for inhibition of spore attachment by PEG-based surfaces is not fully understood or clearly defined in the literature. Spores did not settle (attach) to the PEG monolayers, while on oligoethylene glycol SAMs, high numbers of spores settled and secreted adhesive but they could not bind to the surface so cells were easily washed off by slight disturbance (Schilp, et al. 2009).

Hydrogels, i.e., crosslinked polymer networks that swell in the presence of water, have been studied for antifouling applications. Hydrogel surfaces of alginate, chitosan, and polyvinyl alcohol substituted with stilbazolium groups (PVA-SbQ) inhibited attachment of cypris larvae of *Balanus amphitrite* (Rasmussen et al. 2002) and the marine bacterium *Pseudomonas* sp. NCIMB2021 (Rasmussen and Ostgaard 2003). Hydrogels based on 2-hydroxyethyl methacrylate (HEMA) reduced fouling in two algal colonization bioassays and remained visually clean in field testing for up to 12 weeks with the addition of benzalkonium chloride, a biocidal compound (Cowling et al. 2000). Crosslinked poly(ethylene glycol) diacrylate surfaces have been evaluated as protein-resistant coatings. Surfaces that were more hydrophilic, based on contact angle measurements, exhibited less protein adsorption (Ju et al. 2009). A variety of crosslinked hydrogel compositions including poly(HEMA) were shown to reduce adhesion of cyprids of the barnacle *Balanus amphitrite* (Murosaki et al. 2009).

Surface topographies created in polydimethyl siloxane elastomer (PDMSe) have been proposed as a non-toxic strategy for inhibiting the settlement (attachment) of fouling organisms. A bio-inspired surface topography, Sharklet AF™, reduced attachment of zoospores of *Ulva* by 86% compared to smooth (Carman, et al. 2006). An empirical relationship called the Engineered Roughness Index (ERI) has been used

to quantify topographical roughness based on parameters that describe surface energy (Schumacher, et al. 2007b). A correlation between the attachment of spores of *Ulva* and ERI was demonstrated (Schumacher, et al. 2007b) and a predictive attachment model (Long, et al. 2010) was developed based on a revised version (ERI_{II}). Recently, an extension of the attachment model was reported which correlated the attachment densities of zoospores of *Ulva* and cells of *C. marina* with surface roughness by incorporating the Reynolds number of the organism into the model (Magin, et al. 2010b).

In the present study poly(ethylene glycol) dimethacrylate (PEGDMA), poly(ethylene glycol) dimethacrylate-co-glycidyl methacrylate (PEGDMA-co-GMA), and poly(ethylene glycol) dimethacrylate-co-hydroxyethyl methacrylate (PEGDMA-co-HEMA) hydrogels were made with a thermal curing process using ammonium persulfate (APS) and ascorbic acid (AA) as radical initiators (Shin et al. 2003, Pfister, et al. 2007). The PEGDMA-co-GMA hydrogel composition and a UV curing process were reported previously (Pfister, et al. 2007). The GMA chemistry allows bioactive molecules such as proteins to be covalently grafted to the surface of these hydrogels or for the hydrogel coating to be covalently linked to epoxy paint. Functionalizing the PEGDMA hydrogel with HEMA creates a material with the same average molecular weight between crosslinks as the PEGDMA-co-GMA and hence similar mechanical properties while retaining a surface chemistry similar to that of the PEGDMA composition. It was hypothesized that the ability to vary hydrogel composition and surface topography will allow the investigation of correlations among surface energy, topography and

attachment of cells of fouling organisms. The results extend the attachment model to include substrates other than PDMSe.

Experimental Section

Materials

PEGDMA (<Mn> = 1 kg mol^{-1}) – a tetrafunctional polyethylene glycol macromonomer – was purchased from Polysciences Inc. (Warrington, PA). 2-hydroxyethyl methacrylate 98% stabilized was purchased from Acros Organics (Geel, Belgium). Glycidyl methacrylate >97%, ascorbic acid (AA) 99+%, and ammonium persulfate were purchased from Sigma-Aldrich (Milwaukee, WI). Methacryloxypropyltriethoxysilane was purchased from Gelest Inc. (Morrisville, PA). Ultra-pure water was produced by a Barnstead Nanopure Ultra Pure Water System (Waltham, MA). The base material for standards was a platinum-catalyzed PDMSe (Silastic® T2; Dow Corning Corporation).

Sample Preparation

PEGDMA, PEGDMA-co-GMA, and PEGDMA-co-HEMA hydrogels were produced using a thermally activated polymerization. Aqueous solutions were prepared by combining 25 wt% PEGDMA (<Mn> = 1 kg mol^{-1}) used as is, 0.5 wt % ammonium persulfate and ascorbic acid as chemical initiators, and ultra-pure water to balance. To create a functionalized PEGDMA hydrogel 5 wt% of GMA or HEMA was added to the aqueous solution (Figure 5-1). The hydrogels were either produced as free standing films or coatings attached to 76 x 22 mm silanated microscope glass slides. Glass slides were pretreated with 0.5% methacryloxypropyltriethoxysilane (MPS) in a 95% ethanol/water solution for 10 min, rinsed thoroughly with 95% ethanol, and dried at 120°C for 15 min.

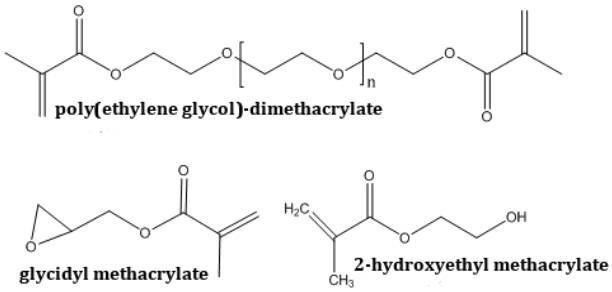

Figure 5-1. Chemical structures of monomers used to produce functionalized hydrogels.

All prepolymer compounds were combined in a glass beaker and stirred until a solution was achieved, i.e., the PEGDMA was dissolved. The prepolymer solution was then poured into two centrifuge tubes and centrifuged for 10 min at 3300 RPM. The centrifuged prepolymer solution was pipette into a mold (Figure 5-2). The mold contained a PDMSe gasket with an opening (2.5 cm x 7.6 cm x 2 mm) for a pre-treated glass slide. The gasket was placed on top of a glass plate (12.7 cm x 12.7 cm x 0.32 cm) and the pretreated slide was fitted into the opening in the gasket. A microtopographically modified silicon wafer was placed on top of the PDMSe spacer, with the topography facing down, to create engineered microtopographies. Smooth samples were cast against a second glass plate. The mold was assembled by adding a second glass plate on the back of the silicon wafer and clamping with 3-2" binder clips. The entire assembly was heated to 45°C for 45 min (Shin, et al. 2003). Hydrogel-coated slides were removed from the assembly by peeling. Two topographies, continuous channels 2.6 µm tall, 2 µm wide and spaced by 2 µm (+2.6CH2x2) and the Sharklet AF™ pattern 2.8 µm tall, 2 µm wide and spaced by 2 µm (+2.8SK2x2) (Schumacher, et al. 2007b) were created with this process.

To create PDMSe smooth standards and topographically modified surfaces the elastomer was prepared by mixing 10 parts by weight of resin and 1 part by weight

curing agent. The mixture was stirred by hand for 5 min and degassed under vacuum (28-30 in Hg) for 30 min to remove bubbles. An allyltrimethoxysilane-coupling agent was applied to clean glass microscope slides (0.5 wt% in 95% ethanol/water solution) and heated for 10 min at 120 °C. The Silastic® T2 was then placed in contact with the treated slides in a mold consisting of two glass plates and aluminum spacers. The elastomer was polymerized at ambient for 24 h. Topographically modified PDMSe samples were prepared in a two-step casting process previously described (Carman, et al. 2006).

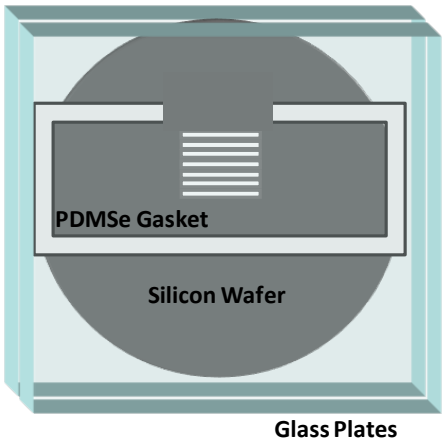

Figure 5-2. Schematic of mold for hydrogel production.

Microtopography Characterization

The +2.8SK2x2 topography (mold dimensions) was replicated as free standing films in PEGDMA-co-GMA and PDMSe. Hydrogel samples were immersed in deionized water for 24 hr prior to characterization. Six height measurements were made at random locations on each sample using a Wyko model NT1000 white light optical profilometer. Hydrogel samples in deionized water were prepared for scanning electron microscopy (SEM) by flash freezing with liquid nitrogen and subsequently freeze drying for 5 d at $9x10^3$ mbar and -42°C (Lyph Lock 4.5 Freeze Dry System, Labconco, Kansas

City, MO). Freeze-dried hydrogel samples and PDMSe samples were mounted onto aluminum SEM stubs with double sided tape. These samples were sputter-coated with gold-palladium for 60 s at 38 mA. Samples were imaged with a JEOL JSM-6400 SEM with a tungsten filament at an accelerating voltage of 15 kV. Feature dimensions were measured using Image J software.

Chemical Composition

Free standing films of PEGDMA, PEGDMA-co-GMA, and PEGDMA-co-HEMA were produced and air dried for 48 h. The attenuated total reflectance Fourier transform infrared (ATR-FTIR) spectrum of each film was recorded on a Perkin-Elmer Spectrum One spectrometer. Spectra were obtained with a ZnSe crystal with an angle of incidence of 60 ° and resolution of 4 cm^{-1}. Twenty scans were performed for each sample. Spectral subtraction was performed to verify composition of the various hydrogel formulations.

Surface Energy Measurements

Captive air and oil bubble contact angles were measured to calculate the surface energy of the functionalized hydrogels (Figure 5-3). Two replicates of each hydrogel were cast onto glass slides. Both sides of five captive air bubbles and five captive n-octane bubbles were measured on each surface (n = 20). Surface energies were calculated using the method previously presented by Hu (Hu and Tsai 1996). Statistical differences between surfaces were evaluated using one-way analysis of variance (ANOVA) and Tukey's test for multiple comparisons ($\alpha = 0.05$).

The surface energy of smooth PDMSe was measured using the Owens-Wendt-Kaelble approach (Owens and Wendt 1969). Static contact angles of water, glycerol and diiodomethane were measured. Both sides of five drops were measured on each of two

replicates (n=20). The polar and dispersive components of the surface energy were calculated using two pairs of polar and non-polar liquids: water and diiodomethane and glycerol and diiodomethane. The contact angles were reduced to surface energies by solving simultaneous equations and averaging the results (Owens and Wendt 1969). The mean and standard deviation for the contact angles of each liquid were determined. However, since the measured values are related to each other by a system of simultaneous equations, it was not trivial to account for the covariance using a small sample size of matching pairs. Standard deviations were calculated by using Minitab Statistical Software to randomly generate 1500-unit sample groups with the same mean and standard deviation as the measured sample groups. The systems of equations were solved multiple times with these data and the results were used for statistical analysis.

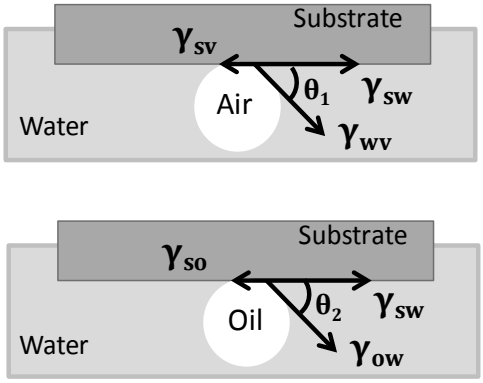

Figure 5-3. Schematic of captive air and oil bubble measurements for calculating surface energy.

Biological Attachment Assays

Coated glass slides were shipped to the University of Birmingham overnight in 50 mL conical centrifuge tubes filled with deionized water. Prior to bioassay, the slides were transferred to sterile (0.22 µm filtered) artificial seawater (ASW) (Tropic Marin^{TM}) for 2 h.

Ulva

A total of four *Ulva* attachment assays were performed. Six replicates of two topographies, +2.6CH2x2 and +2.8SK2x2, and smooth created in PEGDMA-co-HEMA and PDMSe were attached to glass slides and provided for analysis in the fourth assay. Zoospores were obtained from fertile plants of *Ulva linza* collected from Llantwit Major (Wales) and prepared for attachment assays as described previously (Callow, et al. 1997). Briefly, each sample was immersed in 10 mL of a spore suspension containing 1.5×10^6 spores mL^{-1} and incubated in the dark for 45 min.

Attached spores on hydrogel and PDMSe slides were counted using a Zeiss epifluorescence microscope with a 10x objective while the samples were still wet. Thirty counts were taken from each of the three replicates.

Navicula incerta

Cells of *Navicula incerta* were cultured in F/2 medium contained in 250 mL conical flasks until cells reached the logarithmic growth phase, approximately 3 d. Cells were washed 3 times in fresh medium before harvesting and diluting to give a suspension with a chlorophyll a content of approximately 0.25 µg mL^{-1} (Holland, et al. 2004). Six replicates of each hydrogel composition and PDMSe attached to glass slides were placed in Quadriperm dishes to which 10 mL of the diatom suspension were added. Cells were allowed to attach at ambient (~20 °C) on laboratory benches for 2 h. Samples were exposed to a submerged wash in seawater to remove cells which had not attached (the underwater immersion process avoided passing the samples through the air-water interface).

Three replicates were counted wet using an image analysis system attached to a fluorescence microscope. Counts were made for 30 fields of view (0.064 mm^2) on each

sample. The remaining three replicate samples were exposed to a shear stress of 45 Pa in a water channel (Schultz et al. 2000). The number of cells remaining attached was counted using the image analysis method described above.

C. marina

Cultures of *C. marina* (ATCC 25374) (Baumann et al. 1983) were grown in marine broth contained in 100 mL conical flasks, at 18°C on an orbital shaker at 60 rpm overnight. Cells were harvested by centrifugation (8000 rpm for 1 min) and washed 2 times in sterile (0.22 µm filtered) Tropic Marin^{TM} ASW to remove any residual marine broth. The cells were resuspended in sterile ASW and briefly sonicated to aid dispersion. The suspension was diluted to an absorbance of 0.3 at 600 nm. Six replicates of each hydrogel composition and PDMSe attached to glass slides were placed in Quadriperm dishes to which 10 mL of the suspended bacteria were added. The dishes were incubated at ambient (~20°C) on the laboratory bench for 2 h. After incubation, the slides were washed gently in seawater to remove unattached bacteria.

Three replicates were stained with crystal violet (0.01% in seawater) and counted under a 20x objective while still wet. Counts were made for 30 fields of view (2500 µm^2) on each sample. The remaining three replicates with attached bacteria were exposed to a shear stress of 50 Pa in a water channel (Schultz, et al. 2000). The number of cells remaining attached was counted as described above.

The cell density per mm^2 was calculated for each count (n = 90). The mean cell densities were compared using one-way analysis of variance (ANOVA) and Tukey's test for multiple comparisons.

Results

Microtopography Characterization

Fidelity of topographic features replicated in PEGDMA-co-GMA and PDMSe was evaluated with SEM and white light optical profilometry (Figures 5-4 and 5-5). All feature heights were within 0.3 µm of the mold dimensions (Table 5-1).

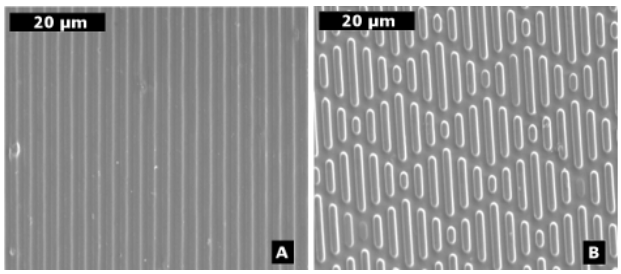

Figure 5-4. Scanning electron micrographs of A)+0.6CH2x2 and B)+1SK2x2 topographies in PEGDMA-co-GMA hydrogel.

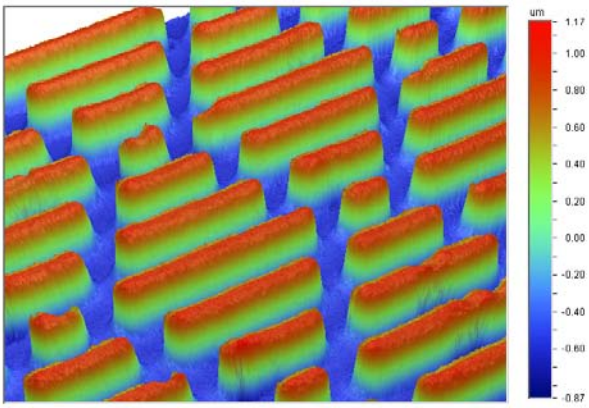

Figure 5-5. White light optical profilometry image of +1SK2x2 topography cast in PEGDMA-co-GMA.

Table 5-1. Average heights plus or minus standard deviation of hydrogel and PDMSe replicates of wafers measured with white light optical profilometry and SEM.

	Feature Height (µm)			
	PEGDMA-co-GMA		PDMSe	
Topography	Profilometer	SEM	Profilometer	SEM
+3SK2x2	3.12 ± 0.1	2.83 ± 0.5	----	3.24 ± 0.1
+3SK2x2	----	----	3.2 ± 0.1	3.17 ± 0.1

Chemical Composition

Spectral subtraction of PEGDMA from PEGDMA-co-HEMA shows characteristic peaks for HEMA, i.e., 3400 to 3200 cm^{-1} (OH stretch), 2863 to 2843 cm^{-1} (CH symmetric stretch), 1750 to 1735 cm^{-1} (C=O stretch), 1485 to 1445 cm^{-1} (CH asymmetric deformation) and 1150 to 1060 cm^{-1} (C-O-C asymmetric stretch). Spectral subtraction of PEGDMA from PEGDMA-co-GMA shows characteristic bands for GMA at 1715 to 1740 cm^{-1} (C=O stretch), 1485 to 1445 cm^{-1} (CH deformation), 1280 to 1230 cm^{-1} (C-O-C symmetric stretch) and 950 to 815 cm^{-1} (asymmetric stretch).

Surface Energy Measurements

The surface energies of PEGDMA and PEGDMA-co-HEMA calculated from measured captive air and oil bubble contact angles were not statistically different (α=0.05, p=0.11). The surface energy of PEGDMA-co-GMA was statistically higher than both PEGDMA and PEGDMA-co-HEMA (α=0.05, p<0). The surface energies of all three hydrogels are higher than that of PDMSe (Tables 5-2 and 5-3).

Table 5-2. Contact angle measurements and calculated surface energies for smooth hydrogels. Surface energies are the interfacial interaction energy (I_{sw}), the free energy between hydrogel and water (γ_{sw}), the polar component of the surface energy of the hydrogel (γ^{p}_{sv}), the dispersion component of surface energy of hydrogel (γ^{d}_{sv}) and the surface energy of the hydrogel (γ_{sv}).

	Contact Angle (°)		Energy (mN/m)				
	Captive Air Bubble	Captive n-Octane Bubble	I_{sw}	γ_{sw}	γ_{sv}^{P}	γ_{sv}^{d}	γ_{sv}
PEGMDA	48 ± 5	47 ± 11	85 ± 7	3 ± 1	35 ± 6	17 ± 9	52 ± 5
PEGDMA-co-GMA	39 ± 2	51 ± 5	83 ± 3	2 ± 1	34 ± 3	25 ± 5	58 ± 2*
PEGDMA-co-HEMA	46 ± 3	48 ± 4	85 ± 3	2 ± 10	35 ± 2	17 ± 2	52 ± 2

*Indicates statistical difference Tukey Test (α=0.05).

Table 5-3. Contact angle measurements and calculated surface energies (γ_S) for smooth PDMSe.

	Contact Angle (°)			Energy (mN/m)
	Water	Glycerol	Diiodomethane	γ_S
PDMSe	109 ± 5	96 ± 1	65 ± 2	19 ± 3

Biological Attachment Assays

***Ulva* attachment**

Results of 3 separate assays showed that PEGDMA, PEGDMA-co-GMA and PEGDMA-co-HEMA consistently reduced the attachment of spores of *Ulva* compared to smooth PDMSe (Figure 5-6). The total average percent reduction for PEGDMA versus PDMSe is 55%, PEGDMA-co-GMA versus PDMSe is 87% and for PEGDMA-co-HEMA versus PDMSe it is 85%.

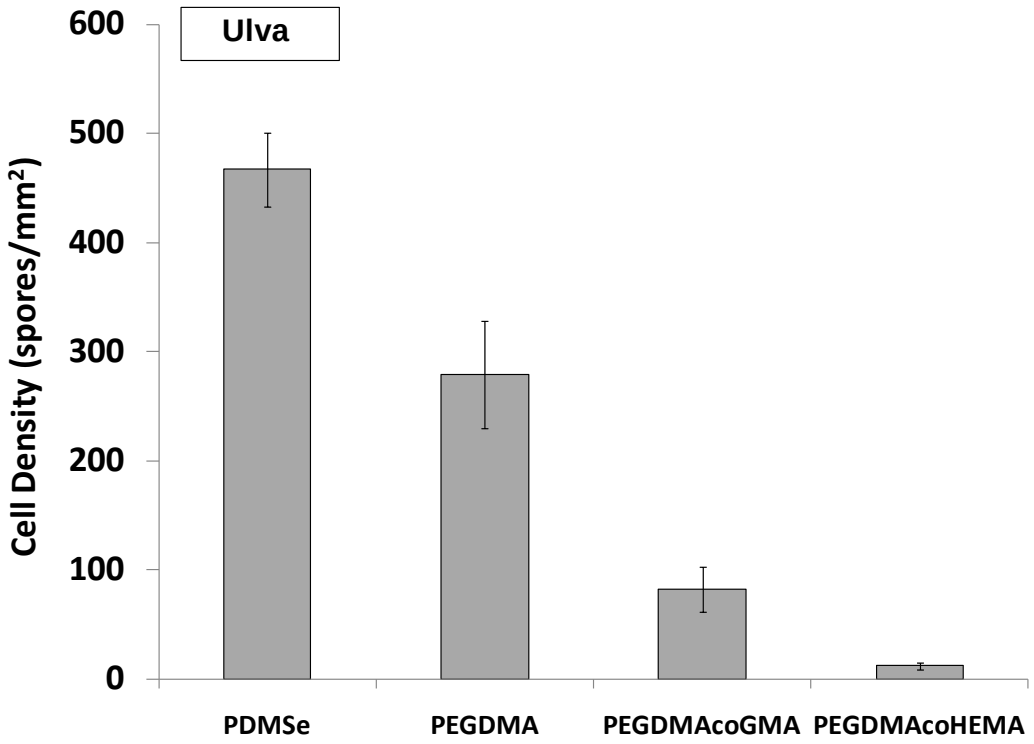

Figure 5-6. Functionalized poly(ethylene glycol)-based hydrogels reduce the attachment density of zoospores of *Ulva*. These data are representative of three separate assays. Error bars indicate 95% confidence intervals.

Attachment of cells of *Navicula*

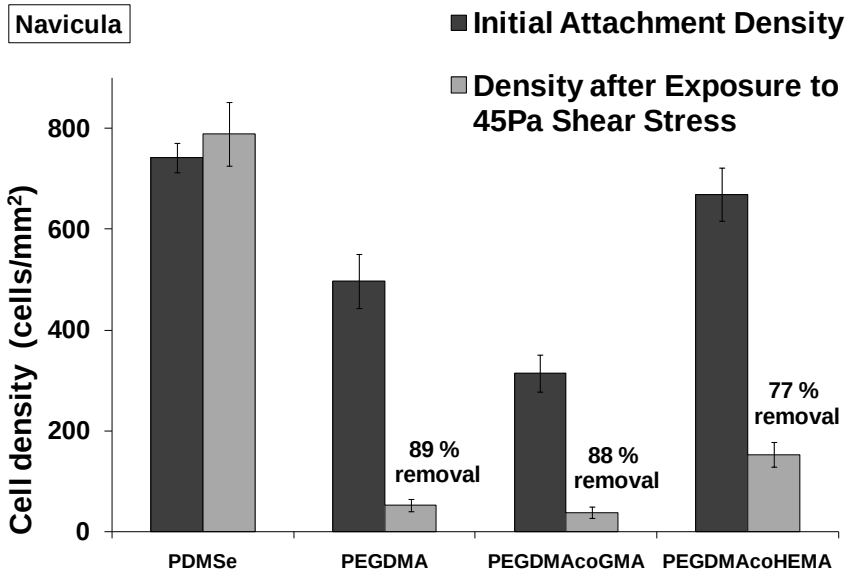

Figure 5-7. Functionalized poly(ethylene glycol)-based hydrogels reduce attachment density and attachment strength of *Navicula*. Error bars indicate 95% confidence intervals.

Diatom cells, unlike spores of *Ulva*, are not motile in the water column. The cells come into contact with a surface by gravity and water currents so at the end of a 2 h incubation period, approximately the same number of diatoms will be in contact with all test surfaces. Differences in the density of attached cells of *Navicula* were quantified following a gentle underwater washing, which washed away cells that were not attached to the surface. The initial attachment density was lowest on PEGDMA-co-GMA which was significantly lower than initial attachment densities on PEGDMA, PDMSe and PEGDMA-co-HEMA ($\alpha = 0.05$, $p<0$) (Figure 5-7). Initial attachment densities on PDMSe and PEGDMA-co-HEMA were not statistically different ($\alpha = 0.05$). Exposure to a shear stress of 45 Pa in the water channel caused removal of 77% or more of diatom cells to be removed from all hydrogel surfaces (Figure 5-7). No cells were removed

from the smooth PDMSe surface. The total percent reduction after removal for PEGDMA-co-GMA versus PDMSe was 95%.

Attachment of cells of *C. marina*

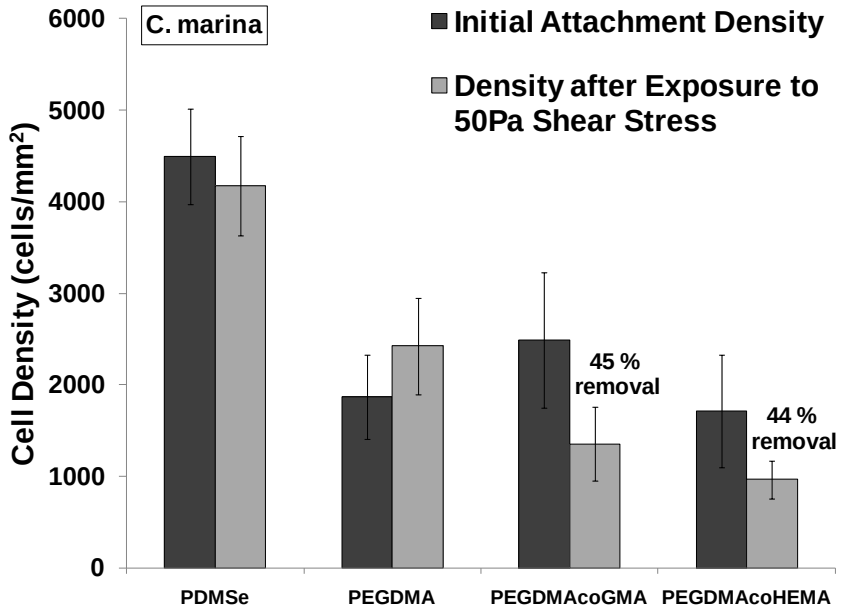

Figure 5-8. Functionalized poly(ethylene glycol)-based hydrogels reduce attachment density and attachment strength of *C. marina*. Error bars indicate 95% confidence intervals.

The initial attachment density of cells of *C. marina* was reduced on the hydrogels compared to a smooth PDMSe standard (up to 62%) with lowest densities on PEGDMA-co-GMA and PEGDMA-co-HEMA (Figure 5-8). Initial attachment densities of *C. marina* were not statistically different among the three hydrogel compositions but all hydrogels significantly reduced attachment versus PDMSe ($\alpha = 0.05$, $p < 0$). Exposure to a 50 Pa shear stress in a water channel caused 44% and 45% removal from PEGDMA-co-GMA and PEGDMA-co-HEMA, respectively (Figure 5-8). There was no statistically significant removal of *C. marina* from PDMSe or PEGDMA. The cell density on PEGDMA-co-HEMA was 77% less, after exposure to a 50 Pa shear stress, than that on PDMSe.

Based on the results from all biological attachment assays, PEGDMA-co-HEMA was selected as the substrate for further testing. The channels (+2.6CH2x2) and Sharklet AF™ (+2.8SK2x2) topographies were replicated in PEGDMA-co-HEMA and PDMSe and tested with the standard *Ulva* zoospore attachment assay. The initial spore attachment density was reduced on both PDMSe +2.6CH2x2 and +2.8SK2x2 versus smooth. Smooth PEGDMA-co-HEMA reduced spore attachment by an average of 75% compared to smooth PDMSe. Topographies produced in PEGDMA-co-HEMA reduced *Ulva* attachment by an average of 82% for +2.6CH2x2 and 93% for +2.8SK2x2 compared to smooth PDMSe.

Discussion

Hydrogel Characterization

White light optical profilometry and SEM were used to confirm that topographies were replicated in hydrogel with high fidelity. Spectral subtraction of ATR-FTIR spectra verified the presence of GMA and HEMA in functionalized PEGDMA hydrogels. Contact angle measurements and surface energy calculations showed that the surface energy of PEGDMA-co-GMA was significantly higher than both PEGDMA and PEGDMA-co-HEMA (Tukey Test α=0.05). The surface energies of PEGDMA and PEGDMA-co-HEMA were not significantly statistically different.

Biological Attachment Assays

Initial attachment density and attachment strength of marine fouling organisms have been attributed to many factors including surface chemistry (Gudipati et al. 2005, Cordiero et al. 2009, Ederth, et al. 2009, Schilp, et al. 2009, Zhang et al. 2009) and surface topography (Callow, et al. 2002, Carman, et al. 2006, Schumacher, et al. 2008, Scardino, et al. 2009a, Scardino et al. 2009b, Aldred et al. 2010, Bers et al. 2010, Long,

et al. 2010, Magin, et al. 2010b). The surface energy of all three PEGDMA-based hydrogels was more than twice that of the PDMSe standard in this report. Hydrogels reduced the initial attachment densities of all three marine organisms compared to the PDMSe standard. These findings are consistent with results from other PEG-based materials that have been evaluated (Ekblad, et al. 2008, Krishnan et al. 2008, Schilp, et al. 2009). The low number of *Ulva* spores removed from the hydrogel surfaces was also expected based on the observation that spores generally attach more firmly to hydrophilic than hydrophobic surfaces (Finlay et al. 2008). All hydrogel compositions reduced the attachment strength of cells of the diatom *Navicula* compared to smooth PDMSe. Diatoms, unlike *Ulva*, have been found to adhere more firmly to hydrophobic silicone elastomers (Holland, et al. 2004) and self-assembled monolayers (SAMs) (Finlay, et al. 2002b) than hydrophilic surfaces.

Initial attachment of cells the diatom *Navicula* on a series of xerogel surfaces was comparable on all surfaces, but the percentage removal of attached cells by hydrodynamic shear stress increased with critical surface tension and increased wettability as measured by the static water contact angle (Finlay, et al. 2010). The functionalized compositions of PEGDMA-co-GMA and PEGDMA-co-HEMA reduced attachment strength of *C. marina* compared to PDMSe. The functionalized compositions of PEGDMA-co-GMA and PEGDMA-co-HEMA reduced attachment strength of *C. marina* compared to PDMSe. The results are consistent with the ‘Baier curve’, a plot which demonstrates the relationship between substratum surface tension and the degree of biological fouling retention (Baier 2006). There are two minima observed on the Baier curve, one between 20 and 30 mN/m and another between 50

and 70 mN/m. The surface tensions of PDMSe and the hydrogel substrates were within these ranges and both exhibited low retention of fouling of specific organisms. Based on these results, PEGDMA-co-GMA and PEGDMA-co-HEMA, in particular, are more effective fouling-release coatings than PDMSe for cells of *Navicula* and *C. marina*.

The normalized, transformed attachment densities of spores of *Ulva* and cells of *C. marina* to various topographies created in PDMSe has been correlated with an attachment model (Magin, et al. 2010b). This equation relates the attachment density on a particular topography to the surface energy of the substratum and the Reynolds number of the fouling organism (Equations 5-1 and 5-2).

$$\ln\left(\frac{A}{A_0}\right) = -m * ERI_{II} \tag{5-1}$$

$$m = m' * Re \tag{5-2}$$

It was shown that attachment density on a variety of topographies could be predicted with this model (Long, et al. 2010). The attachment densities of *Ulva* on PDMSe and PEGDMA-co-HEMA topographies correlated with Equations 5-3 and 5-4, respectively when plotted in the form of the attachment model (Figure 5-9).

$$\ln\left(\frac{A}{A_0}\right) = -0.46 \times 10^{-2} * ERI_{II} \tag{5-3}$$

$$\ln\left(\frac{A}{A_0}\right) = -0.15 \times 10^{-2} * ERI_{II} \tag{5-4}$$

The discrepancy in the slopes of the attachment model was attributed to surface energies of the materials. The effect was incorporated into the attachment model by multiplying by the surface energy of the smooth substrate for each material normalized by the surface energy of PDMSe. The normalized, transformed attachment densities on

both PDMSe and PEGDMA-co-HEMA correlated (R^2 = 0.87) with the attachment model multiplied by the measured surface energy ratio (γ/γ_0) (Figure 5-10).

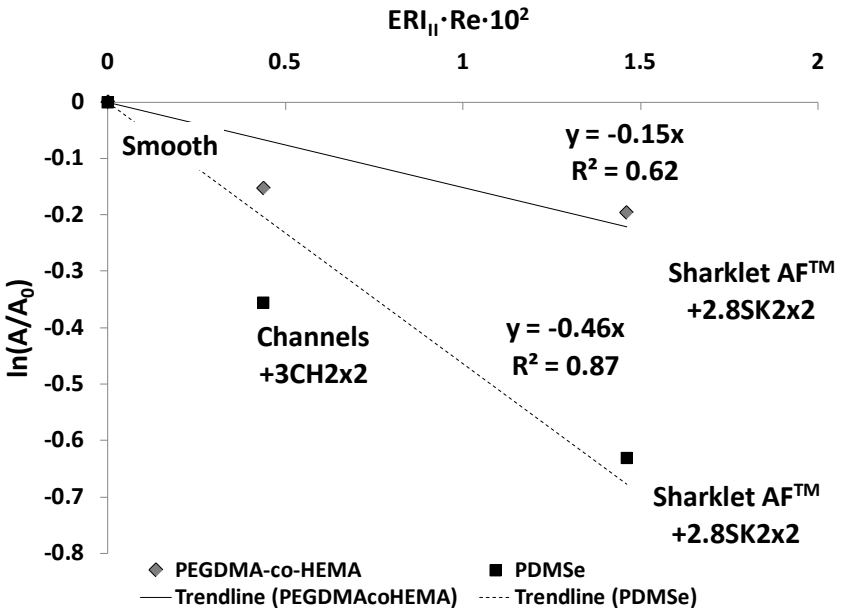

Figure 5-9. Normalized, transformed *Ulva* attachment density on PDMSe and PEGDMA-co-HEMA topographies plotted versus ERI_{II}*Re*10^2. Attachment density on PDMSe and PEGDMA-co-HEMA correlated well with the equation that describes the attachment model (R^2 = 0.87 and R^2 = 0.62, respectively).

The new slope of the attachment model and the negative linear correlation are described by Equations 5-5 and 5-6.

$$m = m'' * Re * \frac{\gamma}{\gamma_0} \tag{5-5}$$

$$\ln\left(\frac{A}{A_0}\right) = (-0.46 \times 10^{-2} * Re * \frac{\gamma}{\gamma_0}) * ERI_{II} \tag{5-6}$$

The normalized, transformed attachment densities of eight assays with spores of *Ulva* and two assays with *C. marina* on various engineered microtopographies created in PDMSe and PEGDMA-co-HEMA correlated to the ERI_{II} with a new slope that consists of the Re of the organisms multiplied by a ratio of the surface energy measured on a smooth substrate to that of a standard (PDMSe) (R^2=0.80) (Figure 5-11).

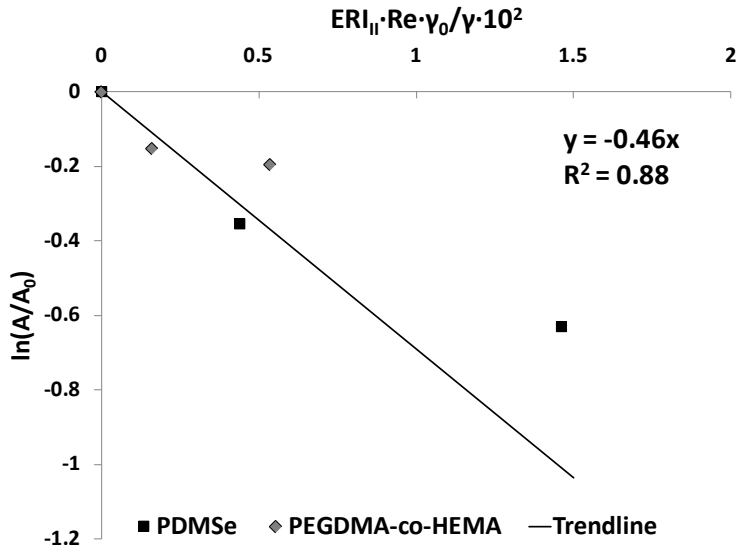

Figure 5-10. Normalized, transformed spore attachment density on PDMSe and PEGDMA-co-HEMA topographies plotted versus $ERI_{II}*Re*10^2$. Attachment density on PDMSe and PEGDMA-co-HEMA show a negative, linear correlation with the attachment model multiplied by γ/γ_0 (R^2=0.88).

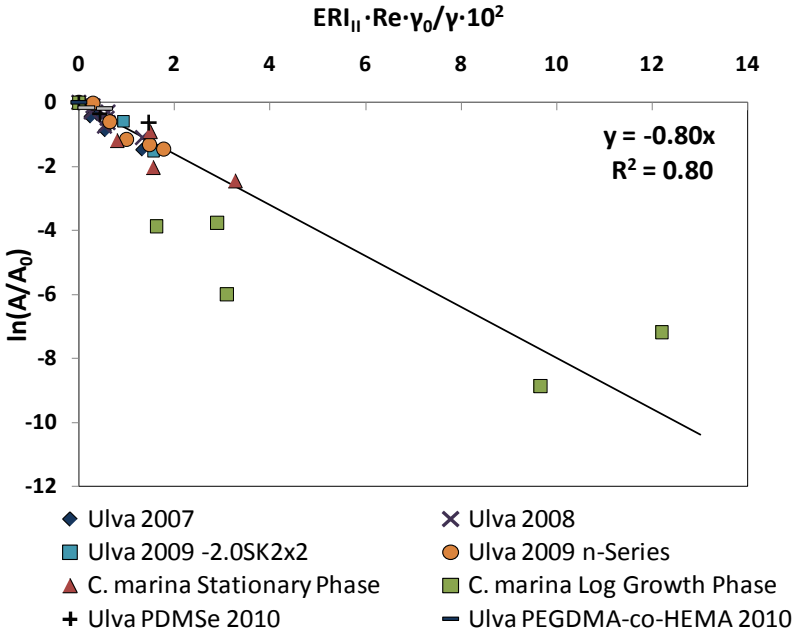

Figure 5-11. Normalized, transformed attachment densities of spores of *Ulva* (Schumacher, et al. 2007b, Schumacher, et al. 2008, Long, et al. 2010) and cells of *C. marina* (Magin, et al. 2010b) on PDMSe and PEGDMA-co-HEMA topographies plotted versus $ERI_{II}*10^2$. Attachment densities on PDMS e and PEGDMA-co-HEMA for eight different assays show a negative, linear correlation with $ERI_{II}*Re*\gamma_0/\gamma*10^2$ (R^2 = 0.80).

The environmental and economic costs of biofouling have led to a need for environmentally neutral antifouling technologies (Magin, et al. 2010a). The results from attachment studies performed with three fouling organisms on functionalized PEGDMA hydrogels provide insight that will lead to improvements in antifouling and fouling release technologies. The role of the slope of the attachment model as an indicator of an organism's sensitivity to a surface was extended by incorporating a ratio of the measured surface energy of a smooth substratum to that of a standard (PDMSe) into the attachment model. The attachment model has now been shown to correlate with the attachment density of cells from two evolutionarily diverse groups on two substrate materials. This equation has been successfully used to model attachment density of zoospores and cells on micro-patterned materials with different surface chemistries. Functionalized, crosslinked hydrogels reduced attachment of fouling organisms from three evolutionarily diverse groups.

CHAPTER 6
ENGINEERED MICROTOPOGRAPHIES AND CHEMISTRIES INFLUENCE ATTACHMENT AND FUNCTION OF ENDOTHELIAL AND SMOOTH MUSCLE CELLS

Background

Coronary heart disease is the leading cause of death in the United States (U.S). According to the latest mortality data, every 38 s an American will die from a coronary event (Heart Disease & Stroke Statistics 2010). Coronary heart disease is a result of atherosclerosis, the narrowing and hardening of artery walls due to a buildup of fatty substances including cholesterol in the arteries that supply blood to the heart muscle. This buildup can block the blood flow and oxygen supply to the heart, ultimately resulting in a heart attack.

Angioplasty and stenting have been used to increase lumen size and restore blood flow in small-diameter vessels such as the coronary arteries, but not without complications. Renarrowing of the blood vessels, referred to as in-stent restenosis, occurs within 6 months in 50% of patients that undergo the procedure (Padera and Schoen 2004). Clot formation or thrombosis begins immediately after circulation is restored to the grafted area; plasma proteins adsorb to the surface of the graft, platelets and leukocytes bind to these proteins, and bulk fibrin formation begins. In areas of low blood flow such as small-diameter vessels, the fiber-forming step of the clotting process occurs and results in a macroscopic thrombus that reduces blood flow (Biomaterials Science: An Introduction to Materials in Medicine 2004). The other common mode of failure for small-diameter vascular grafts is intimal hyperplasia, thickening of the lumen caused by excessive proliferation of smooth muscle cells in the media.

Grafting is the most common way to treat coronary blockages. Autogenous veins or arteries are typically used to reroute blood flow around the blocked arteries in the

grafting procedure. The patient's internal mammary artery or saphenous vein are the most common grafts; however, damage to the native vasculature or a previous grafting procedure may make bypass surgery impossible. Even when healthy autogenous vessels are available, it is less desirable to remove them from their positions than it would be to insert a prosthetic graft (Nerem and Seliktar 2001). However, there are currently no FDA approved small-diameter vascular grafts.

Over the past 20 years researchers have worked diligently to increase patency of small-diameter vascular grafts. The first efforts were directed toward coating synthetic grafts, e.g. Dacron®, a woven poly(ethylene terephthalate) (PET) material and Gore-tex®, expanded poly(tetrafluoroethylene) (ePTFE), with proteins or blood components to reduce blood/material interactions (Rumisek et al. 1986, Drury et al. 1987, Freischlag and Moore 1990). When these attempts did not significantly increase patency, investigators turned to a tissue engineering approach.

Endothelial cells were seeded onto synthetic graft materials to mimic the nonthrombogenic interface that already exists within the blood vessels (Nerem and Seliktar 2001). Since the seminal work of Weinberg and Bell several distinct approaches to vascular tissue engineering have emerged (Weinberg and Bell 1986) (see Appendix B): 1) solid-scaffold (made of synthetic and/or natural materials) and cell seeding in vitro or in vivo, 2) embedding of cells in a matrix, 3) assembly of cell-sheets, and 4) decellurarized tissue constructs. Current small-diameter vascular graft designs focus on recreating the natural extracellular microenvironment. Natural extracellular matrix (ECM) is gel made up of various protein fibers woven together within a hydrated network of glycosaminoglycan chains (Lutolf and Hubbell 2005). Gels made from

collagen, fibrin, and various combinations of these and other proteins are the closest biologically to ECM (Cummings et al. 2004, Chan et al. 2007, Stegemann, et al. 2007, Wu et al. 2007), however, these materials often lack the mechanical stability required in an arterial graft. In vascular tissue engineering, synthetic hydrogels are used as scaffolds to mimic ECM (Nguyen and West 2002, Zhu et al. 2005, Shen et al. 2006), as matrix material in which cells are embedded (Almany and Seliktar 2005), and for microencapsulation of growth factors or other proteins (Lee et al. 2004, Patel et al. 2007). Biodegradable materials such as polylactic acid and polycaprolactone processed by a variety of methods including gel-spinning (Chung et al. 2007a), layer-by-layer construction (Choi et al. 2007, Feng et al. 2007, Zhang et al. 2007), and nonwoven techniques (Roh et al. 2008) are commonly used to create vascular grafts that will allow cellular ingrowth and remodeling in vivo. The technique of electrospinning is a very popular way to mimic the nanofibrillar structure of the ECM. Electrospun vascular prostheses have been made from synthetic elastomers, biodegradable materials, and/or ECM proteins such as collagen and elastin (Stankus et al. 2006, Lee et al. 2008b, Sell and Bowlin 2008, Smith et al. 2008). These structures provide topographical cues to cells along with better mechanical properties than collagen gel matrices.

To obtain ultimate biological and mechanical properties researchers use decellularized ECM from various sources including small intestine submucosa and the vasculature of other species (Badylak 2002, Wang et al. 2007, Zhu et al. 2008). A few investigators have created completely tissue engineered grafts by culturing autologous cells outside of the patient (L'Heureux et al. 2006) or implanting a biodegradable scaffold into the patient and allowing complete cellular remodeling to occur before

grafting (Watanabe et al. 2007). Disadvantages to completely tissue engineered grafts are numerous. Cells must be retrieved from the patient, sometimes surgically and then expanded for several weeks *in vitro* before the graft can be implanted. This process is very time consuming and expensive.

Biology of the Vascular Wall

All blood vessels are made up of three layers: intima, media, and adventitia. The intima is the innermost, subluminal layer composed of the endothelium, basement membrane, and the internal elastic lamina. The endothelium consists of a continuous monolayer of flat endothelial cells (ECs) with a cobblestone-like morphology and extracellular matrix elements. The basement membrane or basal lamina creates a flexible substrate of collagen and glycoproteins for EC attachment. The internal elastic lamina is a layer of circularly arranged elastic fibers that are interlaced with the connective tissue of the basal lamina. These structures form a semi-permeable interface between circulating blood and the rest of the body. The media, the thickest layer, is a circular arrangement of elastic fibers, connective tissue, and smooth muscle cells. It controls the caliber of the blood vessel while providing elasticity. The adventitia is made up mainly of connective tissue. It also contains fibroblasts, nerves, and nutrient capillaries (Biology of the Arterial Wall 1999).

Endothelial cells line the luminal surface of all blood-contacting vessels—arteries, veins, and capillaries. This continuous monolayer of cells creates an ideal anti-thrombogenic surface. ECs possess a glycoprotein coat that is negatively charged and repels platelet and leukocyte adhesion. ECs also secrete bioactive substances that inhibit thrombosis, promote fibrinolysis, and inhibit smooth muscle cell (SMC) proliferation (Biology of the Arterial Wall 1999, Xue and Greisler 2000). Excessive

SMC proliferation, commonly referred to as intimal hyperplasia, is a significant contributor to vascular graft failure. During intimal hyperplasia SMCs in the arteries dedifferentiate from the contractile to the synthetic phenotype and proliferate uncontrollably. Theoretically, coating a small-diameter vascular graft with a confluent layer of ECs would result in a nonthrombogenic blood-material interface that has the ability to reduce intimal hyperplasia (Biology of the Arterial Wall 1999, Xue and Greisler 2000, Nerem and Seliktar 2001). Controlling SMC phenotype could also reduce intimal hyperplasia. *In situ* endothelialization of synthetic prostheses occurs by direct migration of ECs from anastomotic edges, by transmural migration of ECs and by transformation of ECs from EPCs (Sarkar et al. 2006b). Unfortunately, ECs have a limited capacity for regeneration and complete re-endothelialization has never been shown in clinical practice (Xue and Greisler 2000, Sarkar, et al. 2006b). Despite successful re-endothelialization in animal models, it has been shown that transanastomotic endothelial ingrowth does not exceed more than 1 to 2 cm in humans even after years of implantation (Nerem and Seliktar 2001, Zilla et al. 2007).

The regenerative nature of EPCs was first discovered when Asahara, et al (Asahara, et al. 1997) published the first description of isolation of EPCs from human peripheral blood. These cells originate in bone marrow and have the ability to proliferate and to differentiate into mature ECs. Endothelial progenitor cells could be the ideal way to endothelialize a synthetic graft; the cells are autologous and do not require removal from the patient or extensive culture times *ex vivo*.

Topography

A key contributor to the cellular microenvironment is substratum topography. For nearly a century it has been known that substratum topography influences cell

morphology (Harrison 1914). However, to date very little has been reported about the long-term cellular response to topography such as gene expression, proliferation, and differentiation. It has been shown that mRNA expression and protein synthesis change when cell shape is controlled through growth on micropatterned adhesive islands. These outcomes were accompanied by a decreased proliferation time before differentiation (Thomas et al. 2001). Fibroblasts grown on nanoscale topographies showed broad gene up-regulation especially in those that influence cell signaling, proliferation, cytoskeleton, and production of ECM (Dalby, et al. 2002, Dalby et al. 2003). In 2007, it was demonstrated that topography could enhance differentiation of human mesenchymal stem cells into the neuronal lineage (Yim, et al. 2007). It has also been shown that isotropic topographies such as pillars tend to control more collective cell functions such as proliferation, while anisotropic topographies like channels more noticeably alter cell morphology and cytoskeletal organization (Lim and Donahue 2007).

Cell morphology is known to affect proliferation, differentiation, cytoskeletal organization and gene expression (Thomas, et al. 2001, Dalby, et al. 2002, Dalby, et al. 2003, Itano et al. 2003, Lim and Donahue 2007). Itano et al (Itano, et al. 2003) demonstrated that changes in nuclear shape led to the release of nuclear Ca^{2+}, which is known to regulate gene expression in cells. Microchannel scaffolds with discontinuous walls initially supported primary vascular smooth muscle cell proliferation in the synthetic phenotype. Upon reaching confluence, the cells were aligned and transformed towards the contractile phenotype (Cao et al. 2010). This evidence supports the hypothesis that mechanical forces such as those experienced by cells grown on topographies can regulate gene expression.

Approach

The ideal vascular graft should provide sufficient mechanical strength to withstand arterial pressures while matching the compliance of the native artery ($E \approx 600 \pm 100$ kPa) (Holzapfel et al. 2002). For clinical applications, grafts should be readily available in various shapes and sizes, inexpensive, and easy for a surgeon to handle and insert – flexible and kink-resistant with good suture retention (Lee et al. 2008a). For this particular application the graft material must provide mechanical support, good nutrient transport, and support cellular ingrowth. The graft must also create a microenvironment that induces proliferation and differentiation of EPCs to ECs. For this reason, the graft material should mimic the natural ECM, provide sites for grafting bioactive molecules that recruit EPCs and maintain good fidelity of topographical features. Since natural ECM is a combination of hydrated glycosaminoglycan chains and filamentous proteins, synthetic hydrogels have often been used to mimic the extracellular environment (Lutolf and Hubbell 2005). In this case it is hypothesized that a PEGDMA-based hydrogel elastomer will provide good compliance, high fidelity of topographic features, and sites for surface modified with biomolecules. Predefined, engineered surface microtopographies have been created in PEGDMA hydrogels without significant size variations due to swelling (Pfister, et al. 2007). These hydrogels have also been reported to have a highly adjustable shear modulus with a range of G=10kPa to 1Mpa (Pfister, et al. 2007). Substratum elasticity has been shown to direct stem cell differentiation into specific lineages; therefore the ability to fine tune the elastic modulus of the graft will be advantageous when inducing differentiation of EPCs (Engler, et al. 2006).

Since the discovery of circulating EPCs and their regenerative properties, researchers have been investigating ways to increase EPC recruitment and attachment to synthetic stents and grafts. The most widely used approach is to capture EPCs with an antibody against the surface marker CD34. Several clinical trials performed with anti-CD34 coated stents have concluded that these stents are a safe, feasible way to increase EPC attachment and reduce in-stent thrombosis (Aoki et al. 2005, Co et al. 2008, Miglionico et al. 2008). Even though cell capture was reported, very little has been demonstrated about capture kinetics and the final phenotype of captured cells (Markway, et al. 2008). Recently, human umbilical vein endothelial cells (HUVECs) were selectively captured from a flowing, heterogeneous cell population using anti-kinase insert domain receptor (anti-KDR) at a density of approximately 55cells/mm^2 (Markway, et al. 2008). This cell density should be sufficient to produce a monolayer of ECs; it is slightly larger than the EC seeding density (4×10^3 cells cm^{-2}) previously used to culture confluent monolayers of ECs (Carman, et al. 2006). Peptides derived from fibronectin such as connecting segment-1 (CS-1) (Rodenberg and Pavalko 2007) and arginine-glycine-aspartic acid (RGD) (Blindt et al. 2006) have been shown to capture circulating EPCs. Peptides that specifically bind a form of EPCs called human blood outgrowth endothelial cells (HBOECs) with high affinity were selected with phage display technology (Veleva et al. 2007). However, after incorporating these ligands into a polymeric scaffold, testing showed that specific binding was greatly reduced in the presence of serum proteins (Veleva, et al. 2007).

The aim of this work is to create a cell culture substrate for small-diameter vascular graft applications that has the potential to re-endothelialize *in vivo* and/or

control SMC phenotype to reduce neointimal hyperplasia and thrombosis. It was hypothesized that a combination of surface chemistry and topography on a graft surface would capture circulating EPCs in the peripheral blood and promote their differentiation into ECs to create a continuous tissue layer within the lumen of the graft. A biomolecular surface chemistry such as a bioactive peptide or antibody would increase recruitment of endothelial progenitor cells and topographical modification would provide mechanical cues to induce differentiation into the endothelial cell phenotype. The substratum material would provide sufficient mechanical strength and compliance while allowing nutrients to flow to the cells. Anti-CD34 capture methods have demonstrated increased EPC attachment and have been shown to be safe in clinical trials. Since the goal of this research was to use topographical cues to direct differentiation, targeting EPCs with anti-CD34 should provide sufficient EPC capture and retention. An ECM protein, fibronectin, was used as a proof of concept in grafting and cell attachment experiments. Similar work should be completed to show the same effects using anti-CD34.

Materials and Methods

Materials

PEGDMA ($<M_n>$ = 1 kg/mol) was purchased from Polysciences Inc. (Warrington, PA). 2-hydroxyethyl methacrylate 98% stabilized was purchased from Acros Organics (Geel, Belgium). Glycidyl methacrylate >97%, ascorbic acid (AA) 99+%, ammonium persulfate, and albumin from bovine serum were purchased from Sigma-Aldrich (Milwaukee, WI). Methacryloxypropyltriethoxysilane (MPS) was purchased from Gelest Inc. (Morrisville, PA). Ultrapure water was produced by a Barnstead Nanopure Ultra

Pure Water System (Waltham, MA). The base material for standards was a platinum-catalyzed PDMSe (Silastic® T2; Dow Corning Corporation).

Sample Preparation

PEGDMA, PEGDMA-co-GMA, and PEGDMA-co-HEMA hydrogels were produced using a thermally activated polymerization process. Aqueous solutions were prepared by combining 25wt% PEGDMA ($<M_n>$ = 1 kg mol^{-1}), 0.5wt % ammonium persulfate and ascorbic acid as chemical initiators, and ultrapure water to balance. To create a functionalized PEGDMA hydrogel 5 wt% of GMA or HEMA was added to the aqueous solution (Figure 6-1).

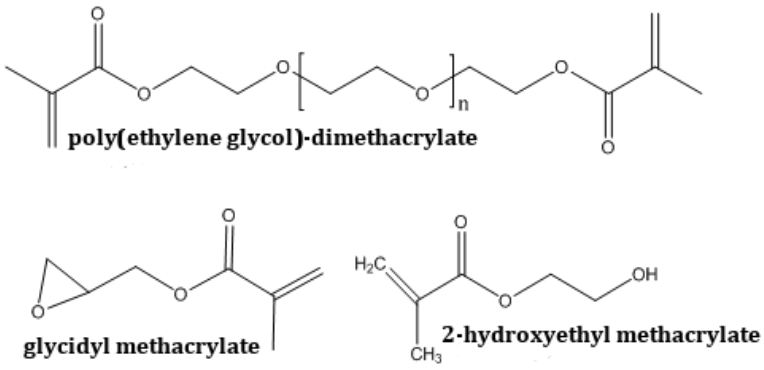

Figure 6-1. Chemical structures of monomers used to produce functionalized hydrogels.

The hydrogels were either produced as free standing films or attached to 76 x 22 mm microscope glass slides during the curing process by way of a silane coupling agent as described in Chapter 5. To produce free standing films all components of the prepolymer solution were combined in a glass beaker and stirred until the PEGDMA was dissolved. The prepolymer solution was then poured into two centrifuge tubes and centrifuged for 10 min at 3300 RPM. A pipette was used to fill a mold made of two glass plates and a PDMSe gasket with the centrifuged prepolymer solution. A

topographically modified silicon wafer was added to the mold to create patterned samples. The mold was then placed in an oven to cure for 45 min at 45°C. Hydrogels were stored in deionized water after curing.

Smooth standards and topographically modified PDMSe standards were also produced. The elastomer was prepared by mixing 10 parts by weight of resin and 1 part by weight curing agent. The mixture was stirred by hand for 5 min and degassed under vacuum (28-30 in Hg) for 30 min to remove bubbles. An allyltrimethoxysilane-coupling agent was applied to clean glass microscope slides (0.5 wt% in 95% ethanol/water solution) and polymerized for 10 min at 120°C. The Silastic® T2 was then placed in contact with the treated slides in a mold consisting of two glass plates and aluminum spacers. The elastomer was polymerized at ambient for 24 h. Topographically modified PDMSe samples were prepared in a two step casting process previously described (Carman, et al. 2006).

Attaching Hydrogels to Glass Slides

Hydrogels were attached to glass slides by way of a silane coupling agent. To prepare a solution of MPS, 30 mL of 190 proof ethanol was pipetted into a polypropylene cup. While mixing with a stir bar 1 to 2 drops of glacial acetic acid was added to adjust the pH of the solution to approximately 4.5-5.5. Then 0.17 mL of MPS was added to the solution and allowed to react for 5 min. Glass slides were cleaned by holding with forceps and passing through a flame 4 to 5 times. Slides were allowed to cool on an aluminum tray covered with Kimwipes®. A plastic transfer pipette was used to cover glass slides with the MPS solution. The MPS solution was allowed to react on the glass slides for 2 to 3 min. The slides were then rinsed with 190 proof ethanol and placed in the oven to dry at 120°C for 10 min. After the slides were treated with MPS, a

slide was placed into a mold consisting of two glass plates and a PDMSe gasket. A topographically modified silicon wafer was placed in this mold to make slides with topographically modified hydrogel. Hydrogel solution was pipetted into the mold and the filled mold was placed into an oven at 45°C for 45 min to cure and attach to the glass slide.

Grafting Fibronectin to Hydrogel Surfaces

Fibronectin was grafted to hydrogel surfaces by reacting the epoxide ring of the GMA with amine nucleophiles on the protein in an alkaline buffer (Volcker et al., 2001). To make the buffer a 0.2 M solution of anhydrous sodium carbonate was prepared by combining 2.12 g of sodium carbonate with 100 mL of deionized water. Then a 0.2 M solution of sodium bicarbonate was prepared by combining 1.68 g of sodium bicarbonate with 100 mL of deionized water. A carbonate-bicarbonate buffer was made by combining 4 mL of the sodium carbonate solution with 6 mL of sodium bicarbonate solution and bringing the volume up to 200 mL with deionized water. The pH of this solution was measured to be 9.8 at 24°C. This buffer was used to make a solution of 50 µg mL^{-1} Fn in buffer. The surface to be grafted was then covered with the Fn buffer solution and incubated at 37°C with 5% CO_2 for one hour. After incubation the Fn solution was removed from the surface and the surface was rinsed three times with phosphate buffered saline (PBS).

Hydrogel Characterization

The average molecular weight between crosslinks ($<M_c>$) was determined experimentally using the method described by Peppas and Barr-Howell (Peppas & Barr-Howell, 1986). Six replicates of each hydrogel formulation: PEGDMA, PEGDMA-co-

GMA, and PEGDMA-co-HEMA were cut from free standing films. The following measurements were made for each sample:

- $W_{a,r}$ the sample weight in air after crosslinking
- $W_{n,r}$ the sample weight in a nonsolvent after crosslinking
- $W_{a,s}$ the sample weight in air after swelling
- $W_{n,s}$ the sample weight in a nonsolvent after swelling
- $W_{a,d}$ the sample weight in air after drying

These measurements were then used to calculate the volume of the hydrogel sample after crosslinking before swelling ($V_{g,r}$) and after equilibrium swelling ($V_{g,s}$). The equations used to calculate the hydrogel volumes are based on Archimedes' buoyancy principle

$$V_{g,r} = \frac{W_{a,r} - W_{n,r}}{\rho_n} \tag{6-1}$$

$$V_{g,s} = \frac{W_{a,s} - W_{n,s}}{\rho_n} \tag{6-2}$$

where ρ_n is the density of the nonsolvent at the temperature of the experiment. The volume of the hydrogel sample after crosslinking but before swelling is described by Equation 6-1 while the volume of the hydrogel after equilibrium swelling is described by Equation 6-2. The volume of the dry polymer was calculated using Equation 6-3

$$\mathrm{V_p} = \frac{\mathrm{W_{a,d}}}{\rho_\mathrm{p}} \tag{6-3}$$

where ρ_p is the density of the polymer. The polymer fractions of each hydrogel sample in both the relaxed and swollen state were calculated using Equation 6-4 and Equation 6-5, respectively:

$$\upsilon_{2,r} = \frac{V_p}{V_{g,r}} \tag{6-4}$$

$$\upsilon_{2,s} = \frac{V_p}{V_{g,s}} \tag{6-5}$$

The solubility parameters (δ) of PEGDMA, PEGDMA-co-GMA and PEGDMA-co-HEMA were determined by swelling three replicates of each hydrogel in seven solvents with a range of solubility parameters (see Table 6-1) for 24 h.

Table 6-1. Properties of solvents used to calculate solubility parameters adapted from (Brandup et al. 1999).

Solvent	Solubility Parameter ($MPa^{1/2}$)	Density (g/cm^3)
Hexane	14.9	0.659
Benzene	17.2	0.874
Toluene	18.2	0.865
Chloroform	19.0	0.568
Acrylonitrile	21.5	0.806
Methanol	29.7	0.791
Water	47.9	1.0

The solubility parameter of the hydrogel was estimated as the maxima of the plot of Equation 6-6 (where m is the mass of the hydrogel after swelling in solvent for 24 h; m_0 is the mass of the hydrogel before swelling after vacuum drying for 45 min; ρ_s is the density of the solvent) versus the solubility parameter of the solvent.

$$Q = \frac{m - m_0}{m_0} * \frac{1}{\rho_s} \tag{6-6}$$

The average molecular weight between crosslinks (<Mc>) for each hydrogel was calculated using the Flory-Rehner Equation (Equation 6-7) (Sperling, 2001)

$$-[\ln(1 - v_2) + v_2 + \chi_1 v_2^2] = V_1 n[v_2^{\frac{1}{3}} - \frac{v_2}{2}] \tag{6-7}$$

where υ_2 is the polymer volume fraction in the equilibrium swollen gel; χ_1 is the solvent-polymer interaction parameter; V_1 is the molar volume of the solvent; and n is the density of active chains between crosslinks. The value of $\chi_1$for the PEGDMA-co-GMA

system was previously determined to be a function of the polymer volume fraction (Pfister et al., 2007):

$$\chi_1(\upsilon_2) = 0.49 + 0.14\upsilon_2 + 0.59\upsilon_2^2 \quad (6\text{-}8)$$

The Young's modulus of an elastomer may be predicted by measure the equilibrium swelling behavior. Young's modulus can be written

$$E = L(\frac{\partial\sigma}{\partial L})_{T,V} \quad (6\text{-}9)$$

which leads to

$$E = nRT\frac{r_i^2}{r_0^2}(2\alpha^2 + \frac{1}{\alpha}) \cong 3n\frac{r_i^2}{r_0^2}RT \quad (6\text{-}10)$$

if equibiaxial extension is assumed $\frac{r_i^2}{r_0^2}\cong 1$.

The Young's modulus of PEGDMA-co-GMA, PEGDMA-co-HEMA and PDMSe were also measured with thermomechanical analysis (TMA). Three discs with a diameter of 10 mm and thickness of 1 mm were cut from free standing films of each hydrogel and tested. Force was applied in 0.1 N increments up to 0.5 N with a TMA2940 from Thermal Instruments. The displacement was recorded in micrometers. The force-displacement curve was used to calculate the shear modulus (G) of the material with Equation 6-11. The average molecular weight between crosslinks was calculated with Equation 6-12. The shear modulus was then converted to the Young's modulus (E) using Equation 6-13.

$$G = \frac{\left[(F_2 - F_1)\left(\frac{\pi d^2}{4}\right)\right]}{[\frac{L_2 - L_1}{L_2}]} \quad (6\text{-}11)$$

$$G = \frac{\rho RT}{<M_c>}(1 - \frac{2<M_c>}{M_n}) \quad (6\text{-}12)$$

$$E = 2G(1 + v) \quad (6\text{-}13)$$

Hydrogel composition and Fn grafting were verified using attenuated total reflectance Fourier transform infrared spectrometry (ATR-FTIR) and immunofluorescence microscopy. Samples of PEGDMA, PEGDMA-co-GMA, PEGMDA-co-HEMA, Fn treated PEGMDA and PEGDMA-co-GMA-graft-Fn were made and dried for 48 hr at ambient temperature. A Perkin Elmer One Spectrometer with a ZnSe crystal (60°) and resolution of 4 cm^{-1} was used to record 20 scans for each sample. Spectral subtraction was performed to verify hydrogel composition and Fn grafting. Additionally, Fn grafting was performed as described above on four samples: PEGDMA-co-GMA smooth, PEGDMA-co-GMA +0.6CH2x2, PEGDMA-co-GMA +1SK2x2, and a smooth PEGDMA standard. A dilution of the primary antibody, anti-Fn produced in mouse, at 1:50 antibody solution to PBS was prepared. Then a dilution of the secondary antibody, anti-mouse IgG-FTIC, at 1:32 antibody solution to PBS was prepared. The Fn-grafted surfaces were covered with the primary antibody and incubated at 37°C with 5% CO_2 for 1 h. The antibody solution was removed from the surfaces and the surfaces were rinsed three times with PBS. The surfaces were then covered with the secondary antibody solution and incubated again for 1 h at 37°C with 5% CO_2. After incubation the surfaces were rinsed three times with PBS. Ten epi-fluorescent micrographs were taken on each sample. ImageJ software was used to determine the average pixel intensity for each image using the Color Histogram plugin. The average fluorescence intensity for smooth PEGDMA and PEGDMA-co-GMA was compared.

Cell Culture Assays

Sample preparation

Free-standing films of PEGDMA, PEGDMA-co-GMA and PDMSe were produced using the method described in the polymer synthesis section. Smooth and topographically modified surfaces were tested. The topographies tested included the n-series of Sharklet topographies and channels with a height of 1 μm and width and spacing of 2 μm. The n-series is a group of topographies designed to have an increasing number of unique features (n) arranged in the Sharklet pattern (Figure 6-2).

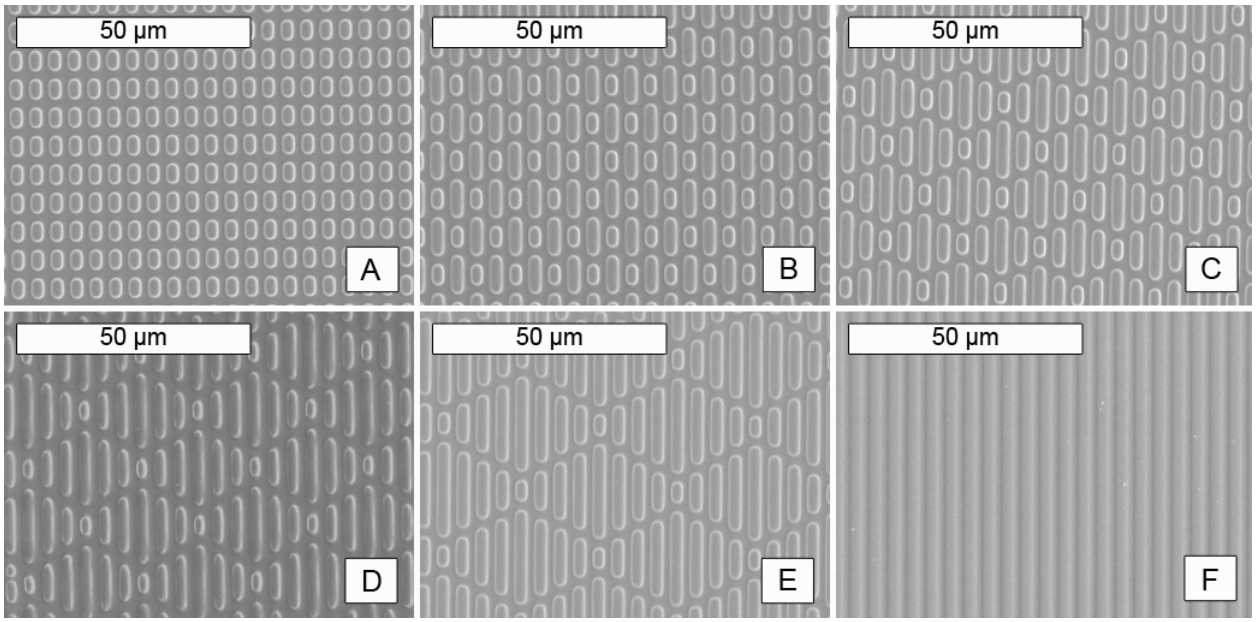

Figure 6-2. Sharklet surfaces varying in the distinct number of features (n) and Channels replicated in PDMSe. A) +1SK2x2_n1, B) +1SK2x2_n2, C) +1SK2x2_n3, D) +1SK2x 2_n4, E) +1SK2x2_n5 and F) +1CH2x2.

The samples were created with features protruding from the surface in a Sharklet pattern with a height of 1 μm and width and spacing of 2 μm. Therefore, using the current nomenclature the n-series surfaces were referred to as +1SK2x2_n4 where n is the number of unique features and ranges from one to five. The channels topography is represented as +1CH2x2. Three 14 mm discs of each film were punched out and glued

into wells of a 24-well plate with uncured polymer. The samples were sterilized by immersion in 70% v/v ethanol in water for 1 h. Samples were then rinsed with PBS three times and exposed to the Fn grafting process described above.

Porcine vascular endothelial cell culture

Porcine vascular endothelial cells (PVECs) from a primary culture provided by Dr. Edward Block's laboratory were seeded onto smooth and +1CH2x2 and +1SK2x2_4 topographies created in PEGDMA-graft-Fn and PEGDMA-co-GMA-graft-Fn at $5x10^4$ cells mL^{-1}. The PVECs were cultured on the hydrogels for 24 h. Cells were fixed with 10% formalin for 5 min and stained with crystal violet. Three transmitted light micrographs were taken per sample at a magnification of 400x using a Zeiss Axioplan 2 Microscope with a digital camera. The number of cells per field of view was counted and the average number of cells mm^{-2} was reported as an indication of PVEC attachment to each hydrogel surface.

Human cell culture

Two types of human cells were provided by Dr. Mark Segal's laboratory: HCAECs and HASMCs. Topographies with a height of 1 μm including the n-series and channels were cast in PDMSe and PEGDMA-co-GMA and prepared as described above. Smooth surfaces and empty tissue culture polystyrene (TCPS) wells were used as standards and controls in these assays. Each cell type was seeded on to an identical plate full of samples at $5x10^4$ or $2.5x10^4$ cells per well and placed into an incubator at 37°C with 5% CO_2. Samples were imaged after 24 h and 7 d using an inverted phase contrast microscope. Cell morphology was observed as an indication of cell attachment and response to the surfaces. Three phase contrast images were taken at 10x magnification for each combination of chemistry and topography.

Image analysis

Phase contrast images were analyzed with ImageJ software. Images of topographically modified surfaces were first rotated until the channels between features were oriented horizontally. The boundaries of HCAECs and HCASMCs were outlined using the freeform select tool and added to the region of interest manager. The projected area (S) and perimeter (L) of each cell were measured. ImageJ was also used to fit an ellipse to each cell and the angle between the major axis of each fitted ellipse and the direction of the channels in each topography was measured. Cell morphology was quantified by calculating the cell shape index (CSI) (Sarkar et al. 2006a, Cao, et al. 2010):

$$CSI = \frac{4\pi S}{L^2} \tag{6-14}$$

Elongated cells will have a CSI approaching 0 while cells with a circular shape will have a CSI closer to 1. Orientation was quantified by tallying the number of cells within ranges of 10 degrees and plotting the percentage of cells in each range (Sarkar, et al. 2006a).

Statistical methods

The mean angle of cell orientation relative to the channels on each topography was calculated using circular statistical methods to calculate the rectangular coordinates of the mean angle (Zar 1984). The following equations were used to calculate the rectangular coordinates of the mean angle from frequence data:

$$X = \sum \frac{f_i \cos a_i}{n} \tag{6-15}$$

$$Y = \sum \frac{f_i \sin a_i}{n} \tag{6-16}$$

In these equations, a_i is the midpoint of the measurement interval recorded and f_i is the frequency of occurrence of an angle within that interval. The magnitude of the mean angle was then calculated with Equation 6-17:

$$r = \sqrt{X^2 + Y^2} \tag{6-17}$$

The mean angle was then taken to be the angle having the following cosine and sine:

$$cos\bar{a} = \frac{X}{r} \tag{6-18}$$

$$sin\bar{a} = \frac{Y}{r} \tag{6-19}$$

Since the dispersion of the data was very small compared with the period of 360°, linear statistics were used to calculate 95% confidence limits and run an ANOVA with Tukey-Kramer Test for multiple comparisons (Batschelet 1981). A Kolmogorov–Smirnov test of each group showed that the mean angle data was not normally distributed. Therefore, the data was transformed by taking the square root. The 95% confidence limits and ANOVA were performed on the transformed data. The mean angle for every topography was plotted in bar charts with error bars representing 95% confidence limits and horizontal bars represent results of the Tukey-Kramer Test (α=0.05).

Results and Discussion

Hydrogel Characterization Results

Solubility parameter

The solubility parameters for the PEGDMA, PEGDMA-co-GMA and PEGDMA-co-HEMA hydrogels were estimated by plotting a volumetric swelling ratio (Q) (Equation 6-6) versus the solubility parameter of several different solvents in which the hydrogels were swollen for 24 h (Figure 6-3). The maximum volumetric swelling ratio corresponds

with the solubility parameter of the hydrogel. Maximum swelling of all three hydrogels occurred in chloroform; therefore δ=19.0 $MPa^{1/2}$.

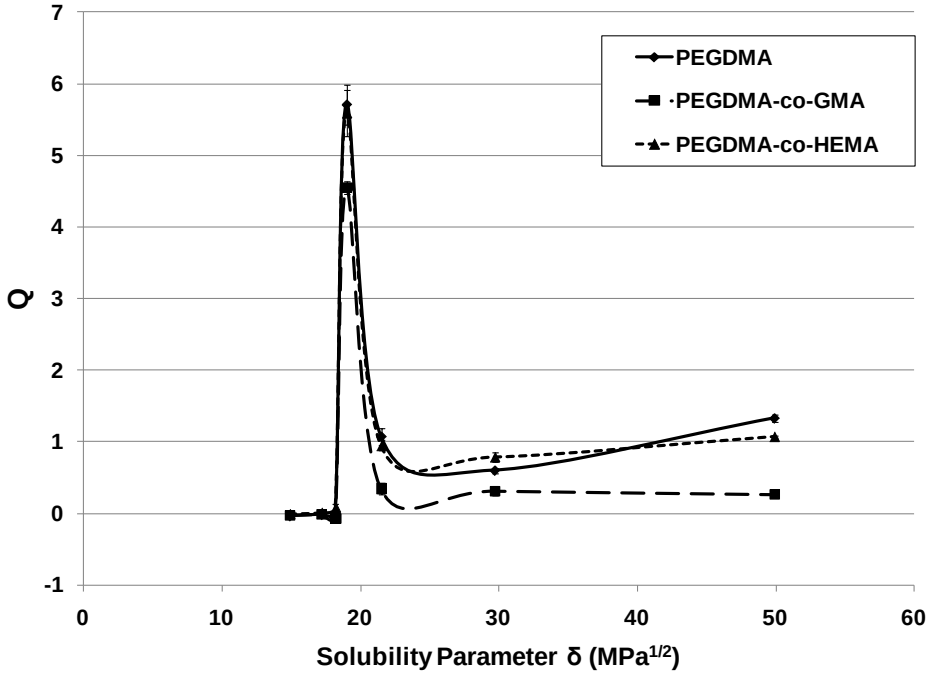

Figure 6-3. Plot of volumetric swelling ratio versus solvent solubility parameter for PEGDMA, PEGDMA-co-GMA and PEGDMA-co-HEMA hydrogels.

Average molecular weight between crosslinks and modulus

The average molecular weight between crosslinks and modulus of PEGDMA-co-HEMA and PEGDMA-co-GMA were measured using TMA and swelling experiments. The Young's modulus of PDMSe was measured to be 150 kPa, which is consistent with previous measurements of Silastic® T2 PDMSe (Feinberg et al. 2003). The measured modulus of PEGDMA-co-GMA was not different from that of PDMSe and both were greater than that of PEGDMA-co-HEMA (Table 6-2). Swelling experiments yielded lower <Mc> values than TMA measurements. The <Mc> was measured to be 160 to 240 g mol-1 and 200 to 280 g mol-1 for PEGDMA-co-HEMA and PEGDMA-co-GMA, respectively.

Table 6-2. Hydrogel characterization results: average molecular weight between crosslinks and modulus values.

	G (kPa)	E (kPa)	<Mc> TMA (g/mol)	<Mc> Swelling (g/mol)
PEGDMA-co-HEMA	30	90	240	160
PEGDMA-co-GMA	50	160	280	200
PDMSe	500	1500	---	---

Hydrogel composition

Spectral subtraction of PEGDMA from PEGDMA-co-GMA shows characteristic bands for GMA at 1715 to 1740 cm^{-1} (C=O stretch), 1485 to 1445 cm^{-1} (CH deformation), 1280 to 1230 cm^{-1} (C-O-C symmetric stretch) and 950 to 815 cm^{-1} (asymmetric stretch) (Figure 6-4). Spectral subtraction of PEGDMA from PEGDMA-co-HEMA shows characteristic peaks for HEMA, i.e., 3400 to 3200 cm^{-1} (OH stretch), 2863 to 2843 cm^{-1} (CH symmetric stretch), 1750 to 1735 cm^{-1} (C=O stretch), 1485 to 1445 cm^{-1} (CH asymmetric deformation) and 1150 to 1060 cm^{-1} (C-O-C asymmetric stretch) (Figure 6-5). These results verified that hydrogels were functionalized by the addition of GMA or HEMA monomer into the prepolymer solution before polymerization.

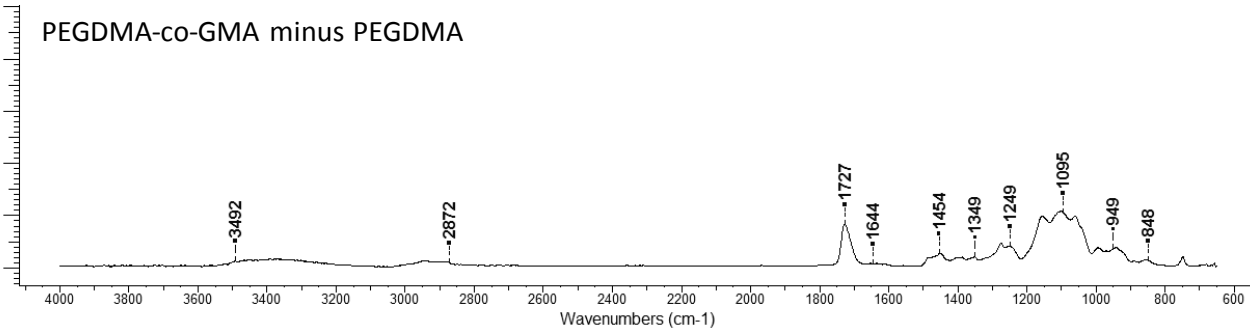

Figure 6-4. Spectral subtraction of ATR-FTIR spectra of PEGDMA-co-GMA minus PEGDMA.

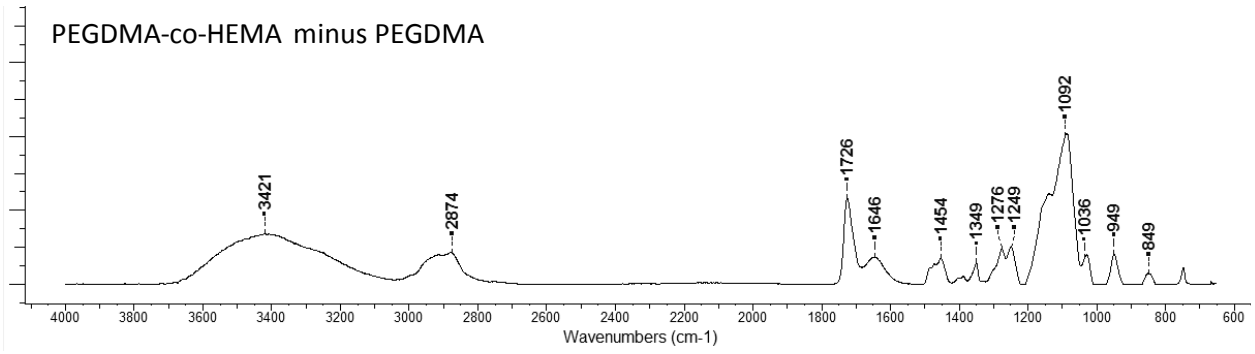

Figure 6-5. Spectral subtraction of ATR-FTIR spectra of PEGDMA-co-HEMA minus PEGDMA.

Fibronectin grafting

Spectral subtraction of PEGDMA-co-GMA from PEGDMA-co-GMA-graft-Fn show characteristic peaks for the protein Fn, i.e., 3400-3200 cm^{-1} (OH stretch) and 1650-1590 cm^{-1} (Amide I Band). Spectral subtraction of PEGDMA from PEGDMA-graft-Fn shows the same peaks; however, these peaks are much less pronounced indicating a smaller amount of protein present on the surface (Figure 6-6).

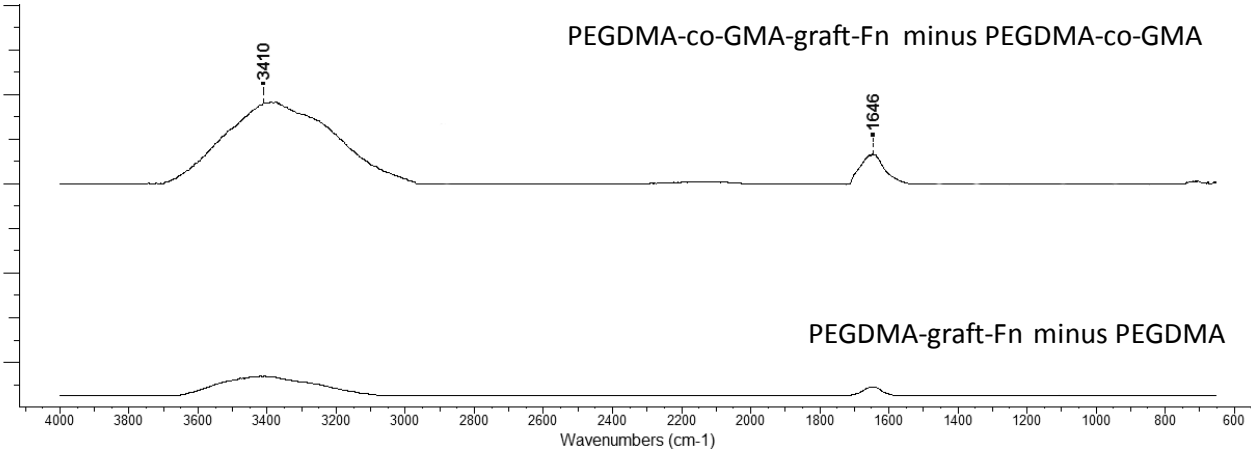

Figure 6-6. Spectral subtraction of ATR-FTIR spectra of PEGDMA-graft-Fn minus PEGDMA and PEGDMA-co-GMA-graft-Fn minus PEGDMA-co-GMA.

The epoxide ring of the GMA was reacted with the amine nucleophiles on the Fn protein in an alkaline buffer solution. PEGDMA without GMA was used as a control surface to show that Fn was grafted, not adsorbed, to the sample surfaces.

Representative fluorescent images (Figure 6-7) indicated there is very little fluorescent signal coming from the PEGDMA surface compared to the three PEGDMA-co-GMA surfaces.

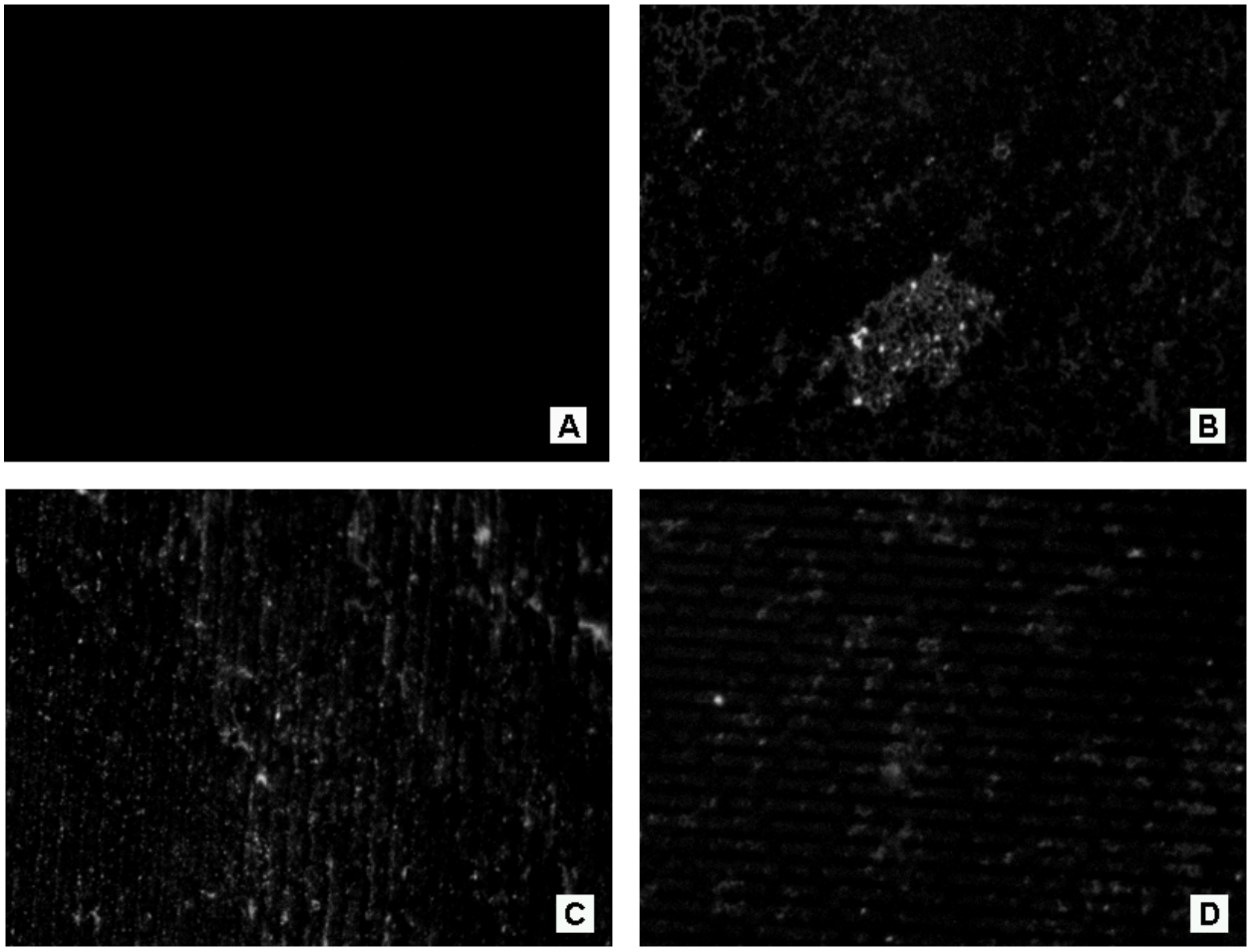

Figure 6-7. Epi-fluorescent micrographs (magnification 500x) of immunofluorescently labeled Fn. A) PEGDMA Smooth, B) PEGDMA-co-GMA Smooth, C) PEGDMA-co-GMA +0.6CH2x2, D) PEGDMA-co-GMA +1SK2x2

Average fluorescence intensity measurements confirmed that there is a statistically significant difference between the average fluorescence intensity on the smooth PEGDMA and PEGDMA-co-GMA samples (see Figure 6-8). These results along with those from ATR-FTIR indicated that Fn was grafted, not adsorbed to PEGDMA-co-GMA hydrogels.

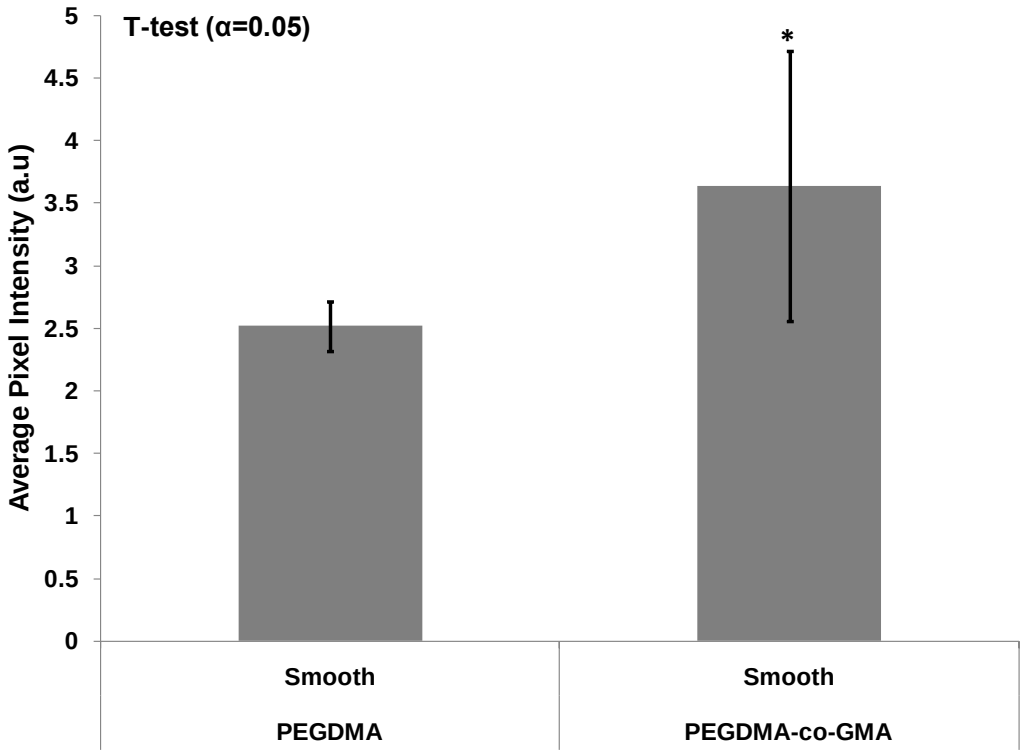

Figure 6-8. Fluorescence intensity of immunofluorescently labeled Fn. The asterisk indicates a significant statistical difference between groups based on a T-test (α=0.05, n=10).

Cell Culture Assay Results

PVEC assay

The average number of cells mm^{-2} was calculated for PEGDMA and PEGDMA-co-GMA hydrogels that had been exposed to the Fn grafting process. The average number of cells mm^{-2} was 190 and 310 for PEGDMA-graft-Fn and PEGMDA-co-GMA-graft-Fn, respectively (Figure 6-10). A Student's T-test (α=0.05) showed that there was a statistically significant difference between the average number of cells attached to each hydrogel. These results represent a 1.6-fold increase in cells attached to the Fn grafted PEGDMA-co-GMA surface versus the PEGDMA control. The average number of cells mm^{-2} attached to PEGDMA-co-GMA-graft-Fn surfaces was 160 for the +1SK2x2_n4 topography versus 50 and 60 for smooth and +1CH2x2, respectively.

There was a 3.2-fold increase in the average number of cells attached to +1SK2x2_n4 compared to the smooth and +1CH2x2 topography.

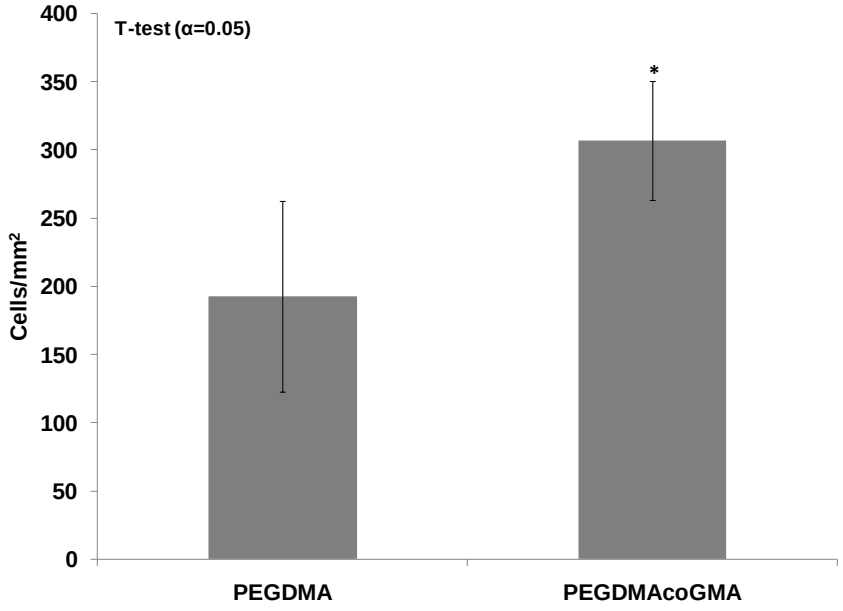

Figure 6-9. PVEC cell culture assay results: average number of cells mm^{-2} on smooth surfaces. The asterisk indicates a significant statistical difference between groups based on a T-test (α=0.05, n=30).

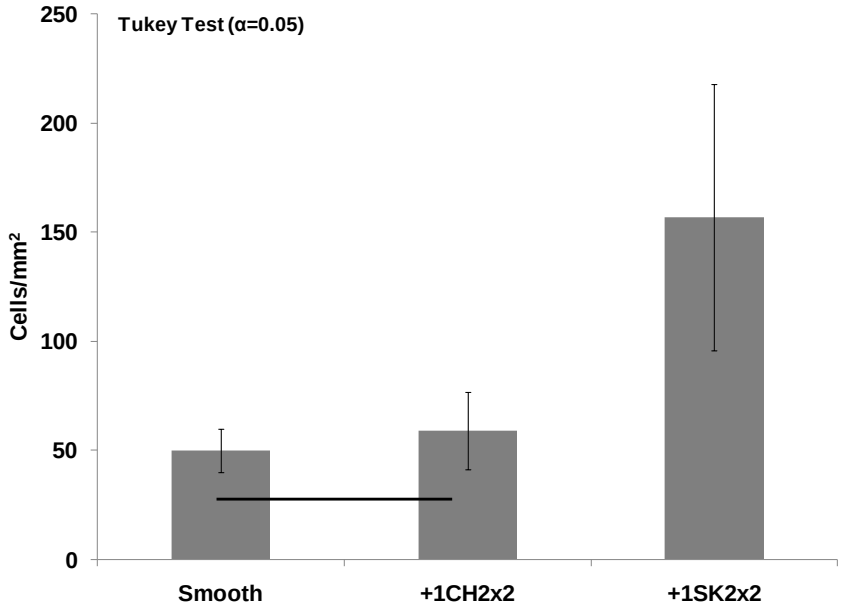

Figure 6-10. PVEC cell culture assay results: average number of cells mm^{-2} on smooth and topographically modified surfaces. The horizontal bar indicates no statistically significant difference based on a T-test (α=0.05, n=30).

Human cell assays

Cell morphology was observed as an indication of cell attachment and spreading on PEGDMA-co-GMA-graft-Fn and PDMSe surfaces. Phase contrast images show that ECs, SMCs and EPCs attached to but did not spread on PEGDMA-co-GMA-graft-Fn (Figures 6-13 and 6-17). Therefore, cell culture assays on hydrogels were discontinued after 48 h. Both HCAECs and HASMCs showed attachment and spreading on PDMSe surfaces at 24 h and 7 d. Phase contrast micrographs were taken at 10 x magnification and the orientation of the channels in each topography is indicated with an arrow as described in Figure 6-11. A blank box with no arrow indicates a smooth surface.

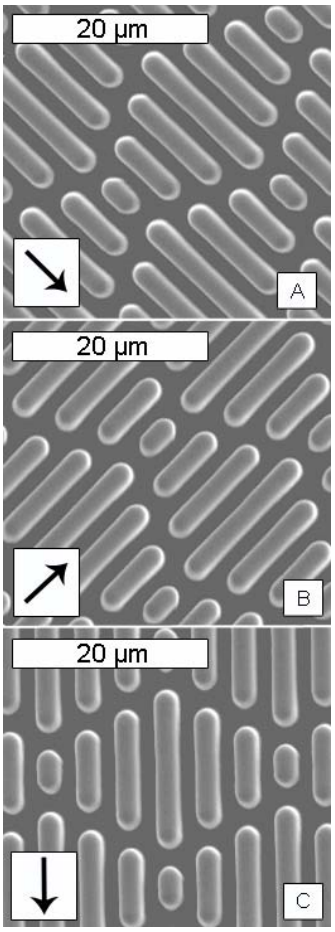

Figure 6-11. Arrows indicate the direction of the channels in each topography on phase contrast micrographs.

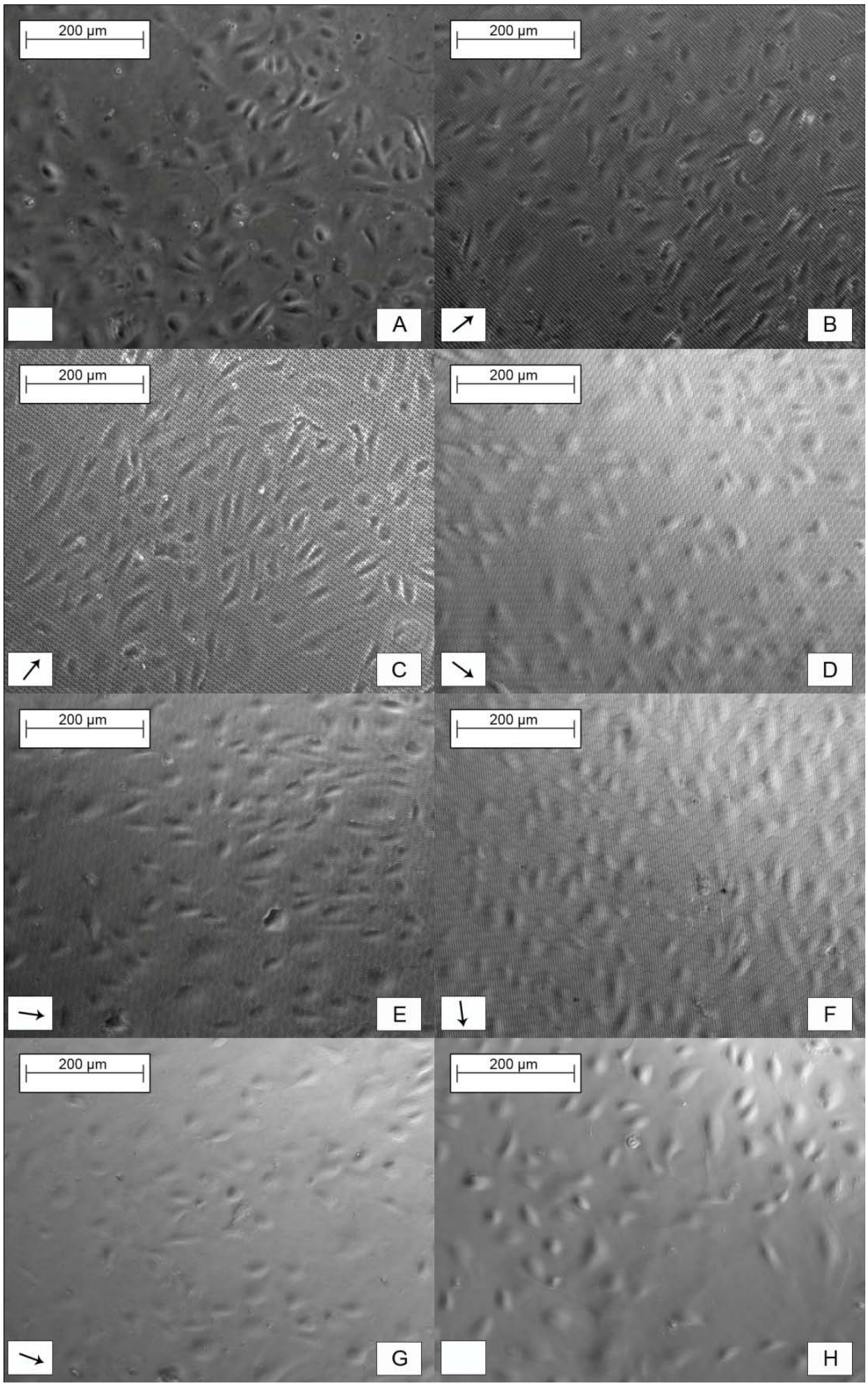

Figure 6-12. HCAECs seeded at $5x10^4$ cells/well on PDMSe A) smooth, B) +1SK2x2_n1, C) +1SK2x2_n2, D) +1SK2x2_n3, E) +1SK2x2_n4, F) +1SK2x2_n5, G) +1CH2x2 and H) TCPS after 24 h.

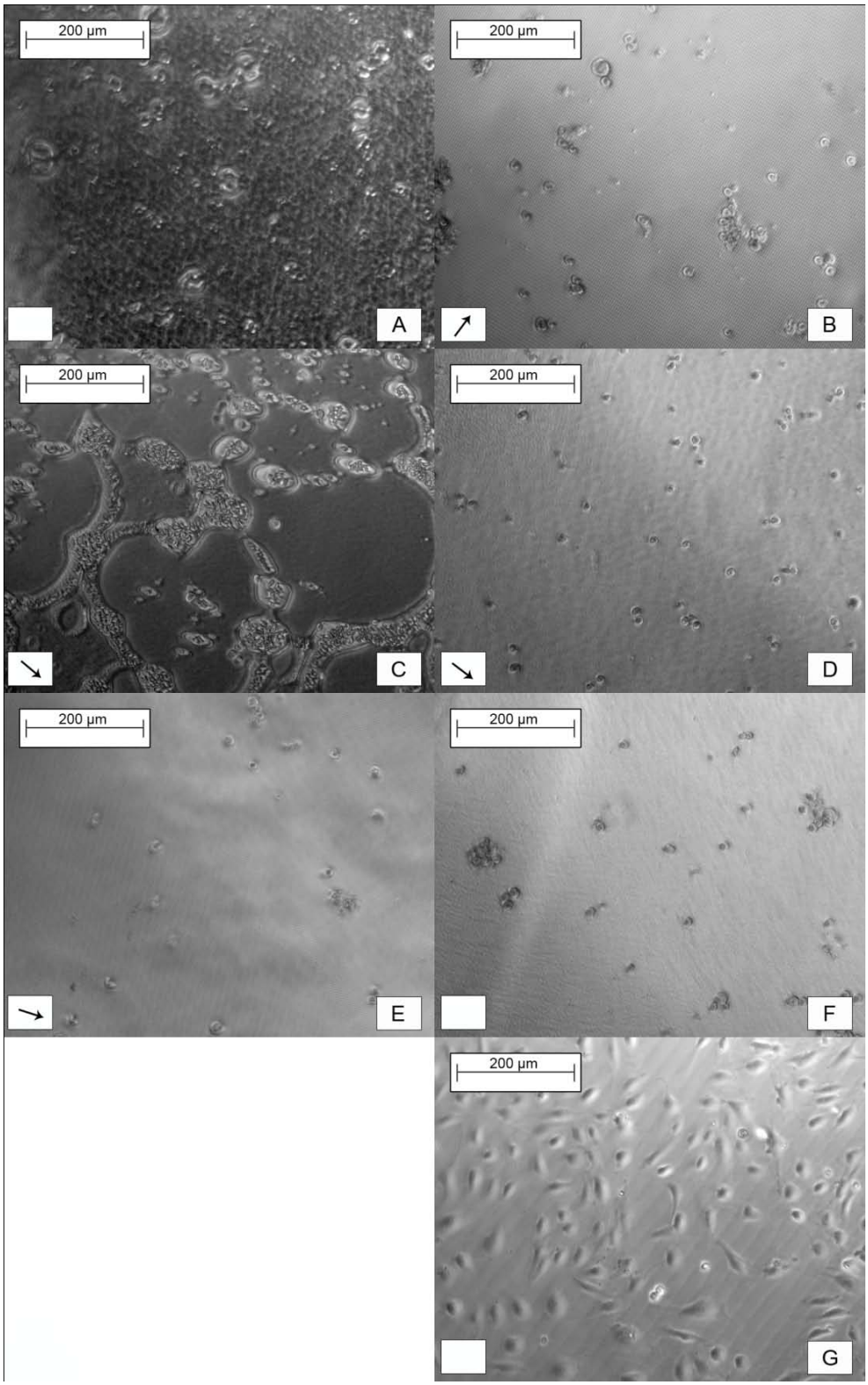

Figure 6-13. HCAECs seeded at $5x10^4$ cells/well on PEGDMA-co-GMA-graft-Fn A) smooth, B) +1SK2x2_n1, C) +1SK2x2_n2, D) +1SK2x2_n3, E) +1SK2x2_n4, F) +1SK2x2_n5, and G) TCPS after 24 h.

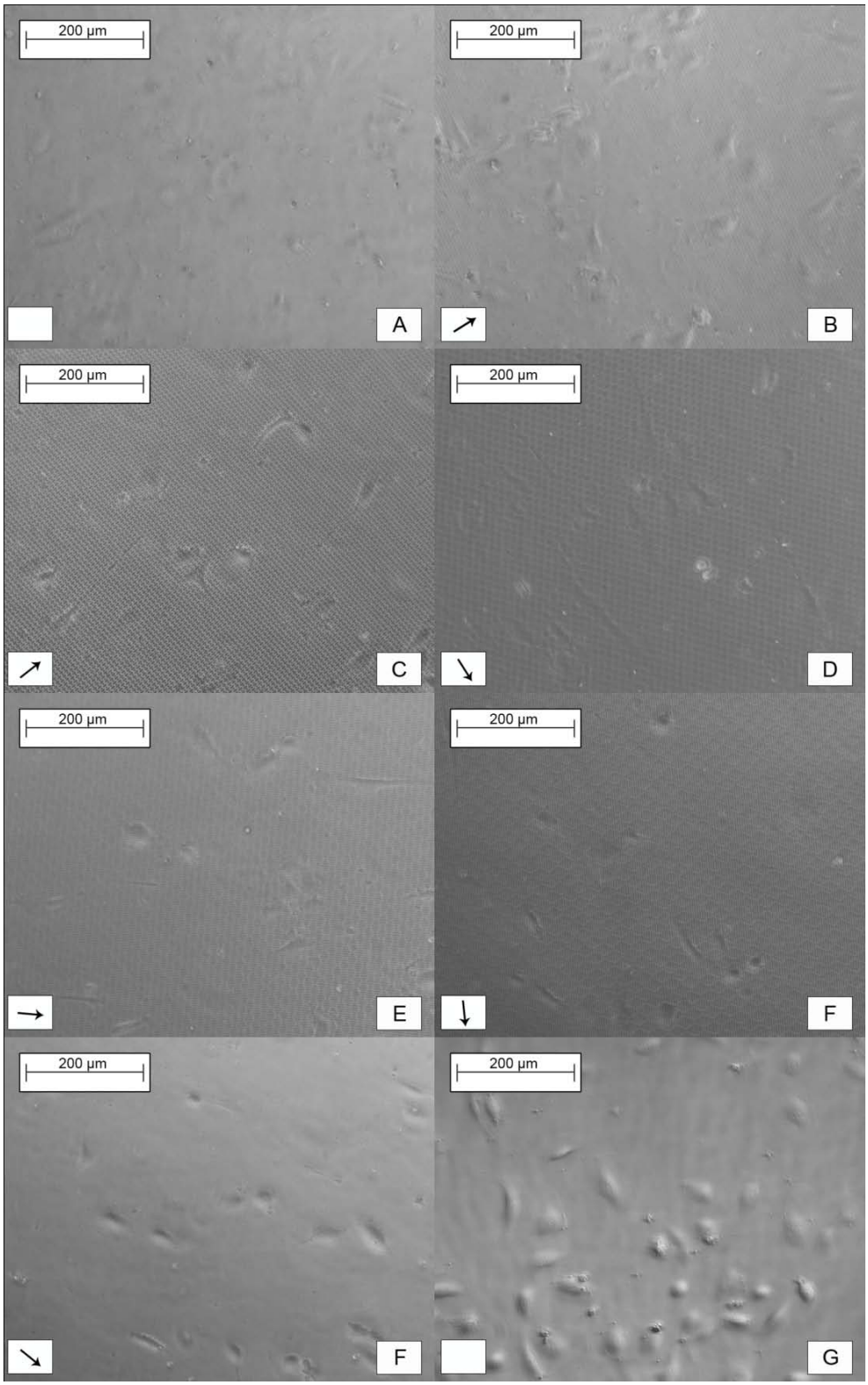

Figure 6-14. HCAECs seeded at $2.5x10^4$ cells/well on PDMSe A) smooth, B) +1SK2x2_n1, C) +1SK2x2_n2, D) +1SK2x2_n3, E) +1SK2x2_n4, F) +1SK2x2_n5, G) +1CH2x2 and H) TCPS after 24 h.

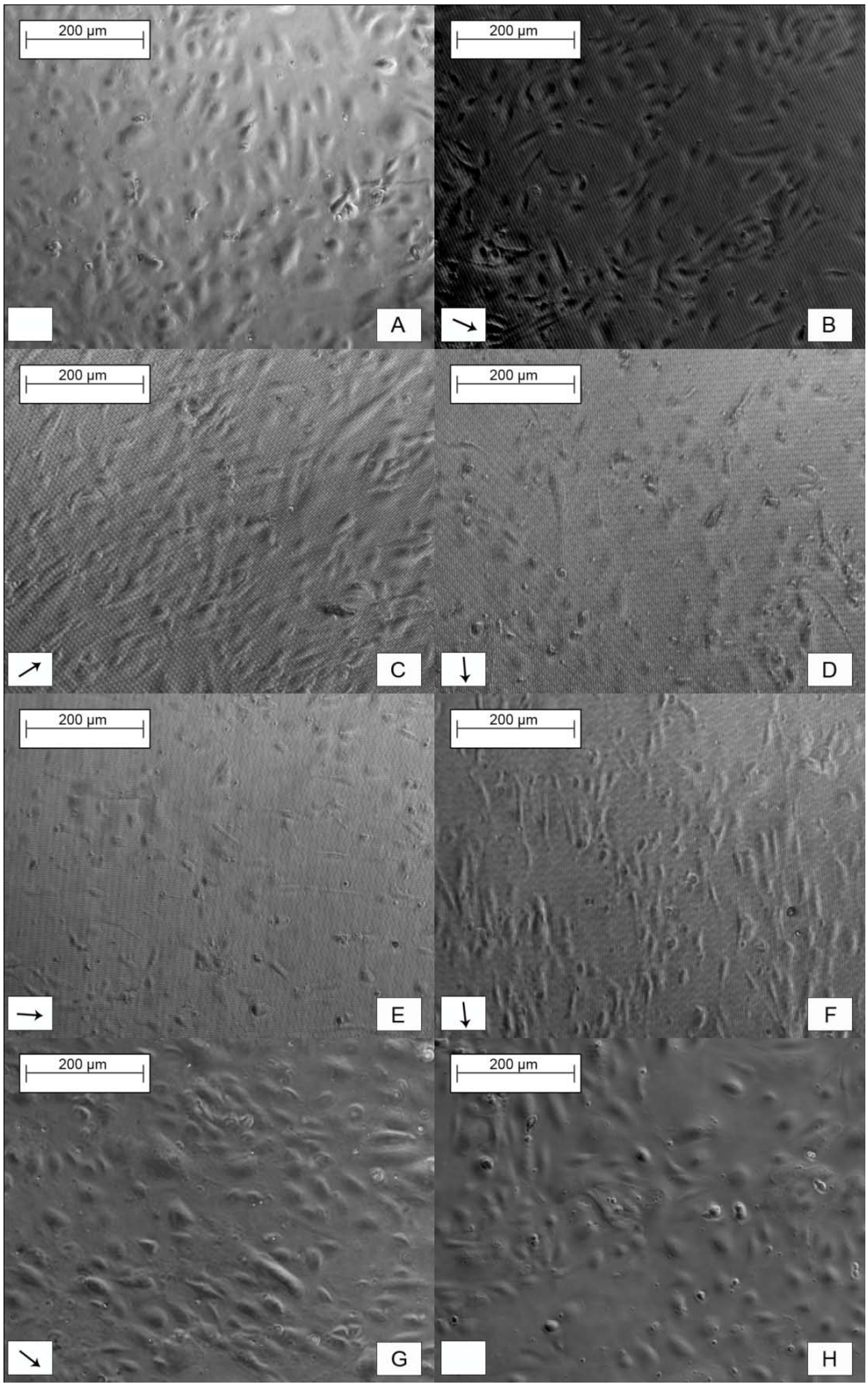

Figure 6-15. HCAECs seeded at $2.5x10^4$ cells/well on PDMSe A) smooth, B) +1SK2x2_n1, C) +1SK2x2_n2, D) +1SK2x2_n3, E) +1SK2x2_n4, F) +1SK2x2_n5, G) +1CH2x2 and H) TCPS after 7 d.

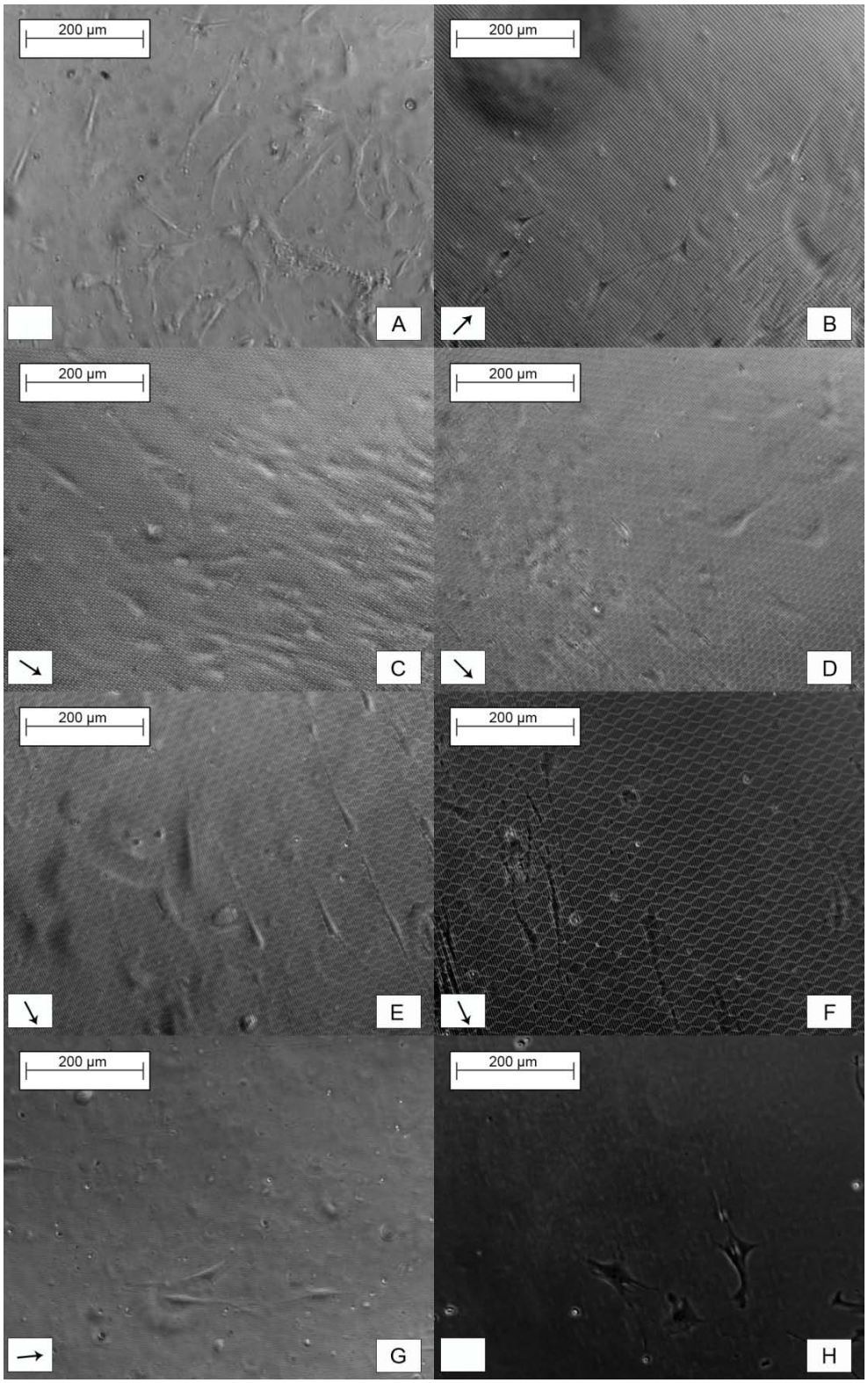

Figure 6-16. HASMCs seeded at 2.5x10^4 cells/well on PDMSe A) smooth, B) +1SK2x2_n1, C) +1SK2x2_n2, D) +1SK2x2_n3, E) +1SK2x2_n4, F) +1SK2x2_n5, G) +1CH2x2 and H) TCPS after 24 h.

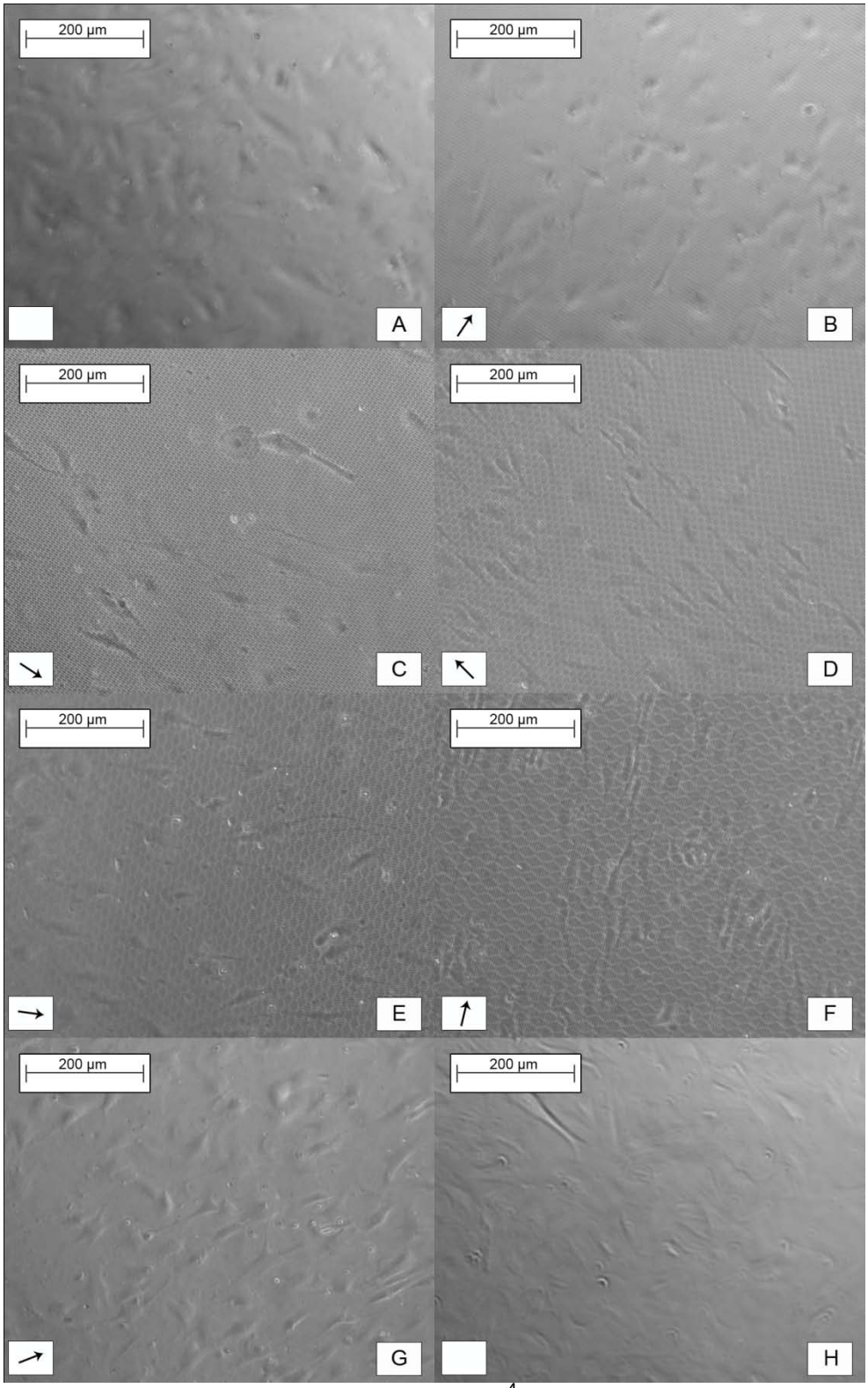

Figure 6-17. HASMCs seeded at $2.5x10^4$ cells/well on PDMSe A) smooth, B) +1SK2x2_n1, C) +1SK2x2_n2, D) +1SK2x2_n3, E) +1SK2x2_n4, F) +1SK2x2_n5, G) +1CH2x2 and H) TCPS after 7 d.

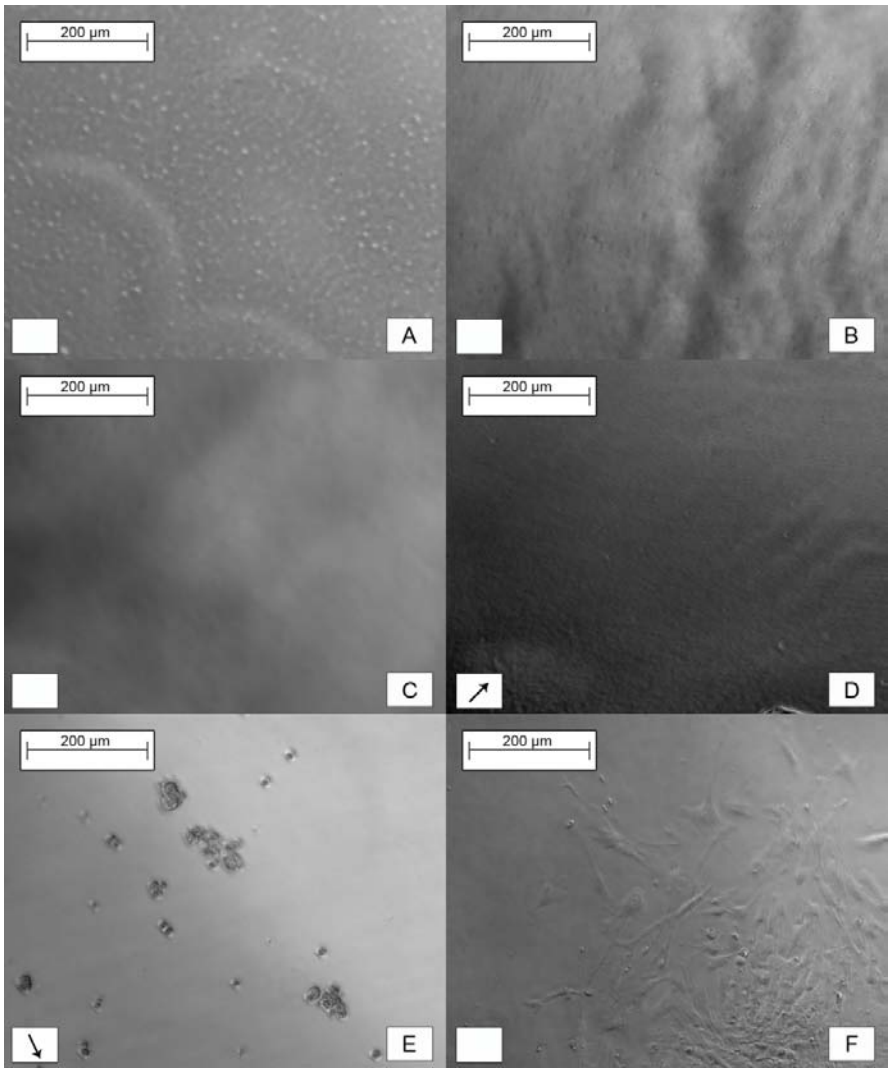

Figure 6-18. HASMCs seeded at $2.5x10^4$ cells/well on PEGDMA-co-GMA-graft-Fn A) smooth, B) +1SK2x2_n1, C) +1SK2x2_n2, D) +1SK2x2_n3, E) +1SK2x2_n4 and F) TCPS after 24 h.

Cell morphology was quantified by calculating the CSI index for each cell. The CSI ranges from 0 (elongated, linear cells) to 1 (circular shaped cells). After 24 h HCAECs showed no statistically significant elongation compared to a smooth PDMSe standard and a TCPS control (Figure 6-19). The average CSI for HCASMCs after 24 h was lowest on +1SK2x2_n4, however this value was only statistically different from +1SK2x2_n2 and the TCPS control (Tukey test α=0.05).

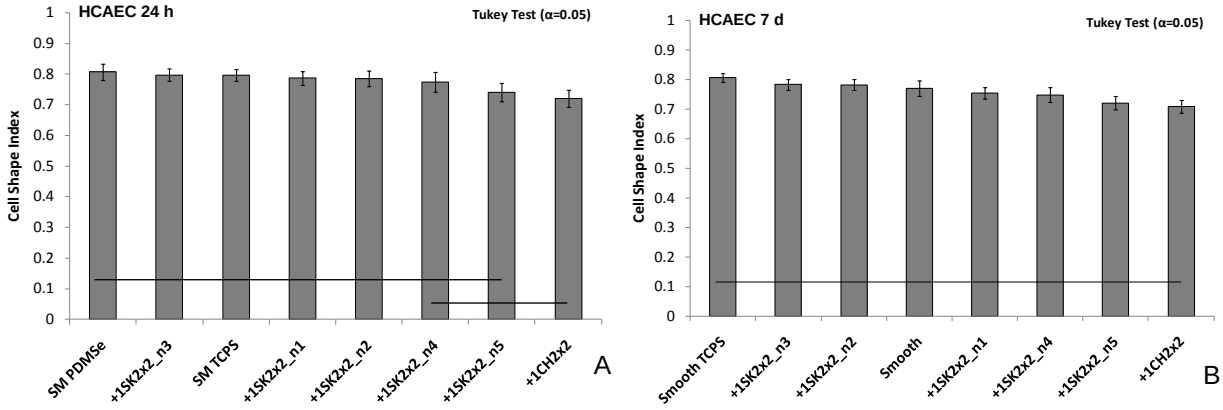

Figure 6-19. Average CSI for HCAECs cultured on topographies replicated in PDMSe A) after 24 h and B) after 7 d. Horizontal bars indicate no statistical differences.

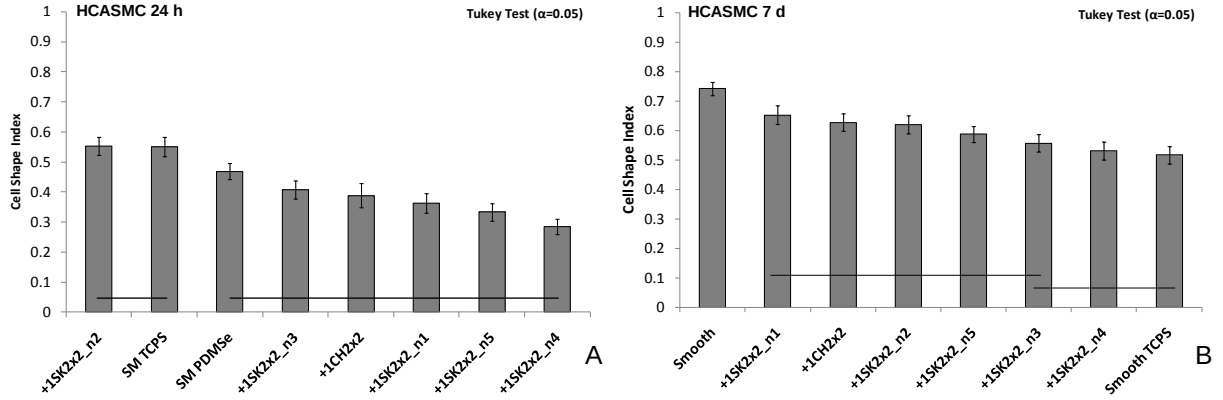

Figure 6-20. Average CSI for HCASMCs cultured on topographies replicated in PDMSe A) after 24 h and B) after 7 d. Horizontal bars indicate no statistical differences.

The average CSI for HCAECs cultured for 7 d was lowest on +1CH2x2, which was not statistically different from +1SK2x2_n5, +1SK2x2_n4 and +1SK2x2_n1 (Figure 6-20). Elongation was highest on +1SK2x2_n3 and +1SK2x2_n4 for HCASMCs after 7 d. The average CSI for these surfaces was not statistically different from the TCPS control (Figure 6-20) (Tukey test α=0.05). All topographies increased HCASMC elongation after 7 d compared to smooth PDMSe (Tukey test α=0.05).

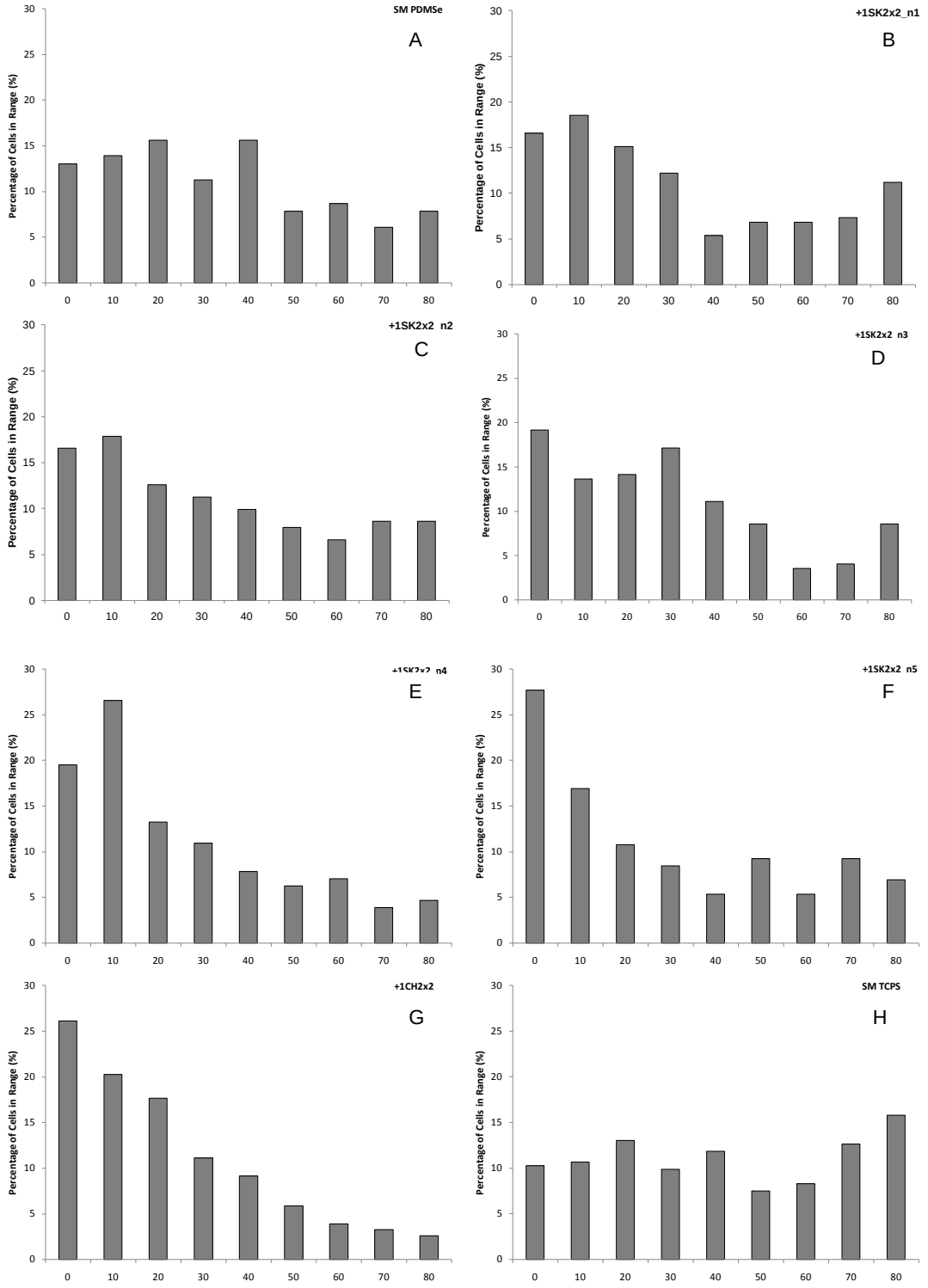

Figure 6-21. Distribution of the percentage of HCAECs at angles in each 10 degree range after 24 h on A) Smooth PDMSe, B)+1SK2x2_n1, C)+1SK2x2_n2, D)+1SK2x2_n3, E) +1SK2x2_n4, F) +1SK2x2_n5, G) +1CH2x2 and H) TCPS.

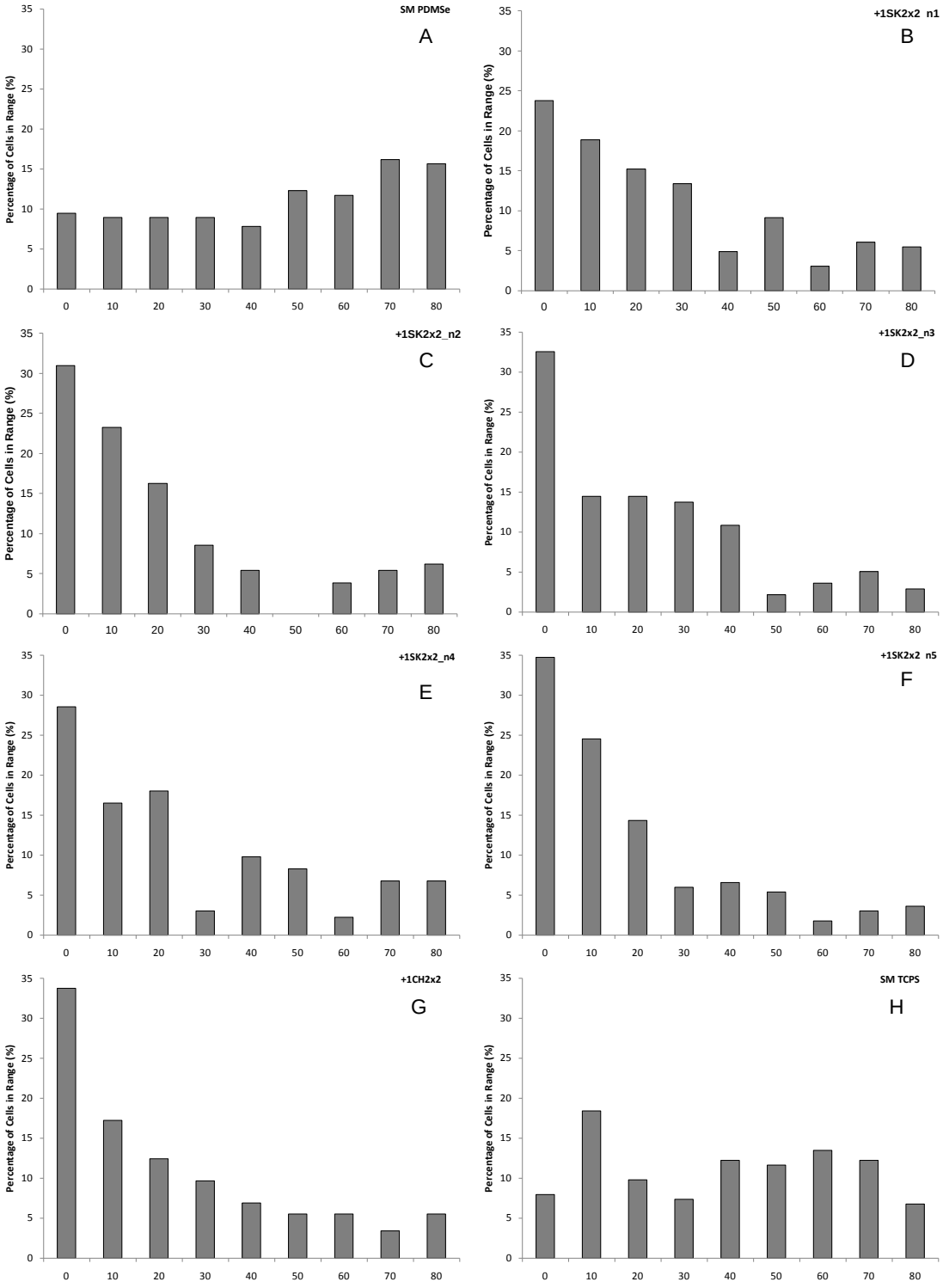

Figure 6-22. Distribution of the percentage of HCAECs at angles in each 10 degree range after 7 d on A) Smooth PDMSe, B)+1SK2x2_n1, C)+1SK2x2_n2, D)+1SK2x2_n3, E) +1SK2x2_n4, F) +1SK2x2_n5, G) +1CH2x2 and H) TCPS.

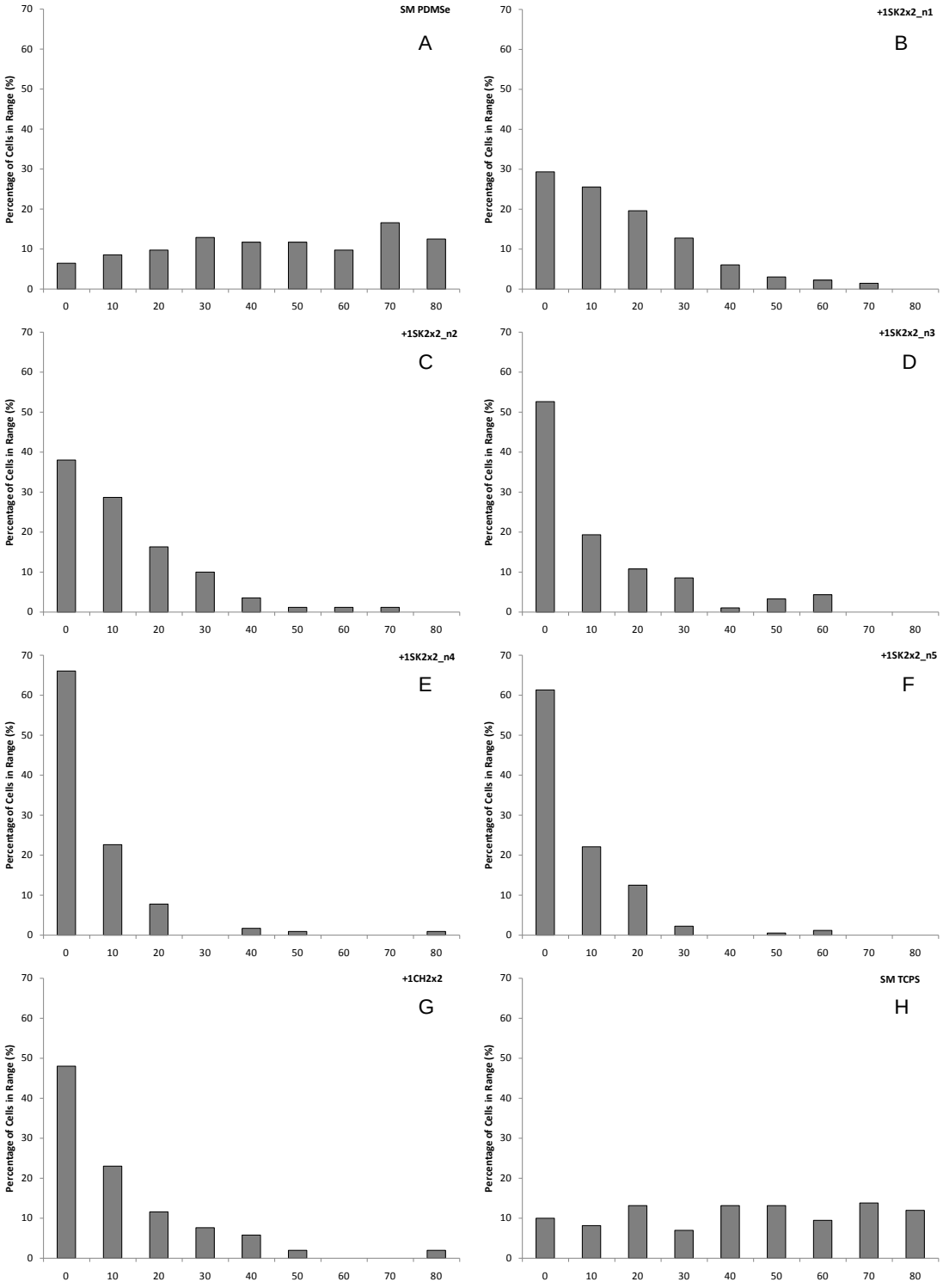

Figure 6-23. Distribution of the percentage of HCASMCs at angles in each 10 degree range after 24 h on A) Smooth PDMSe, B)+1SK2x2_n1, C)+1SK2x2_n2, D)+1SK2x2_n3, E) +1SK2x2_n4, F) +1SK2x2_n5, G) +1CH2x2 and H) TCPS.

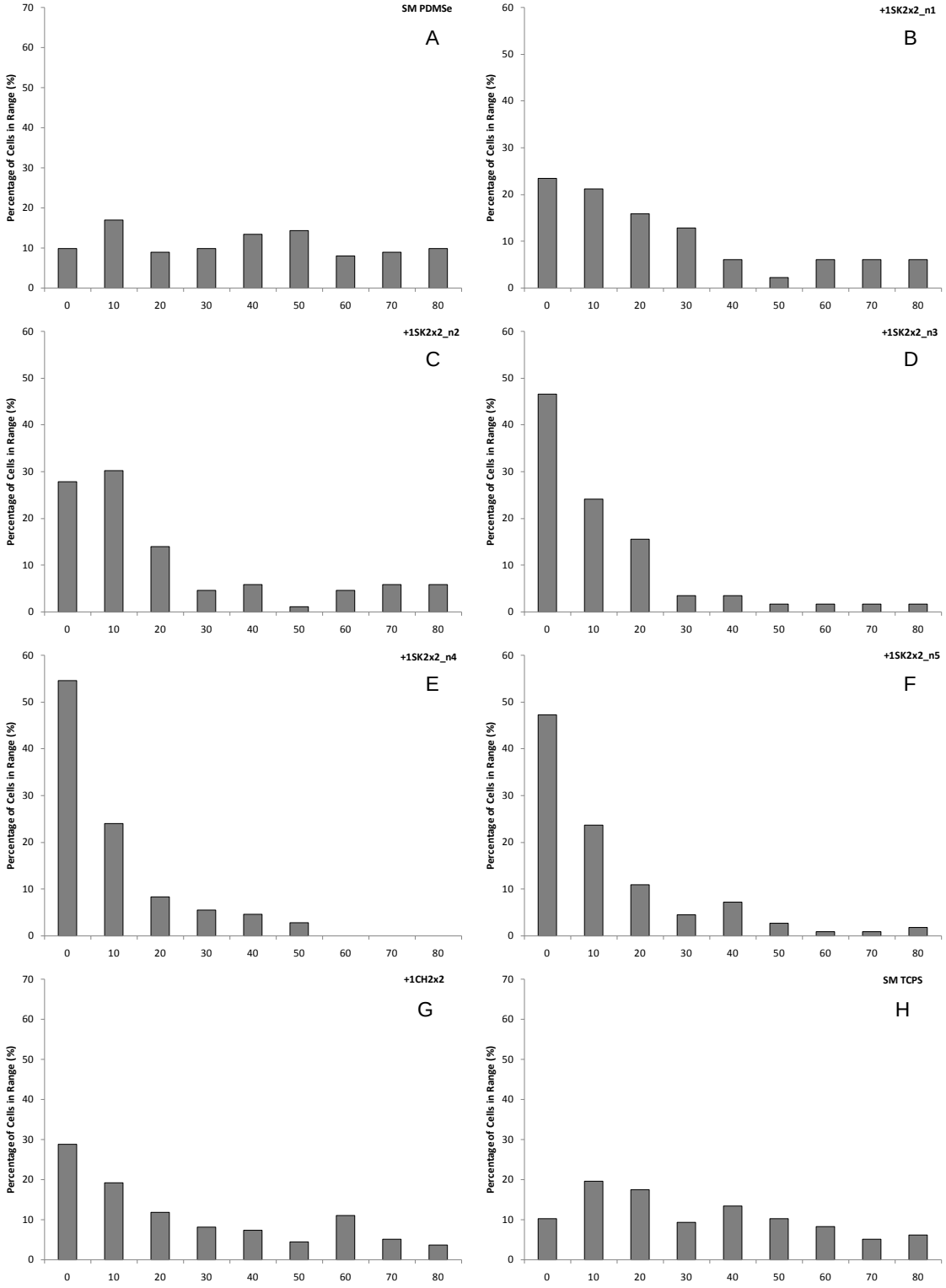

Figure 6-24. Distribution of the percentage of HCASMCs at angles in each 10 degree range after 7 d on A) Smooth PDMSe, B)+1SK2x2_n1, C)+1SK2x2_n2, D)+1SK2x2_n3, E) +1SK2x2_n4, F) +1SK2x2_n5, G) +1CH2x2 and H) TCPS.

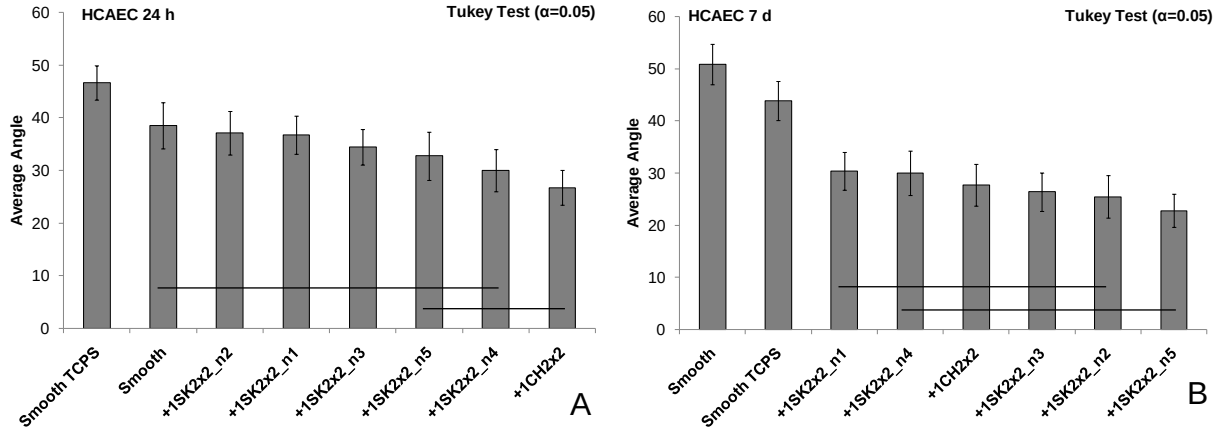

Figure 6-25. Average angle of cell orientation relative to the channels in the topography is plotted for A) HCAEC after 24 h in culture and B) HCAEC after 7 d in culture.

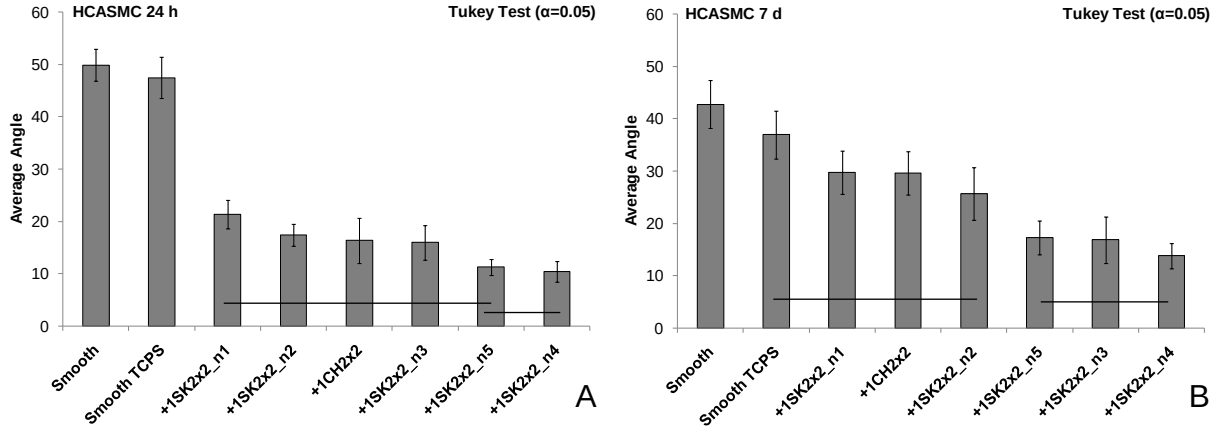

Figure 6-26. Average angle of cell orientation relative to the channels in the topography is plotted for A) HCASMC after 24 h in culture and B) HCASMC after 7 d in culture.

Both HCAECs and HCASMCs showed increasing orientation along the direction of the channels in the topographies after 24 h with increasing number of features (n) when cultured on the n-series Sharklet AF™ topographies. The highest degree of orientation was observed on the +1CH2x2 topography for HCAECs cultured for 24 h. Cells cultured on the smooth PDMSe standard and TCPS control did not show preferential orientation, i.e., the mean angles on these topographies were approximately 45°. After 7 d the highest degree of orientation was observed on +1SK2x2_n5 for HCAECs

(Figure 6-25). More HCAECs were orientated along the direction of the channels in each topography after 7 d than after 24 h. The mean angles were lower on topographically modified surfaces after 7 d. The highest degree of orientation was observed on +1SK2x2_n4 for HCASMCs after 24 h and 7 d (Figure 6-26).

Discussion

Functionalized PEGDMA hydrogels were created, characterized, topographically modified and tested as cell culture substrates. The solubility parameters were measured for all three hydrogels. Maximum swelling occurred in chloroform indicating a solubility parameter of 19 $MPa^{1/2}$ which corresponds well with the ranges of experimental and theoretical values of solubility parameter for crosslinked poly(ethylene oxide) (PEO) reported in the literature, 19 to 40 $MPa^{1/2}$ and 18 to 31 $MPa^{1/2}$ respectively (Barton, 1990; Graham et al., 1981; Katz & Salee, 1968). The average molecular weight between crosslinks and Young's modulus were measured for each hydrogel using swelling experiments and TMA. Subtraction of ATR-FTIR spectra verified that the hydrogels were functionalized by the addition of GMA or HEMA monomer into the prepolymer solution before polymerization. Spectral subtraction and immunofluorescence microscopy both confirmed grafting of Fn to the PEGDMA-co-GMA hydrogel by way of the epoxide ring.

Assays with PVECs showed a 1.6-fold increase in cells attached to the Fn grafted PEGDMA-co-GMA surface versus the PEGDMA control. This value corresponds well to the 2-fold increase that was predicted in the hypothesis and is consistent with previously reported results (Markway, et al. 2008). The average number of cells attached to +1SK2x2_n4 was 3.2-fold larger than the average number of cells attached to the smooth and +1CH2x2 topography after 24 h. Topographical modification of PEG-based

biomaterials was shown to increase fibroblast attachment versus smooth (Schulte, et al. 2009). Channels ranging in size from 5 to 50 μm and pillars 3 μm in diameter with 3 or 6 μm spacing increased attachment and spreading of fibroblasts after 4 h and 24 h (Schulte, et al. 2009). It is possible that the topographical modification led to a change in the amount, type and/or conformation of protein adsorbed to the PEG surfaces. The topographically modified surfaces could also direct or promote cytoskeletal organization which could also lead to better attachment and spreading of the cells. The +1SK2x2_n4 topography showed a clear increase in PVEC attachment and spreading versus smooth after 24 h while the +1CH2x2 topography did not. This increase was most likely due to cytoskeletal organization. The small feature spacing did not allow cells to settle within the topographies and this difference may explain why cell attachment did not increase on the channels topography versus a smooth surface as it did in the report by Schulte, et al.

Hydrogels based on PEG are known to be non-adhesive surfaces i.e., non-specific protein adsorption is minimized (Ostuni, et al. 2001, Balamurugan, et al. 2005, Schulte, et al. 2009). These materials were selected as a cell culture substrate so that protein adsorption and therefore cellular attachment could be controlled by chemical and topographical modification. All surfaces made of PEGDMA-co-GMA-graft-Fn hydrogel showed attachment of HCAECs and HASMCs after 24 h. Minimal cell spreading was observed after 3 d in culture indicating these hydrogels did not provide an ideal substrate for cell culture. Assays on the PEGDMA-co-GMA-graft-Fn hydrogels were discontinued after 48 h. Both cell types attached to and spread on all PDMSe surfaces.

Elongation and alignment of HCAECs and HASMCs were quantified. Topographies with the greatest number of distinct features (n=4 and n=5) in the n-series and +1CH2x2 resulted in the largest elongations and orientations of HCAECs and HCASMCs after 24 h and 7 d. Discontinuous microchannels were shown to increase expression of proteins representative of the contractile phenotype in vascular smooth muscle cells (Cao, et al. 2010). Topography may trigger alignment and elongation, as well as some intracellular signal that triggers the expression of the contractile phenotype (Thakar et al. 2003, Sarkar, et al. 2006a, Beamish et al. 2010). Using topography to direct HCASMCs to express the contractile phenotype could be a strategy to reduce intimal hyperplasia in small diameter vascular graft applications. Protein expression of HCASMCs should be quantified in cells cultured on both topographically modified and smooth PDMSe to determine if any of the n-series topographies could be used to regulate not only orientation, but also phenotype of these cells. Proteins expressed by SMCs in the contractile phenotype include α-smooth muscle actin and myosin heavy chain. Immunostaining assays could be used to quantify the expression of these proteins by cells cultured on each topography (Beamish, et al. 2010).

Functionalized PEGDMA hydrogels are not an ideal cell culture substrate for small diameter vascular graft applications. Cells attached to but did not spread on both smooth and topographically modified surfaces created in PEGDMA-co-GMA-graft-Fn. It is, however, still feasible to use topographies created in PDMSe to direct cell morphology and possibly phenotype. Further studies should be performed to quantify protein expression of HCAECs and HASMCs on both smooth and topographically modified surfaces. The ability to use topography to select a certain cell phenotype

would advance small diameter vascular graft technology. Studies should also be continued with EPCs to determine the influence of topography on differentiation.

CHAPTER 7
CONCLUSIONS AND FUTURE WORK

Conclusions

Non-Toxic Antifouling Strategies

Biofouling is a technically complex problem that remains an economic and environmental concern. New combinations of material chemistries and topographies were evaluated for antifouling properties with organisms representing three diverse phylogenetic groups, viz. the eukaryotic Plantae (*Ulva*), the eukaryotic Chromista (*Navicula*) and the prokaryotic Bacteria (*Cobetia*) (Cavalier-Smith 2004). Engineered antifouling topographies in PDMSe inhibited attachment of *C. marina* up to 99% versus a smooth standard. The factors contributing to the slope of the line created when plotting the attachment model were investigated. The size and motility of bacterial cells and algal spores were incorporated into the attachment model (Long, et al. 2010) by multiplying the ERI_{II} by the Re of the cells. The results showed a negative linear correlation of the normalized transformed attachment densities for both organisms with ERI_{II}*Re ($R^2 = 0.77$) (Magin, et al. 2010b).

The same microtopographies also created in PDMSe reduced the attachment density and attachment strength of cells of the diatoms *Navicula* and *Seminavis* compared to smooth PDMSe. However, the results did not correlate with current models, i.e., the attachment model and attachment point theory. A new analysis showed that the average normalized, transformed attachment density of *Navicula* after exposure to shear stress (48 Pa) correlated with the contact area between the diatom and a topographically modified surface ($R^2 = 0.82$).

Functionalized PEGDMA hydrogels significantly reduced attachment and attachment strength of *Navicula* and *C. marina*. All three hydrogel compositions reduced significantly (p=0.05) initial attachment of cells of *Navicula* (up to 58%) and *C. marina* (up to 62%), as well as zoospores of *Ulva linza* (up to 97%) compared to a smooth PDMSe standard. A shear stress (45 Pa), in a water channel, eliminated up to 95% of the initially attached *Navicula* cells from the topopgraphically patterned surfaces relative to smooth PDMSe surfaces. Compared to the smooth PDMSe standard 79% of the *C. marina* cells were removed from all hydrogel compositions when exposed to the same shear stress. The Sharklet AF™ microtopography patterned PEGDMA-co-HEMA surfaces reduced attachment of *Ulva* by 97% compared to a smooth PDMSe standard. The attachment of spores of *Ulva* to engineered microtopographies in PDMSe and PEGDMA-co-HEMA negatively correlated with the attachment model that includes the engineered roughness index (ERI_{II}) multiplied by the Reynolds number (Re) of the organism. The attachment model was extended with the addition of a surface energy term. Attachment densities of cells from two evolutionarily diverse groups correlated with the attachment model for various engineered topographies replicated in materials other than PDMSe ($R^2 = 0.80$). The extension of the attachment model to incorporate new fouling organisms and new surface chemistries creates an algorithm that can be used to design non-toxic antifouling surfaces.

Cell Culture Substrates

Hydrogels based on PEGDMA and standards made of PDMSe were topographically modified and evaluated as substratum materials for mammalian cell culture. Capturing endothelial progenitor cells (EPCs) and inducing differentiation into the endothelial cell (EC) phenotype is the ideal way to re-endothelialize a small-

diameter vascular graft. Likewise, modulation of the SMC phenotype is a way to reduce intimal hyperplasia after the implantation of a synthetic graft. Substratum elasticity has been reported to direct stem cell differentiation into specific lineages (Engler, et al. 2006). Functionalized PEGDMA hydrogels provided good compliance, high fidelity of topographic features and sites for surface modification with biomolecules. Fibronectin grafting and topography both increased EC attachment. This combination of adjustable elasticity, surface chemistry and topography has the potential to promote the capture and differentiation of EPCs into a confluent EC monolayer.

Engineered microtopographies replicated in PDMSe directed alignment and elongation of HCAECs and HCASMCs compared to smooth surfaces. Both elongation and alignment along the channels of the features in the topographies increased with increasing (n), the number of unique features, on the Sharklet AF™ patterns. The ability to control cell morphology is important for developing healthy cell cultures that function in the same way as cells grown *in vivo*.

Future Work

Non-Toxic Antifouling Strategies

The attachment model can be used to design new combinations of surface chemistry and engineered microtopography for antifouling applications. However, the model does not completely describe all of the complex factors that contribute to biofouling. The model should be tested to investigate other factors contributing to the slope of the model and validate its current form. The incorporation of the Re of the organism into the model can be validated by running additional assays using swimming organisms in static assays or non-swimming organisms under flow conditions. Flagellated marine bacteria, for example, would have a different Re than *C. marina* and

could be used as a test organism. Since diatoms are not motile in the water column the attachment of these cells could be measured under flow conditions so that an average Re could be calculated for the organism. These results may lead to the incorporation of a third marine fouling organism into range described by the current model.

Biodiversity within a cell or spore population is another factor that could be incorporated into the attachment model. One way to test this concept is to transfect a population of cells or spores at one age with green fluorescent protein and an older population of the same cells or spores with yellow fluorescent protein and track attachment. Older cells or spores may attach with different affinity or in different preferential locations on topographies.

Engineered antifouling topographies should be created with a range of surface energies and evaluated for fouling resistance with a standard *Ulva* attachment assay. These data can be used to validate the addition of the surface energy term to the current attachment model.

Cell Culture Substrates

Increased alignment and elongation of HCASMCs could be triggering a switch from the synthetic to the contractile phenotype. Cells in the contractile phenotype contract in response to molecular signals and have a low proliferative index. Both of these qualities are desired in cells growing on a newly implanted vascular graft. Intimal hyperplasia, a result of excessive smooth muscle cell proliferation, is one of the leading causes of restenosis in small diameter vascular grafts. Controlling the phenotype of HCASMCs that are in contact with a graft could reduce the probability of graft occlusion. The expression of contractile proteins in HCASMCs cultured on engineered

microtopographies, such as α-smooth muscle actin and myosin heavy chain should be quantified to confirm phenotypic expression.

The aim of the cell culture substrate work was to create a cell culture substrate for small-diameter vascular graft applications that has the potential to re-endothelialize *in vivo* to reduce neointimal hyperplasia and thrombosis. It was hypothesized that a combination of surface chemistry and topography on a graft surface would capture circulating EPCs in the peripheral blood and promote their differentiation into ECs to create a continuous tissue layer within the lumen of the graft. A biomolecular surface chemistry such as a bioactive peptide or antibody would increase recruitment of endothelial progenitor cells and topographical modification would provide mechanical cues to induce differentiation into the endothelial cell phenotype. This research should be continued in order to examine the ability of physical cues such as engineered microtopographies to induce cell differentiation.

Engineered topographies that induce differentiation into the EC phenotype could be combined with those that direct SMCs to remain in the contractile phenotype to create a platform for building vascular graft materials. Since SMCs have a higher aspect ratio than ECs, i.e., SMCs are much longer than they are wide, changing the width and spacing of the topographies could influence differentiation to one phenotype over the other or provide for selection of SMCs and/or ECs from a co-culture population. The influence of engineered microtopographies on the formation of an EC monolayer could also be evaluated by staining for a protein present in EC gap junctions such as vascular endothelial caderhin. The formation of functional gap junctions is essential for EC function *in vivo*.

Cell stiffness has been shown to be influenced by substrate modulus (Engler, et al. 2006, Feinberg, et al. 2009). Cell stiffness may also play a role in how cells interact with engineered microtopographies. A stiffer cell, for example, could deform microtopographic features to settle in between features, while a less stiff cell might spread across the features. To investigate cell stiffness the antimitotic agent, nocodazole, could be added to cells to decrease cell stiffness when seeding cells onto the surfaces. Nocodazole disrupts microtubules by binding to β-tubulin and preventing the formation of disulfide linkages. This action inhibits microtubule polymerization within cells. Nocodazole can easily be rinsed from the cells after attachment to the surface to restore a normal degree of stiffness. This treatment could be used to create functional monolayers of cells on engineered microtopographies.

APPENDIX A
REYNOLDS NUMBER CALCULATIONS

C. marina:

Stationary Phase L = 1 µm

Logarithmic Growth Phase L = 2 µm

Flow Cell Parameters:

Q = $2x10^{-5}$ L/s h = 1.27 $x10^{-4}$ m w = $1.27x10^{-2}$ m

v = $9.7x10^{-5}$ L μ = 1 $x10^{-2}$ kg/m-s ρ = $1x10^{3}$ kg/m^3

$$Q = \langle v_x \rangle hw \tag{A-1}$$

$$\langle v_x \rangle = \frac{\left(\frac{2*10^{-5}L}{s}\right)*\left(\frac{0.001\ m^3}{1\ L}\right)}{1.27*10^{-2}\ m*1.27*10^{-4}\ m} \tag{A-2}$$

$$\langle v_x \rangle = 1.2 * 10^{-3}\ m/s \tag{A-3}$$

$\langle v_x \rangle$ is the average velocity within the flow cell. The velocity of the bacteria relative to the fluid (V) near the wall was estimated to be 20% of the average fluid velocity in the flow cell.

$$Re = \frac{\rho VL}{\mu} \tag{A-4}$$

C. marina:

Stationary Phase Re = 2.5 x 10^{-3} in the flow cell

Logarithmic Growth Phase Re = 5 x 10^{-3} in the flow cell

Ulva:

The diameter of the spore body was taken to be the characteristic length: L = 5 µm. The average swimming speed was reported to be 150 µm/s (Heydt et al. 2007). This value was taken to be the velocity of the spore relative to the fluid (V).

$Re = 7.7 \times 10^{-4}$

APPENDIX B
SUMMARY OF RECENT SMALL-DIAMETER VASCULAR GRAFT LITERATURE

Table B. Summary of recent literature on small-diameter vascular grafts.

Author(s) Year	Material(s)	Processing	Cell Type(s)	Advantages	Disadvantages
(Wu, et al. 2007)	Type I Collagen glutaraldehyde crosslinked	Bi-layer membrane	SMC EC Implated in rat	Good mechanical properties Regenerated rat vena cava in vivo	Have to remove and culture cells ex vivo
(Chan, et al. 2007)	Type I Collagen photochemically crosslinked with rose Bengal	gel	Subcutaneous implantation in rat	Better mechanical properties than uncrosslinked collagen gels Good stability and tissue compatibility	Not tested with vascular cells or in vasculature Only loose connective tissue grew on implant
(Cummings, et al. 2004)	Type I Collagen Fibrin	3D matrix gel	Rat aortic SMC	Fibrin can be used to change mechanical properties of collagen gel	No difference in cell proliferation among samples Mechanical properties still do not match artery No cell differentiation / endothelialization
(Nguyen and West 2002)	PEG-co-poly(α-hydroxy acid)	Photopolymerizable hydrogels	ECs Implanted in rat SMC	Can control modulus, permeability, bioerodability Cells grow and spread Can attach grow factors and adhesion molecules	Must optimize mechanical properties
(Zhu, et al. 2005)	PCL-*b*-PEG-*b*-PCL-DA	Micropatterned foldable hydrogel UV embossing	3T3 fibroblasts	Biocompatible Biodegradable Patternable High water content Permeability	Shrinking/Swelling of patterned surface Not tested with ECs or SMCs
(Stankus, et al. 2006)	Poly(l-lactide-co-ε-caprolactone), poly(ester urethane)	Electrospun fiber	SMCs electrosprayed in hydrogel	Strong, flexible, elastic High cell density	Have to remove and culture cells ex vivo
(He et al. 2005)	Poly(l-lactide-co-ε-caprolactone), collagen	Electrospun fiber Nanofiber mesh	Human coronary artery ECs	Enhanced spreading, viability, and attachment Preserved phenotype	Have to remove and culture cells ex vivo

(Sell and Bowlin 2008)	Synthetic polymers Proteins	Electrospun fiber	ECs SMCs	Good mechanical properties Mimics ECM Good cell growth	Have to remove and culture cells ex vivo
(Smith, et al. 2008)	polydioxanone, elastin, sutures	Electrospun fiber	SMC and EC	Great mechanical properties Biodegradable Bioactivity	Tendency to form aneurysm Uneven degradation No mechanism for endothelialization
(Lee, et al. 2008a)	PCL, collagen	Electrospun fiber	SMC and EC	Great mechanical properties Resist high pressure over long time Support cell growth	Have to remove and culture cells ex vivo No mechanism for endothelialization
(Lee et al. 2007)	PCL Collagen Elastin Glutaraldehyde crosslinked	Electrospun fiber	Ovine SMC	Improved mech props Cell infiltration Can control size and mech props	Have to remove and culture cells ex vivo No mechanism for endothelialization
(Chung, et al. 2007a)	PLCL	Gel-spun	Implanted in mouse	Controllable mech props	No mechanism for endothelialization
(Zhang, et al. 2007)	PLGA, PU	layered	Bone marrow stromal cell seeded then implanted in canine	Good mech strength 3 month patency *in vivo* Endothelialized	Have to remove and culture cells ex vivo Low degradation rate might increase inflammatory response
(Feng, et al. 2007)	PCLLGA Collagen Type I hydrogel	Layer by layer Microgrooves	SMC layered in grooves with or without collagen	Good alignment of SMCs Rapid 3D fabrication	Have to remove and culture cells ex vivo No mechanism for endothelialization
(Choi, et al. 2007)	PLA-ePTFE-PLA	Layered biodegradable and nonbiodegradable PLA made porous by gas foaming	SMC with pulsatile flow	Good mech props Biodegradable	Have to remove and culture cells ex vivo No mechanism for endothelialization
(Roh, et al. 2008)	PGA or PLA	Nonwoven with polyester glue	Implanted in mouse	No thrombosis or aneurysm	Foreign body immune response in 3 weeks

				Endothelialization and collagen deposits at 3 weeks	Mouse model not representative of human endothelialization
(Fidkowski et al. 2005)	Poly(glycerol sebacate)	Biodegradable elastomer Etched capillary patterns onto silicon for molds	EC perfused with syringe at physiological flow rate	Endothelialized in vitro in 14 days	Have to remove and culture cells ex vivo No mechanism for endothelialization
(Xu et al. 2008)	PU, polyester, spandex	Knitted	No cell testing yet	Improved mech props Controllable dimensions	No cell testing
(Nieponice et al. 2008)	PEUU	Porous matrix tube	Seeded with muscle derived stem cells	Cell proliferation and viability	Stem cell phenotype preserved, no differentiat ion Have to remove and culture cells ex vivo No mechanism for endothelialization
(Almany and Seliktar 2005)	PEG-fibrinogen	Biosynthetic hydrogel scaffolds	EC and SMC cured inside scaffold	Bioactive Fibrinogen should enhance EC attachment Controllable mech props Proteolytic biodegradation	Need to test endothelializtion in vivo
(Patel, et al. 2007)	Hydrogel poly(acrylamide), poly (ethylene glycol-co-acrylic acid)	GRGDSP on interpenetrating polymer network	ECs	Increased EC adhesion and spreading Proliferation rate unchanged	EC migration inhibited under flow conditions
(Lee, et al. 2004)	Alginate Hydrogels	Microencapsulation of growth factors coated with heparin and chitosan VEGF and FGF	No cell testing	Can locally deliver growth factors	Delivery complete after 5-10 days not long enough to enhance cell attachment or differentiation
(Watanabe, et al. 2007)	Autologous ECM and cells	Implanted in body to collect tissue	Autoimplantation up to 2 months	No formation of aneurysm or rupturing Autologous	Must create an implantation site to form tube then graft
(Badylak 2002)	Small intestine	ECM, explanted	Xenogeneic and	Recruitment of	Sourcing

	submucosa	from porcine	allogeneic ECM grafts	circulating progenitors ECM remodeling Extensive angiogenesis Rapid scaffold degradation	Optimizing mech props Immunologic response to the scaffolds
(Wang, et al. 2007)	Decellularized xenografts	With and without heparin	From canine to rabbit	Showed cellular reconstruction with EC and SMC after 6 months	Without heparin thrombosis rate was 58% Sourcing Immunologic response
(L'Heureux, et al. 2006)	Completely TE	Fibroblasts from skin biopsy made into sheets and wrapped around mandrel Matured 10 weeks Seeded ECs	Implanted in nude rats and primates	Cell infiltration Good mech props	Long ex vivo maturation time Have to remove and culture cells ex vivo Endothelialization models do not mimic human
(Aoki, et al. 2005)	Stainless Steel stent with CD 34 antibody	Covalently coupled polysaccharide intermediate coating with murine monoclonal anti-human CD34 antibodies	Human Clinical Trial (16 patients)	Safe and feasible for treatment of coronary artery disease Luminal loss after 6 months ~0.63mm Increased in vitro cell capture >3 fold	Intravascular volume obstruction ~27% Intimal hyperplasia not significantly reduced
(Co, et al. 2008)	Stainless Steel stent with CD 34 antibody	Covalently coupled polysaccharide intermediate coating with murine monoclonal anti-human CD34 antibodies	Human Clinical Trial (120 patients)	Low rate of major cardiac events at 6 months ~5.8% Low rate of late stent thrombosis ~0.28%	No in vitro cell testing No characterization of removed stents or cell differentiation or endothelialization
(Markway, et al. 2008)	Glass coverslips	Coated w/	HUVECs,	KDR is a leading	Captured ECs not EPCs

	with or without protein G spacer	monoclonal mouse anti-human KDR IgG1 or anti-TGFβ1, blocked w/ heat denat. BSA, BSA controls	BaSMCs	candidate for selection of EPCs Anti-KDR with protein G spacer captured 2.5 fold more cells	No data on differentiation
(Rodenberg and Pavalko 2007)	Microplate wells or glass slides	Coated with recombinant fibronectin peptide fragments	HCAECs, HUVECs	Both EC types adhered maximally to CS-1 (1.6 fold increase)	Tested only with ECs not EPCs No capture data for EPCs No differentiation data for EPCs
(Blindt, et al. 2006)	PEUU coated Guidant Tetra stents	Controlled release of cRGD	Polymer coated w/ or w/o cRGD and bare metal stents implanted in porcine coronary arteries, infused with EPCs Culture plate coated and perfused in parallel plate flow chamber	cRGD significant increase over control cRGD stimulates out-growth, shear-resistant recruitment, invasion of EPCs	Recruited and counted EPCs but did not investigate differentiation of EPCs into ECs
(Veleva, et al. 2007)	Biopanning	12-mer peptide ligands selected with phage display that bind HBOEC	Human blood outgrowth ECs	Isolated clones display cell specificity No significant binding is observed on panel of other cell types	No differentiation studies
(Veleva et al. 2008)	Peptide-modified terpolymers	Peptides incorporate into mehtacyrlic terpolymers via chain transfer free radical polymerization	Human blood outgrowth ECs	Ligands do not interfere with EC function Ligand bound HBOEC but not HUVEC	No studies on progenitor differentiation
(Esguerra et al. 2010)	Bacterial cellulose	Hydrogel produced by	SMCs Implantation in	Low inflammatory response	Cell ingrowth less than PGA Angiogenesis less

	scaffolds	bacteria	dorsal skinfold chamber of hamsters	Increased cell growth versus ePTFE Angiogenesis in border zones	pronounced in borders than for ePTFE and PGA
(Soletti et al. 2010)	Poly(ester-urethane) urea	Electrospinning Thermally induced phase separation	Rotational vacuum seeding of muscle derived stem cells	Mechanical properties similar to artery High cell seeding Dynamic culture	Mechanical properties not assessed after cell seeding or in wet conditions Have to remove and culture cells ex vivo before implantation
(Nichol et al. 2010)	Gelatin methacrylate	Hydrogel	Immortalized human umbilical vein ECs NIH 3T3 cells	Cell attachment, proliferation and spreading on surfaces Can micropattern	Mechanical properties not assessed Topographical resolution only 100μm
(Kibbe et al. 2010)	poly(1,8 octanediol citrate) coated ePTFE grafts	Shear spinning	Implanted in porcine model	POC-ePTFE grafts similar extent of neointimal hyperplasia and leukocyte and monocyte/ macrophage infiltration as control ePTFE grafts POC supported ECs	Not tested in small diameter vessels Results were from 28d study
(Gui et al. 2009)	Decellularized human umbilical arteries	Explantation and cleaning	HUVECs Implanted into nude rats	Re-endothelialized with HUVECs Retained function up to 8 weeks in mice Burst pressure similar to native arteries	Obtaining human umbilical arteries is a challenge
(Zhou et al. 2009)	Decellularized canine carotid arteries coated with heparin and VEGF	Explantation and treatment	HUVECs Implantation into dog model	Reduced in vivo thrombogenicity Improved early patency rate of graftsT Patent at 6 months High degree of reendothelialization	Studies performed in dog model for only 6 months Infection, calcification, aneurismal dilation, and vasoreactivity need to be assessed
(Stekelenburg et al. 2009)	Fast-degrading polyglycolic acid scaffold coated	PGA sheet wrapped around mandrel and	Myofibroblasts from discarded saphenous	Similar mechanical properties to native vessel	All assays performed in vitro

	with poly-4-hydroxybutyrate combined with fibrin gel	dip-coated	veins Grown in bioreactor with dynamic strain	Cell infiltration and collagen deposition	
(Tillman et al. 2009)	PCL/Collagen	Electrospinning	Rabbit aortoiliac bypass model	Supported adherence and growth of vascular cells under physiologic conditions Endothelialized grafts resisted adherence of platelets Implanted in Vivo scaffolds retained structural integrity over 1 mo	Rabbit model does not mimic human re-endthelialization well Short assay time period
(Hong et al. 2009)	Poly(ester urethane)urea Poly(2-methacryloyloxy ethyl phosphorylcholine-co-methacryloyloxy ethyl butylurethane)	Electrospinning	Rat SMCs Rat abdominal aorta implantation	Good mechanical properties Slowed proliferation of rat SMCs Thin neo-intimal layer with endothelial coverage and good anastomotic tissue integration after 8 weeks	Rat model does not mimic human conditions well 8 week study
(Koens et al. 2010)	Elastin Collagen	Casting, moulding, freezing and lyophilization Carbodiimide cross-linked and heparinized	Platelet aggregation tests	Burst pressures similar to native vessel No platelet aggregation	No cell culture in vitro or in vivo has been performed
(Zhang et al. 2006)	Poly(propylene carbonate)	Electrospinning	Genetically modified MSCs	Cells form 3D network NO produced by grafts seeded with eNOS-modified MSCs was comparable to that produced by native blood vessels	Cell sourcing Genetically modified cells could elicit immune response

LIST OF REFERENCES

Abarzua S and Jakubowski S. 1995. Biotechnological investigation for the prevention of biofouling. I. Biological and biochemical principles for the prevention of biofouling. Marine Ecology Progress Series. 123:301-312.

Aldred N, Scardino A, Cavaco A, de Nys R and Clare AS. 2010. Attachment strength is a key factor in the selection of surfaces by barnacle cyprids (*Balanus amphitrite*) during settlement. Biofouling. 26(3):287-299.

Almany L and Seliktar D. 2005. Biosynthetic hydrogel scaffolds made from fibrinogen and polyethylene glycol for 3D cell cultures. Biomaterials. 26(15):2467-2477.

Andrewartha J, Perkins K, Sargison J, Osborn J, Walker G, Henderson A and Hallegraeff G. 2010. Drag force and surface roughness measurements on freshwater biofouled surfaces. Biofouling. 26(4):487-496.

Aoki J, Serruys PW, van Beusekom H, Ong ATL, McFadden EP, Sianos G, van der Giessen WJ, Regar E, de Feyter PJ, Davis HR, Rowland S and Kutryk MJB. 2005. Endothelial Progenitor Cell Capture by Stents Coated with Antibody Against CD34. Jornal of the American College of Cardiology. 45(10):1574-1579.

Asahara T, Murohara T, Sullivan A, Silver M, van der Zee R, Li T, Witzenbichler B, Schatteman G and Isner JM. 1997. Isolation of Putative Progenitor Endothelial Cells for Angiogenesis. Science. 275:964.

Badylak SF. 2002. The extracellular matrix as a scaffold for tissue reconstruction. Seminars in Cell & Developmental Biology. 13(5):377-383.

Baier RE. 2006. Surface behaviour of biomaterials: The *theta surface* for biocompatibility. Journal of Materials Science: Materials in Medicine. 17:1057-1062.

Bakker DP, Busscher HJ, van Zanten J, de Vries J, Klijnstra JW and van der Mei HC. 2004. Multiple linear regression analysis of bacterial deposition to polyurethane coatings after conditioning film formation in the marine environment. Microbiology. 150:1779-1784.

Balamurugan S, Ista LK, Yan J, Lopez GP, Fick J, Himmelhaus M and Grunze M. 2005. Reversible Protein Adsorption and Bioadhesion on Monolayers Terminated with Mixtures of Oligo(ethylene glycol) and Methyl Groups. J Am Chem Soc. 127:14548-14549.

Batschelet E editor 1981. Circular Statistics in Biology. London, England: Academic Press, Inc.

Baumann L, Bowditch RD and Baumann P. 1983. Description of *Deleya* gen. nov. Created to Accommodate the Marine Species *Alcaligenes aestus*, A. *pacificus*, A. *cupidus*, A. *venustus*, and *Pseudomonas marina*. International Journal of Systematic Bacteriology. 33(4):793-802.

Beamish JA, He P, Kottke-Marchant K and Marchant RE. 2010. Molecular Regulation of Contractile Smooth Muscle Cell Phenotype: Implications for Vascular Tissue Engineering. Tissue Engineering: Part B.

Bechert DW, Bruse M and Hage W. 2000. Experiments with three-dimensional riblets as an idealized model of shark skin. Experiments in Fluids. 28:403-412.

Bers AV, Diaz ER, da Gama BAP, Vieira-Silva F, Dobretsov S, Valdivia N, Thiel M, Scardino AJ, McQuaid CD, Sudgen HE, Thomason JC and Wahl M. 2010. Relevance of mytilid shell microtopographies for fouling defence - a global comparison. Biofouling. 26(3):367-377.

Bers VA and Wahl M. 2004. The Influence of Natural Surface Microtopographies on Fouling. Biofouling. 20(1):43-51.

Bettinger CJ, Langer R and Borenstein JT. 2009. Engineering Substrate Topography at the Micro- and Nanoscale to Control Cell Function. Angew Chem Int Ed. 48:5406=5415.

Bico J, Marzolin C and Quere D. 1999. Pearl drops. Europhys Lett. 47(2):220-226.

Bico J, Thiele U and Quere D. 2002. Wetting of texture surfaces. Colloids Surf, A. 206(1-3):41-46.

Biology of the Arterial Wall. 1999. Dordrecht/Boston/London: Kluwer Academic Publishers.

Biomaterials Science: An Introduction to Materials in Medicine. 2004. 2 ed. San Diego: Elsevier Academic Press.

Blindt R, Vogt F, Astafieva I, Fach C, Hristov M, Krott N, Seitz B, Kapurniotu A, Kwok C, Dewor M, Bosserhoff A-K, Bernhagen J, Hanrath P, Hoffmann R and Weber C. 2006. A Novel Drug-Eluting Stent Coated With an Integrin-Binding Cyclic Arg-Gly-Asp Peptide Inhibits Neointimal Hyperplasia by Recruiting Endothelial Progenitor Cells. Journal of the American College of Cardiology. 47(9):1786-1795.

Bowen J, Pettitt ME, Kendall K, Leggett GJ, Preece JA, Callow ME and Callow JA. 2007. The influence of surface lubricity on the adhesion of *Navicula perminuta* and *Ulva linza* to aklanethiol self-assembled monolayers. J R Soc Interface. 4(473-477).

Brady RF and Singer IL. 2000. Mechanical Factors Favoring Release from Fouling Release Coatings. Biofouling. 15(1-3):73-81.

Brandup J, Immergut EH and Grulke EA editors. 1999. Polymer Handbook. 4 ed. New York, NY: John Wiley & Sons, Inc.

Callow ME, Callow JA, Pickett-Heaps JD and Wetherbee R. 1997. Primary adhesion of *enteromorpha* (chlorophyta, ulvales) propagules: quantitative settlement studies and video microscopy. J Phycol. 33:938-947.

Callow ME, Callow JA, Ista LK, Coleman SE, Nolasco AC and Lopez GP. 2000. Use of Self-Assembled Monolayers of Different Wettabilities To Study Surface Selection and Primary Adhesion Processes of Green Algal (*Enteromorpha*) Zoospores. Applied and Environmental Microbiology. 66(8):3249-3254.

Callow ME, Jennings AR, Brennan AB, Seegert CA, Gibson AL, Wilson LH, Feinberg AW, Baney R and Callow JA. 2002. Microtopographic Cues for Settlement of Zoospores of the Green Fouling Alga *Enteromorpha*. Biofouling. 18(3):237-245.

Cao Y, Poon YF, Feng J, Rayatpisheh S, Chan V and Chan-Park MB. 2010. Regulating orientation and phenotype of primary vascular smooth muscle cells by biodegradable films patterned with arrays of microchannels and discontinuous mircowalls. Biomaterials. 31(24):6228-6238.

Carman ML, Estes TG, Feinberg AW, Schumacher JF, Wilkerson W, Wilson LH, Callow ME, Callow JA and Brennan AB. 2006. Engineered antifouling microtopgraphies - correlating wettability with cell attachment. Biofouling. 22(1):11-21.

Carman ML. Engineered Microtopographies to Induce *In Vitro* Endothelial Cell Morphologies Stable to Shear [Dissertation]. Gainesville FL: University of Florida.

Cassie ABD and Baxter S. 1944. Wettability of Porous Surfaces. Trans Faraday Society. 40:546-551.

Cavalier-Smith T. 2004. Only six kingdoms of life. Proc R Soc Lond B. 271:1251-1262.

Chai C and Leong KW. 2007. Biomaterials Approach to Expand and Direct Differentiation of Stem Cells. Molecular Therapy. 15(3):467-480.

Chan BP, Hui TY, Chan OCM, So KF, Lu W, Cheung KMC, Salomatina E and Yaroslavsky A. 2007. Photochemical Cross-Linking for Collagen-Based Scaffolds: A Study on Optical Properties, Mechanical Properties, Stability, and Hemetocompatibility. Tissue Engineering. 13(1):73-85.

Chaudhury MK, Finaly JA, Chung JY, Callow ME and Callow JA. 2005. The influence of elastic modulus and thickness on the release of the soft-fouling green alga *Ulva linza* (syn. *Enteromorpha linza*) from poly(dimethylsiloxane) (PDMS) model networks. Biofouling. 2(1):41-48.

Chiovitti A, Dugdale TM and Wetherbee R editors. 2006. Diatom Adhesives: Molecular and Mechanical Properties. Berlin: Springer-Verlag.

Choi Y-J, Kim M-S and Noh I. 2007. Tissue Regeneration of a Hybrid Vascular Graft Composed of Biodegradable Layers and Non-Biodegradable Layer by Static and Pulsatile Flows. Key Engineering Materials. 342-343:61-64.

Chung E, Kim S-H, Ko Y-G, Kwon J-H, Han J-W, Park I-S, Han S-S and Kim S-H. 2007a. Characterization of Gel-spun Tubular Scaffold for Cardiovascular Tissue Engineering. Key Engineering Materials. 342-343:321-324.

Chung KK, Schumacher JF, Sampson EM, Burne RA, Antonelli PJ and Brennan AB. 2007b. Impact of engineered surface microtopographies on biofilm formation of Staphylococcus aureus. Biointerphases. 2(2):89-94.

Co M, Tay E, Lee CH, Poh KK, Low A, Lim J, Lim IH, Lim YT and Tan HC. 2008. Use of endothelial progenitor cell capture stent (Genous Bio-Engineered R Stent) during primary percutaneous coronary intervention in acute myocardial infarction: Intermediate - to long-term clinical follow-up. American Heart Journal. 155(1):128-132.

Cordiero A, Nitschke M, Janke A, Helbig R, D'Souza F, Donnelly G, Willemsen P and Werner C. 2009. Fluorination of poly(dimethylsiloxane) surfaces by low pressure CF4 plasma - physicochemical and antifouling properties. Express Polymer Letters. 3(2):70-83.

Cowling MJ, Hodgkiess T, Parr ACS, Smith MJ and Marrs SJ. 2000. An alternative approach to antifouling based on analogues of natural processes. The Science of the Total Environment. 258:129-137.

Cummings CL, Gawlitta D, Nerem RM and Stegemann JP. 2004. Properties of engineered vascular constructs made from collagen, fibrin, and collagen-fibrin mixtures. Biomaterials. 25(17):3699-3706.

Curtis ASG and Wilkinson CD. 1998. Reactions of cells to topography. J Biomater Sci Polymer Edn. 9(12):1313-1329.

Dalby MJ, Yarwood SJ, Riehle MO, Johnstone HJH, Affrossman S and Curtis ASG. 2002. Increasing Fibroblast Response to Materials Using Nanotopography: Morphological and Genetic Measurements of Cell Response to 13-nm-High Polymer Demixed Islands. Experimental Cell Research. 276(1):1-9.

Dalby MJ, Childs S, Riehle MO, Johnstone HJH, Affrossman S and Curtis ASG. 2003. Fibroblast reaction to island topography: changes in cytoskeleton and morphology with time. Biomaterials. 24(6):927-935.

Dalby MJ. 2005. Topographically induced direct cell mechanotransduction. Medical Engineering and Physics. 27:730-742.

de Mel A, Jell G, Stevens MM and Seifalian AM. 2008. Biofunctionalization of Biomaterials for Accelerated in Situ Endothelialization: A Review. Biomacromolecules. Epub ahead of print.

Drury J, Ashton T, Cunningham J, Maini R and Pollock J. 1987. Experimental and clinical experience with a gelatin impregnated Dacron prosthesis. Ann Vasc Surg. 1(5):542-547.

Ederth T, Pettitt ME, Nygren P, Du C-X, Ekblad T, Zhou Y, Falk M, Callow ME, Callow JA and Liedberg B. 2009. Interactions of Zoospores of *Ulva linza* with Arginine-Rich Oligopeptide Monolayers. Langmuir. 25(16):9375-9383.

Edgar LA. 1982. Diatom Locomotion: A Consideration of Movement in a Highly Viscous Situation. Br phycol J. 17:243-251.

Edgar LA and Pickett-Heaps JD. 1984. Diatom locomotion. Prog Phycol Res. 3:47-88.

Ekblad T, Bergstrom G, Ederth T, Conlan SL, Mutton R, Clare AS, Wang S, Liu Y, Zhao Q, D'Souza F, Donnelly GT, Willemsen PR, Pettitt ME, Callow ME, Callow JA and Liedberg B. 2008. Poly(ethylene glycol)-Containing Hydrogel Surfaces for Antifouling Applications in Marine and Freshwater Environments. Biomacromolecules. 9:2775-2783.

Engler AJ, Sen S, Sweeney HL and Discher DE. 2006. Matrix Elasticity Directs Stem Cell Lineage Specification. Cell. 126(4):677-689.

Esguerra M, Fink H, Laschke M, Jeppsson A, Delbro D, Gatenholm P, Menger MD and Risberg B. 2010. Intravital fluorescent microscopic evaluation of bacterial cellulose as scaffold for vascular grafts. Journal of Biomedical Materials Research Part A. 93A:140-149.

Feinberg AW, Gibson AL, Wilkerson W, Seegert CA, Wilson LH, Zhao LC, Baney R, Callow JA, Callow ME and Brennan AB. Investigating the Engergetics of Bioadhesion on Micro-engineered Siloxane Elastomers: Characterizing the Topography, Mechanical Properties and Surface Engergy and its Effect on Cell Contact Guidance. In: S Clarson, J Fitzgerald, M Owen, S Smith and M Dyke editors: Am Chem Soc.

Feinberg AW, Schumacher JF and Brennan AB. 2009. Engineering high-density endothelial cell monolayers on soft substrates. Acta Biomaterialia. 5:2013-2024.

Feng J, Chan-Park MB, Shen J and Chan V. 2007. Quick Layer-by-Layer Assembly of Aligned Multilayers of Vascular Smooth Muscel Cells in Deep Microchannels. Tissue Engineering. 13(5):1003-1012.

Fidkowski C, Kaazempur-Mofrad M, Borenstein J, Vacanti JP, Langer R and Wang Y. 2005. Endothelialized Microvasculature Based on a Biodegradable Elastomer. Tissue Engineering. 11(1/2):302-309.

Finlay JA, Callow ME, Ista LK, Lopez GP and Callow JA. 2002a. The Influence of Surface Wettability on the Adhesion Strength of Settled Spores of the Green Alga *Enteromorpha* and the Diatom *Amphora*. Integr Comp Biol. 42:1116-1122.

Finlay JA, Callow ME, Schultz MP, Swain GW and Callow JA. 2002b. Adhesion Strength of Settled Spores of the Green Alga *Enteromorpha*. Biofouling. 18(4):251-256.

Finlay JA, Krishnan S, Callow ME, Callow JA, Dong R, Asgill N, Wong K, Kramer EJ and Ober CK. 2008. Settlement of *Ulva* Zoospores on Patterned Fluorinated and PEGylated Monolayer Surfaces. Langmuir. 24:503-510.

Finlay JA, Bennett SM, Brewer LH, Sokolova A, Clay G, Gunari N, Meyer AE, Walker GC, Wendt DE, Callow ME, Callow JA and Detty MR. 2010. Barnacle settlement and the adhesion of protein and diatom microfouling to xerogel films with varying surface energy and water wettability. Biofouling. 26(6):657-666.

Freischlag J and Moore W. 1990. Clinical experience with a collagen-impregnated knitted Dacron vascular graft. Ann Vasc Surg. 4(5):499-454.

Genzer J and Efimenko K. 2006. Recent developments in superhydrophobic surfaces and their relevance to marine fouling: a review. Biofouling. 22(5):339-360.

Gudipati CS, Finlay JA, Callow JA, Callow ME and Wooley KL. 2005. The Antifouling and Fouling-Release Performance of Hyperbranched Fluoropolymer (HBFP)-Poly(ethylene glycol) (PEG) Composite Coatings Evaluated by Adsorption of Biomacromolecules and the Green Fouling Alga *Ulva*. Langmuir. 21:3044-3053.

Gui L, Muto A, Chan S, Breuer CK and Niklason LE. 2009. Development of Decellularized Human Umbilical Arteries as Small-Diameter Vascular Grafts. Tissue Engineering: Part A. 15(9):2665-2676.

Harrison R. 1914. The reaction of embryonic cells to solid structures. The Journal of Experimental Zoology. 17(4):521-544.

Hatcher BM, Seegert CA and Brennan AB. 2002. Polyvinylpyrrolidone modified bioactive glass fibers as tissue constructs: *In vitro* mesenchymal stem cell response. Journal of biomedical Materials Research Part A. 66A(4):840-849.

He W, Ma ZW, Yong T, Teo WE and Ramakrishna S. 2005. Fabrication of collagen-coated biodegradable polymer nanofiber mesh and its potential for endothelial cells growth. Biomaterials. 26:7606-7615.

Heart Disease & Stroke Statistics Dalls, Texas: American Heart Association

Heydt M, Rosenhahn A, Grunze M, Pettitt ME, Callow ME and Callow JA. 2007. Digital In-line Holography as a Three-Dimensional Tool to Study Motile Marine Organisms During Their Exploration of Surfaces. The Journal of Adhesion. 83:417-430.

Hoagland KD, Rosowski JR, Gretz MR and Roemer SC. 1993. Diatom Extracellular Polymeric Substances: Function, Fine Structure, Chemistry and Physiology. J Phycol. 29:537-566.

Hoffman AS. 2002. Hydrogels for biomedical applications. Advanced Drug Delivery Reviews. 54(1):3-12.

Holland R, Dugdale T, Wetherbee R, Brennan A, Finlay JA, Callow JA and Callow ME. 2004. Adhesion and Motility of Fouling Diatoms on a Silicone Elastomer. Biofouling. 20(6):323-329.

Holm ER, Schultz MP, Haselbeck EG, Talbott WJ and Field AJ. 2004. Evaluation of hydrodynamic drag on experimental fouling-release surfaces, using rotating disks. Biofouling. 20(4/5):219-226.

Holm ER, Kavanagh CJ, Meyer AE, Wiebe D, Nedved BT, Wendt D, Smith C, Hadfield MG, Swain G, Wood CD, Truby K, Stein J and Montemarano J. 2006. Interspecific variation in patterns of adhesion of marine fouling to silicone surfaces. Biofouling. 22(4):233-243.

Holzapfel GA, Gasser TC and Stadler M. 2002. A structural model for the viscoelastic behavior of arterial walls: Contimuum formulation and finite element analysis. European Journal of Mechanics A/Solids. 21:441-463.

Hong Y, Sang-Ho Y, Nieponice A, Soletti L, Vorp DA and Wagner WR. 2009. A small diameter, fibrous vascular conduit generated from a poly(ester urethane)urea and phospholipid polymer blend. Biomaterials. 30:2457-2467.

Hu DS-G and Tsai C-e. 1996. Correlation Between Interfacial Free Energy and Albumin Adsorption in Poly(acrylonitrile-acrylamide-acrylic acid) Hydrogels. Journal of Applied Polymer Science. 59:1809-1817.

Ista LK, Mendez S and Lopez GP. 2010. Attachment and detachment of bacteria on surfaces with tunable and switchable wettability. Biofouling. 26(1):111-118.

Itano N, Okamoto S-i, Zhang D, Lipton SA and Ruoslahti E. 2003. Cell spreading controls endoplasmic and nuclear calcium: A physical gene regulation pathway from the cell surface to the nucleus. Proc Natl Acad Sci USA. 100(9):5181-5186.

Jain A and Bhosle NB. 2009. Biochemical composition of the marine conditioning film: implications for bacterial adhesion. Biofouling. 25(1):13-19.

Joint I, Tait K, Callow ME, Callow JA, Milton D, Williams P and Camara M. 2002. Cell-to-Cell Communication Across the Prokaryote-Eukaryote Boundary. Science. 298:1207.

Ju H, McCloskey BD, Sagle AC, Kusuma VA and Freeman BD. 2009. Preparation and characterization of crosslinked poly(ethylene glycol) diacrylate hydrogels as fouling-resistant membrane coatings. Journal of Membrane Science. 330:180-188.

Kibbe MR, Martinez J, Popowich DA, Kapadia MR, Ahanchi SS, Aalami OO, Jiang Q, Webb AR, Yang J, Carroll T and Ameer G. 2010. Citric acid-based elastomers provide a biocompatible interface for vascular grafts. Journal of Biomedical Materials Research Part A. 93A:314-324.

Koens MJW, Faraj KA, Wismans RG, van der Vliet JA, Krasznai AG, Cuijpers VMJI, Jansen JA, Daamen WF and van Kuppevelt TH. 2010. Controlled fabrication of triple layered and molecularly defined collagen/elastin vascular grafts resembling the native blood vessel. Acta Biomaterialia.

Krishnan S, Weinman CJ and Ober CK. 2008. Advances in polymers for anti-biofouling. Journal of Materials Chemistry. 18:3405-3413.

L'Heureux N, Dusserre N, Konig G, Victor B, Keire P, Wight TN, Chronos NAF, Kyles AF, Gregory CR, Hoyt G, Robbins RC and McAllister TN. 2006. Human tissue-engineered blood vessels for adult arterial revascularization. Nature Medicine. 12(3):361-365.

Lee KW, Yoon JJ, Lee JH, Kim SY, Jung HJ, Kim SJ, Joh JW, Lee HH, Lee DS and Lee SK. 2004. Sustained release of vascular endothelial growth factor from calcium-induced alginate hydrogels reinforced by heparin and chitosan. Transplantation Proceedings. 36(8):2464-2465.

Lee SJ, Yoo JJ, Lim GJ, Atala A and Stitzel J. 2007. *In vitro* evaluation of electrospun nanofiber scaffolds for vascular graft application. Journal of biomedical Materials Research Part A. 83A(4):999-1008.

Lee SJ, Liu J, Oh SH, Soker S, Atala A and Yoo JJ. 2008a. Development of a composite vascular scaffolding system that withstands physiological vascular conditions. Biomaterials. 29:2891-2898.

Lee SJ, Oh SH, Liu J, Soker S, Atala A and Yoo JJ. 2008b. The use of thermal treatments to enhance the mechanical properties of electrospun poly([var epsilon]-caprolactone) scaffolds. Biomaterials. 29(10):1422-1430.

Liliensiek SJ, Wood JA, Yong J, Auerbach R, Nealey PF and Murphy CJ. 2010. Modulation of human vascular endothelial cell behaviors by nanotopographic cues. Biomaterials. 31:5418-5426.

Lim JY and Donahue HJ. 2007. Cell Sensing and Response to Micro- and Nanostructured Surfaces Produced by Chemical and Topographic Patterning. Tissue Engineering. 13(8):1879-1891.

Long CJ. Analytic Methods for Predicting Biosettlement on Patterned Surfaces [Dissertation]. Gainesville, FL: University of Florida.

Long CJ, Schumacher JF, Robinson P, II, Finaly JA, Callow ME, Callow JA and Brennan AB. 2010. A Model that Predicts the Attachment Behavior of Ulva linza Zoospores on Surface Topography. Biofouling. 26(4):411-419.

Lutolf MP and Hubbell JA. 2005. Synthetic biomaterials as instructive extracellular microenvironments for morphogenesis in tissue engineering. Nature Biotechnology. 23(1):47-55.

Magin CM, Cooper SP and Brennan AB. 2010a. Non-Toxic Antifouling Strategies. Materials Today. 13(4):36-44.

Magin CM, Long CJ, Cooper SP, Ista LK, Lopez GP and Brennan AB. 2010b. Engineered Antifouling Microtopographies: The role of Reynolds number in a model that predicts attachment of zoospores of *Ulva* and cells of *Cobetia marina*. Biofouling. 26(6):719-727.

Markway BD, McCarty OJT, Marzec UM, Courtman DW, Hanson SR and Hinds MT. 2008. Capture of Flowing Endothelial Cells Using Surface-Immobilized Anti-Kinase Insert Domain Receptor Antibody. Tissue Engineering. 14(2).

Marmur A. 2006. Super-hydrophobicity fundamentals: implications to biofouling prevention. Biofouling. 22(2):107-115.

Miglionico M, Patti G, D'Ambrosio A and Di Sciascio G. 2008. Percutaneous Coronary Intervention Utilizing a New Endothelial Progenitor Cells Antibody-Coated Stent: A Prospective Single-Center Registry in High-Risk Patients. Cathetherication and Cardiovascular Interventions. 71:600-604.

Molino PJ and Wetherbee R. 2008. The biology of biofouling diatoms and their role in the development of microbial slimes. Biofouling. 24(5):365-379.

Molino PJ, Campbell E and Wetherbee R. 2009a. Development of the initial diatom microfouling layer on antifouling and fouling-release surfaces in temperate and tropical Australia. Biofouling. 25(8):685-694.

Molino PJ, Childs S, Hubbard MRE, Carey JM, Burgman MA and Wetherbee R. 2009b. Development of the primary bacterial microfouling layer on antifouling and fouling release coatings in temperate and tropical environments in Eastern Australia. Biofouling. 25(2):149-162.

Moon JJ, Hahn M, Kim I, Nsiah B and West JL. 2009. Micropatterning of Poly(Ethylene Glycol Diacrylate Hydrogels with Biomolecules to Regulate and Guide Endothelial Morphogenesis. Tissue Engineering: Part A. 15(3):579-585.

Murosaki T, Noguchi T, Kakugo A, Putra A, Kurokawa T, Furukawa H, Osada Y, Gong JP, Nogata Y, Matsumura K, Yoshimura E and Fusetani N. 2009. Antifouling activity of synthetic polymer gels against cyprids of the barnacle (*Balanus amphitrite*). Biofouling. 25(4):313-320.

Nerem RM and Seliktar D. 2001. Vascular Tissue Engineering. Annu Rev Biomed Eng. 3:225-243.

Nguyen KT and West JL. 2002. Photopolymerizable hydrogels for tissue engineering applications. Biomaterials. 23(22):4307-4314.

Nichol JW, Koshy ST, Bae H, Hwang CM, Yamanlar S and Khademhosseini A. 2010. Cell-laden microengineered gelatin methacrylate hydrogels. Biomaterials. 31:5536-5544.

Nieponice A, Soletti L, Guan J, Deasy BM, Huard J, Wagner WR and Vorp DA. 2008. Development of a tissue-engineered vascular graft combining a biodegradable scaffold, muscle-derived stem cells and a rotational vacuum seeding technique. Biomaterials. 29(7):825-833.

Ostuni E, Chapman RG, Holmlin RE, Takayama S and Whitesides GM. 2001. A Survey of Structure-Property Relationships of Surfaces that Resist the Adsorption of Protein. Langmuir. 17:5605-5620.

Otani M, Oumi T, Uwai S, Hanyuda T, Prabowo RE, Yamaguchi T and Kawai H. 2007. Occurrence and diversity of barnacles on international ships visiting Osaka Bay, Japan, and the risk of their introduction. Biofouling. 23(3/4):277-286.

Owens DK and Wendt RC. 1969. Estimation of Surface Free Energy of Polymers. J Appl Polym Sci. 13(8):1741-1747.

Padera RF and Schoen FJ editors. 2004. Cardiovascular Medical Devices. San Diego: Elsevier Academic Press.

Patel S, Tsang J, Harbers GM, Healy KE and Li S. 2007. Regulation of endothelial cell function by GRGDSP peptide grafted on interpenetrating polymers. journal of biomedical Materials Research Part A. 83A(2):423-433.

Perkins KJ, Andrewartha JM, McMinn A, Cook SS and Hallegraeff GM. 2010. Succession and physiological health of freshwater microalgal fouling in a Tasmanian hydropower canal. Biofouling. 26(6):637-644.

Pettengill JB, Wendt DE, Schug MD and Hadfield MG. 2007. Biofouling likely serves as a major mode of dispersal for the polychaete tubeworm *Hydroides elegans* as inferred from microsatellite loci. Biofouling. 23(3/4):161-169.

Pfister PM, Wendlandt M, Neuenschwander P and Suter UW. 2007. Surface-textured PEG-based hydrogels with adjustable elasticity: Synthesis and characterization. Biomaterials. 28(4):567-575.

Pickford AR, Smith SP, Stauton D, Boyd J and Campbell ID. 2001. The hairpin structure of the (6)F1(1)F2(2)F2 fragment from human fibronectin enhances gelatin binding. EMBO J. 20(7):1519-1529.

Piola RR and Johnston EL. 2008. The potential for translocation of marine species via small-scale disruptions to antifouling surfaces. Biofouling. 24(3):145-155.

Quere D. 2008. Wetting and Roughness. Annu Rev Mater Res. 38:71-99.

Ralston E and Swain G. 2009. Bioinspiration - the solution for biofouling control? Bioinsp Biomim. 4.

Rasmussen K, Willemsen PR and Ostgaard K. 2002. Barnacle Settlement on Hydrogels. Biofouling. 18(3):177-191.

Rasmussen K and Ostgaard K. 2003. Adhesion of the marine bacterium *Pseudomonas* sp. NCIMB 2021 to different hydrogel surfaces. Water Research. 37:519-524.

Reilly GC and Engler AJ. 2010. Intrinsic extracellular matrix properties regulate stem cell differentiation. Biomaterials. 43:55-62.

Rodenberg EJ and Pavalko F. 2007. Peptides Derived from Fibronectin Type III Connecting Segments Promote Endothelial Cell Adhesion but Not Platelet Adhesion: Implications in Tissue-Engineered Vascular Grafts. Tissue Engineering. 13:2653-2666.

Roh JD, Nelson GN, Brennan MP, Mirensky TL, Yi T, Hazlett TF, Tellides G, Sinusas AJ, Pober JS, Saltzman WM, Kyriakides TR and Breuer CK. 2008. Small-diameter biodegradable scaffolds for functional vascular tissue engineering in the mouse model. Biomaterials. 29(10):1454-1463.

Rosenhahn A, Schilp S, Kreuzer HJ and Grunze M. 2010. The role of "inert" surface chemistry in marine biofouling prevention. Physical Chemistry Chemical Physics. 12:4275-4286.

Rumisek J, Wade C, Brooks D, Okerberg C, Barry M and Clarke J. 1986. Heat-denatured albumin-coated Dacron vascular grafts: physical characteristics and in vivo performance. Journal of Vascular Surgery. 4(2):136-143.

Saha K, Pollock JF, Schaffer DV and Healy KE. 2007. Designing synthetic materials to control stem cell phenotype. Current Opinion in Chemical Biology. 11(4):381-387.

Sarkar S, Lee GY, Wong JY and Desai TA. 2006a. Development and characterization of a porous micro-patterned scaffold for vascular tissue engineering applications. Biomaterials. 27:4775-4782.

Sarkar S, Sales KM, Hamilton G and Seifalian AM. 2006b. Addressing Thrombogenicity in Vascular Graft Construction. journal of Biomedical Materials Research Part B: Applied Biomaterials. 82B(1):100-108.

Scardino AJ, Harvey E and De Nys R. 2006. Testing attachment point theory: diatom attachment on microtextured polyimide biomimics. Biofouling. 22(1):55-60.

Scardino AJ, Guenther J and de Nys R. 2008. Attachment point theory revisited: the fouling response to a microtextured matrix. Biofouling. 24(1):45-53.

Scardino AJ, Hudleston D, Peng Z, Paul NA and de Nys R. 2009a. Biomimetic characterisation of key surface parameters for the development of fouling resistant materials. Biofouling. 25(1):83-93.

Scardino AJ, Zhang H, Cookson DJ, Lamb RN and de Nys R. 2009b. The role of nano-roughness in antifouling. Biofouling. 25(8):757-767.

Schilp S, Kueller A, Rosenhahn A, Grunze M, Pettitt ME, Callow ME and Callow JA. 2007. Settlement and adhesion of algal cells to hexa(ethylene glycol)-containing self-assembled monolayers with systematically changed wetting properties. Biointer*phases*. 2(4):143-150.

Schilp S, Rosenhahn A, Pettitt ME, Bowen J, Callow ME, Callow JA and Grunze M. 2009. Physicochemical Properties of (Ethylene Glycol)-Containing Self-Assembled Monolayers Relevant for Protein and Algal Cell Resistance. Langmuir. 25(17):10077-10082.

Schulte VA, Diez M, Moller M and Lensen MC. 2009. Surface Topography Induces Fibroblast Adhesion on Intrinscially Nonadhesive Poly(ethylene glycol) Substrates. Biomacromolecules. 10:2795-2801.

Schultz MP, Finlay JA, Callow ME and Callow JA. 2000. A Turbulent Channel Flow Apparatus for the Determination of the Adhesion Strength of Microfouling Organisms. Biofouling. 15(4):243-251.

Schultz MP. 2007. Effects of coating roughness and biofouling on ship resistance and powering. Biofouling. 23(5):331-341.

Schumacher JF, Aldred N, Callow ME, Finaly JA, Callow JA, Clare AS and Brennan AB. 2007a. Species-specific engineered antifouling topographies: correlations between the settlement of algal zoospores and barnacle cyprids. Biofouling. 23(5):307-317.

Schumacher JF, Carman ML, Estes TG, Feinberg AW, Wilson LH, Callow ME, Callow JA, Finlay JA and Brennan AB. 2007b. Engineered antifouling microtopographies -- effect of feature size, geometry, and roughness on settlement of zoospores of the green alga *Ulva*. Biofouling. 23(1):55-62.

Schumacher JF, Long CJ, Callow ME, Finaly JA, Callow JA and Brennan AB. 2008. Engineered Nanforce Gradients for Inhibition of Settlement (Attachment) of Swimming Algal Spores. Langmuir. 24:4931-4937.

Sell SA and Bowlin GL. 2008. Creating small diameter bioresorbable vascular grafts through electrospinning. J Mater Chem. 18:260-263.

Shen JY, Chan-Park MB, He B and Zhu AP. 2006. Three-Dimensional Microchannels in Biodegradable Polymeric Films for Control Orientation and Phenotype of Vascular Smooth Muscel Cells. Tissue Engineering. 12(8):2229-2240.

Shin H, Temenoff JS and Mikos AG. 2003. In Vitro Cytotoxicity of Unsaturated Oligo[poly(ethylene glycol) fumarate] Macromers and Their Cross-Linked Hydrogels. Biomacromolecules. 4(3):552-560.

Smith M, J., McClure MJ, Sell SA, Barnes CP, Walpoth BH, Simpson DG and Bowlin GL. 2008. Suture-reinforced electrospun polydioxanone-elastin small-diameter tubes for use in vascular tissue engineering: A feasibility study. Acta Biomaterialia. 4:58-66.

Soletti L, Hong Y, Guan J, Stankus JJ, El-Kurdi MS, Wagner WR and Vorp DA. 2010. A bilayered elastomeric scaffold for tissue engineering of small diameter vascular grafts. Acta Biomaterialia. 6:110-122.

Stankus JJ, Guan J, Fujimoto K and Wagner WR. 2006. Microintegrating smooth muscle cells into a biodegradable elastomeric fiber matrix. Biomaterials. 27:735-744.

Stegemann JP, Kaszuba SN and Rowe SL. 2007. Review: Advances in Vascular Tissue Engineering Using Protein-Based Biomaterials. Tissue Engineering. 13(11):2601-2613.

Stekelenburg M, Rutten MCM, Snoeckx LHEH and Baaijens FPT. 2009. Dynamic Straining Combined with Fibrin Gel Cell Seeding Improves Stregth of Tissue-Engineered Small-Diameter Vascular Grafts. Tissue Engineering: Part A. 15(5):1081-1089.

Thakar RG, Ho F, Huang NF, Liepmann D and Li S. 2003. Regulation of vascular smooth muscle cells by micropatterning. Biochemical and Biophysical Research Communications. 307:883-890.

Thomas CH, Collier JH, Sfeir CS and Healy KE. 2001. Engineering gene expression and protein synthesis by modulation of nuclear shape. Proc Natl Acad Sci USA. 99(4):1972-1977.

Thompson SEM, Taylor AR, Brownlee C, Callow ME and Callow JA. 2008. The role of nitric oxide in diatom adhesion in relation to substratum properties. J Phycol. 44:967-976.

Tillman BW, Yazdani SK, Lee SK, Geary RL, Atala A and Yoo JJ. 2009. The *in vivo* stability of electrospun polycaprolactone-collagen scaffolds in vascular reconstruction. Biomaterials. 30:583-588.

van Kooten TG and von Recum AF. 1999. Cell adhesion to textured silicone surfaces: The influence of time of adhesion and texture on focal contact and fibronectin fibril formation. Tissue Engineering. 5(3):223-240.

Veleva AN, Cooper SL and Patterson C. 2007. Selection and Initial Characterization of Novel Peptide Ligands that Bind Specifically to Human Blood Outgrowth Endothelial Cells. Biotechnology and Bioengineering. 98(1):306-312.

Veleva AN, Heath DE, Cooper SL and Patterson C. 2008. Selective endothelial cell attachment to peptide-modified terpolymers. Biomaterials. 29(27):3656-3661.

Verran J and Boyd RD. 2001. The Relationship Between Substratum Surface Roughness and Microbiological and Organic Soiling: a Review. Biofouling. 17(1):59-71.

Wang X-N, Chen C-Z, Yang M and Gu YJ. 2007. Implantation of Decellularized Small-caliber Vascular Xenografts With and Without Surface Heparin Treatment. Artificial Organs. 31(2):99-104.

Watanabe T, Kanda K, Ishibashi-Ueda H, Yaku H and Nakayama Y. 2007. Development of biotube vascular grafts incorporating cuffs for easy implantation. J Artif Organs. 10:10-15.

Weinberg CB and Bell E. 1986. A Blood Vessel Model Constructed from Collagen and Cultured Vascular Cells. Science. 231(4736):397-400.

Weiss P. 1945. Experiments on cell and axon orientation *in vitro*: the role of collodial exudates in tissue organization. Journal of Experimental Zoology. 100(3):353-386.

Wendt DE, Kowalke GL, Kim J and Singer IL. 2006. Factors that influence elastomeric coating performance: the effect of coating thickness on basal plate morphology, growth and critical removal stress of the barnacle *Balanus amphitrite*. Biofouling. 22(1):1-9.

Wenzel RN. 1936. Resistance of Solid Surfaces to Wetting by Water. Industrial and Engineering Chemistry. 28(8):988-994.

Wetherbee R, Lind JL, Burke J and Quatrano RS. 1998. The First Kiss: Establishment and Control of Initial Adhesion by Raphid Diatoms. J Phycol. 34:9-15.

Wu H-C, Wang T-W, Kang P-L, Tsuang Y-H, Sun J-S and Lin F-H. 2007. Coculture of endothelial and smooth muscle cells on a collagen membrane in the development of a small-diameter vascular graft. Biomaterials. 28:1385-1392.

Xu W, Zhou F, Ouyang C, Cui W, Yao M and Wang X. 2008. Small Diameter Polyurethane Vascular Graft Reinforced by Elastic Weft-Knitted Tubular Fabric of Polyester/Spandex. Fibers and Polymers. 9(1):71-75.

Xue L and Greisler HP. 2000. Blood Vessels. In: Principles of Tissue Engineering. 2 ed. New York: Academic Press.

Yamaguchi T, Prabowo RE, Ohshiro Y, Shimono T, Jones D, Kawai H, Otani M, Oshino A, Inagawa S, Akaya T and Tamura I. 2009. The introduction to Japan of the Titan barnacle, *Megabalanus coccopoma* (Darwin, 1854) (Cirripedia: Balanomorpha) and the role of shipping in its translocation. Biofouling. 25(4):325-333.

Yebra DM, Kiil S and Dam-Johansen K. 2004. Antifouling technology -- past, present and future steps towards efficient and environmentally friendly antifouling coatings. Prog Org Coat. 50:74-104.

Yim EKF, Pang SW and Leong KW. 2007. Synthetic nanostructures inducing differentiation of human mesenchymal stem cells into neuronal lineage. Experimental Cell Research. 313:1820-1829.

Zar JH. 1984. Biostatistical Analysis. Second ed. Englewood Cliffs, N.J.: Prentice-Hall, Inc.

Zhang J, Qi H, Wang H, Hu P, Ou L, Guo S, Li J, Che Y, Yu Y and Kong D. 2006. Engineering of Vascular Grafts with Genetically Modified Bone Marrow Mesenchymal Stem Cells on Poly(Propylene Carbonate) Graft. Artifical Organs. 30(12):898-905.

Zhang L, Zhou J, Lu Q, Wei Y and Hu S. 2007. A Novel Small-Diameter Vascular Graft: In Vivo Behavior of Biodegradable Three-Layered Tubular Scaffolds. Biotechnology and Bioengineering. 99(4):1007-1015.

Zhang Z, Finlay JA, Wang L, Gao Y, Callow JA, Callow ME and Jiang S. 2009. Polysulfobetaine-Grafted Surfaces as Environmentally Benign Ultralow Fouling Marine Coatings. Langmuir. 25(23):13516-13521.

Zhao C, Brinkhoff T, Burchardt M, Simon M and Wittstock G. 2009. Surface selection, adhesion and retention behavior of marine bacteria on synthetic organic surfaces using self-assembled monolayers and atomic force microscopy. Ocean Dynamics. 59:305-315.

Zhou M, Liu Z, Wei Z, Liu C, Quiao T, Ran F, Bai Y, Jiang X and Ding Y. 2009. Development and Validation of Small-diameter Vascular Tissue From a Decellularized Scaffold Coated with Heparin and Vascular Endothelial Growth Factor. Artifical Organs. 33(3):230-239.

Zhu AP, Chan-Park MB and Gao JX. 2005. Foldable Micropatterned Hydrogel Film Made from Biocompatible PCL-*b*-PEG-*b*-PCL Diacrylate by UV Embossing. Journal of Biomedical Materials Research Part B: Applied Biomaterials. 76B(1):76-84.

Zhu C, Ying D, Mi J, Li L, Zeng W, Hou C, Sun J, Yuan W, Wen C and Zhang W. 2008. Development of anti-atherosclerotic tissue-engineered blood vessel by A20-regulated endothelial progenitor cells seeding decellularized vascular matrix. Biomaterials. 29(17):2628-2636.

Zilla P, Bezuidenhout D and Human P. 2007. Prosthetic vascular grafts: Wrong models, wrong questions and no healing. Biomaterials. 28:5009-5027.

BIOGRAPHICAL SKETCH

Chelsea Marie Magin, daughter of Gregory Allen Magin and Tina Marie Capizzi, was born in Ocala, Florida on a Saturday, in November. Growing up, Chelsea enjoyed playing softball, building model rockets with her father and swimming with her family in the cool, clear waters of the Silver River. She was a safety patrol and a proud Hornet at Ward Highlands Elementary School, and a Fort King Middle School Falcon. In 1999, she entered the International Baccalaureate program at Ocala's Vanguard High School. While there, Chelsea maintained an unweighted 4.0 and played varsity softball.

After graduating high school, Chelsea attended the University of Florida, where she maintained her excellent GPA, earning a bachelor's degree with highest honors in materials science and engineering. During her undergraduate career, she served for four years in the Society of Women Engineers, holding many leadership positions in that organization including Vice President. Chelsea also established the inaugural "Introduce a Girl to Engineering Day," a fixture at UF's Engineers Week. She also founded the UF chapter of the Phi Sigma Rho Engineering Sorority. Towards the end of her undergraduate career, Chelsea interned for two summers with Kimberly-Clark Corporation in Neenah, Wisconsin, submitting three patent applications during her time there.

Chelsea entered the J. Crayton Pruitt Family Department of Biomedical Engineering at UF for her graduate studies, working in Dr. Anthony Brennan's research group. Her graduate work focused on the use of topographically modified surfaces in applications ranging from marine antifouling to directed differentiation of human cells. Chelsea published several papers during her time in the Brennan research group. Her research has taken her all over the world, presenting posters and talks at conferences

from England to Japan. During her graduate studies, Chelsea founded the SWE Graduate Organization of Women Engineers, served as President of the University of Florida chapter of the Society for Biomaterials (SFB) and served on SFB's National Bylaws Committee. Chelsea is also a member of the Alachua County Habitat for Humanity Women Build Group's steering committee. She has been recognized for her contributions as the recipient of the 2010 UF Women's Leadership Council Phyllis M. Meek Spirit of Susan B. Anthony Award and the 2010 Attributes of a Gator Engineer Recognition Award for Leadership. Chelsea enjoys cycling, swimming, throwing pottery and gardening as a member of UF's Organic Garden Co-op. Chelsea is engaged to Steve Kirschner, an attorney and fellow University of Florida graduate. They have two cats, a dog named Yoshi, matching road bikes and a love for Stevie Ray Vaughan. After graduating from the University of Florida, Chelsea will be working as a postdoctoral researcher in Dr. Kristi Anseth's research group in the Department of Chemical and Biological Engineering at the University of Colorado-Boulder.